Ecole Doctorale :
Ressources Procédés Produits Environnement (RP2E)

Ecole Nationale Supérieure des Industries Chimiques (ENSIC)

Laboratoire Réactions et Génie des Procédés (LRGP-CNRS)

Étude de la Cinétique de Polymérisation Radicalaire du Styrène dans un Réseau Tridimensionnel et Application à la Valorisation de Pneus Usagés

T H È S E

Présentée en vue de l'obtention du

DOCTORAT DE L'UNIVERSITE DE LORRAINE
Spécialité : Génie des Procédés et des Produits

par

Ning YU

Thèse soutenue confidentiellement le 8 Décembre 2015

Composition du Jury:

Rapporteurs :	Yves HOLL	Professeur (Université de Strasbourg)
	Nida OTHMAN	Chargée de recherche CNRS
Examinateurs :	Guo-Hua HU	Professeur (Université de Lorraine)
	Dimitrios MEIMAROGLOU	Maître de Conférences (Université de Lorraine)
Invités :	Razak LATIFI	Professeur (Université de Lorraine)
	Sandrine HOPPE	Chargée de recherche CNRS

Ecole Doctorale :
Ressources Procédés
Produits Environnement
(RP2E)

Ecole Nationale
Supérieure des Industries
Chimiques
(ENSIC)

Laboratoire Réactions
et Génie des Procédés
(LRGP-CNRS)

Study of the Kinetics of Free Radical Polymerization of Styrene in a Three Dimensional Network and Applications for Used Tire Recycling

P h D T H E S I S

Requirement for the Diploma of

Doctor of Philosophy

at The University of Lorraine

Specialty: Process and Product Engineering

Defended by

Ning YU

defended on December 8th, 2015

Jury:

Advisors:	Guo-Hua HU	Professor (University of Lorraine)
	Dimitrios MEIMAROGLOU	Associate Professor (University of Lorraine)
Reviewers:	Yves HOLL	Professor (University of Strasbourg)
	Nida OTHMAN	Researcher (CNRS(CR1))
Invited Members:	Razak LATIFI	Professor (University of Lorraine)
	Sandrine HOPPE	Researcher (University of Lorraine)

Résumé

Les caoutchoucs ont de nombreuses applications, y compris les pneus. Cependant, une fois usagé ils sont souvent considérés comme des déchets qui finissent par se trouver dans les décharges ou sont valorisés en tant que ressource énergétique ou ressource matière première secondaire de basse qualité.

Cette thèse a pour objet de développer une nouvelle méthodologie pour valoriser les poudrettes de pneus usagés (PPU). Celles-ci résultent du broyage de la partie caoutchoutique des pneus usagés qui conserve l'excellente élasticité. L'idée est de profiter de leur élasticité pour renforcer la résistance au choc des polymères fragiles tels que le polystyrène (PS) en y incorporant les PPU.

Cependant, la réalisation de cette idée a besoin de relever deux défis majeurs : (1) les PPU commerciales ont typiquement des diamètres de l'ordre de plusieurs centaines de micromètres. Or elles doivent être deux ordres de grandeur plus petits en taille pour pouvoir améliorer la résistance au choc des polymères fragiles. (2) L'adhésion interfaciale entre les polymères et les PPU est mauvaise et constitue donc des défauts mécaniques du matériau. Ces deux défis sont liés à la nature même des PPU qui sont intrinsèquement des réseaux réticulés chimiquement.

Cette thèse choisit le PS pour représenter les polymères fragiles. La méthodologie visant à renforcer sa résistance au choc est de polymériser le styrène par voie radicalaire au sein des PPU. Cette polymérisation forme à la fois des chaines en PS libres et des greffons en PS liés chimiquement aux mailles du réseau des PPU. Les inclusions des chaines en PS libres facilitent la dispersion des PPU en taille plus petite lorsqu'une action mécanique leur est appliquée lors de l'extrusion par exemple. La formation des greffons en PS sur les mailles du réseau des PPU renforce l'adhésion interfaciale entre le PS et les PPU.

Cette thèse a développé un modèle complet permettant de décrire la cinétique de polymérisation radicalaire du PS libre et celle des greffons en PS liés aux mailles du réseau des PPU. Elle l'a validé par un plan d'expériences judicieux.

Abstract

Rubber has many applications including tires. However, once used it is considered as a waste which ends up either in landfills or being recycled as an energy resource or a secondary raw material resource of low quality.

This thesis aims to develop a novel approach to value ground tire rubber (GTR). The latter results from grounding of the rubber part of used tires which retains excellent elasticity. The idea is to take the advantage of its elasticity to toughen brittle polymers such as polystyrene (PS) upon incorporating GTR into them.

However, two challenges have to be overcome to realize this idea. (1) Commercial GTR is typically in the form of particles of a few hundreds of micrometers in diameter. However, it has to be at least one to two orders of magnitude smaller when incorporated in a brittle polymer so as to be able to improve its impact resistance. (2) The interfacial adhesion between the polymer and GTR is weak. These two challenges are related to the intrinsic nature of the GTR which is chemically cross-linked.

This thesis chooses PS to represent brittle polymers. The approach aiming at toughening it is to polymerize styrene in a free radical manner inside cross-linked GTR particles. This leads to the formation of both free PS and PS that is grafted onto the GTR, denoted as grafted PS. The inclusions of the free PS inside the GTR particles help break them down by mechanical shear in a screw extruder for example and the formation of grafted PS improves the interfacial adhesion between the PS and the GTR.

This thesis has developed a comprehensive kinetic model for the polymerization of free PS and that of grafted PS. This model is validated by experimental designs.

Remerciements

I would like to express my gratitude to all those who have helped and inspired me during my doctoral study. I would like to express my deep and sincere gratitude to my advisor, Prof. Guo-Huo HU. His wide knowledge and his logical way of thinking have been of great value for me. His understanding, encouraging and personal guidance have provided a good basis for the present thesis.

I am deeply grateful to my co-advisor, Dr. Dimitrios MEIMAROGLOU. He was always accessible and willing to help his students with their research. His ideas and concepts have had a remarkable influence on my entire research.

I warmly thank Dr. Sandrine HOPPE and Mr. Richard LAINE, for their valuable advice and friendly help. Their extensive discussions around my work and interesting explorations in operations have been very helpful for this study. All my lab buddies at LRGP made it a convivial place to work. In particular, I would like to thank Zheng-hui LI, Fang YUAN, Yu-yin LI, Sara RONASI, Romain Tessier, Francois BESSON and Binod SHRESTHA for their friendship and help in the past four years.

My sincere thanks are due to the official reviewers, Prof. Yves HOLL, Dr. Nida OTHMAN and Prof. Razak LATIFI, for their detailed review, constructive criticism and excellent advice during the preparation of this thesis.

My deepest gratitude goes to my family and my friends for their unflagging love and support throughout my life. I owe my loving thanks to my parents Yin-yuan YU and Xiu-ying ZHANG, my girlfriend Dexin LIUWANG. Without their encouragement and understanding, it would have been impossible for me to finish this work. Furthermore, the generous support of scholarship from China Scholarship Council (CSC) is greatly appreciated.

Table of contents

Nomenclature

Symbol	Designation	Unit
I	Initiator	$mol \cdot L^{-1}$
I_0	Initial initiator concentration	$mol \cdot L^{-1}$
$R*$	Primary radical	$mol \cdot L^{-1}$
M	Monomer	$mol \cdot L^{-1}$
AH	Diels-Alder adduct	$mol \cdot L^{-1}$
$\dot{A}$	1-Phenyltetralyl radical	$mol \cdot L^{-1}$
$\dot{M}$	Styryl	$mol \cdot L^{-1}$
RM_1^*	Monomer radical	$mol \cdot L^{-1}$
GTR_1^*	Rubber radical	$mol \cdot L^{-1}$
$GTRM_1^*$	Rubber-monomer radical	$mol \cdot L^{-1}$
k_d	Initiator decomposition rate constant	s^{-1}
f	Initiator efficiency	-
k_I	Initiation reaction rate constant	$L \cdot mol^{-1} \cdot s^{-1}$
k_1	Styrene dimerization rate constant	$L \cdot mol^{-1} \cdot s^{-1}$
$k\text{-}_1$	Diels-Alder decomposition reaction rate constant	s^{-1}
k_2	Styrene-induced homolysis reaction rate constant	$L \cdot mol^{-1} \cdot s^{-1}$
k_A	Thermal initiation reaction rate constant	$L \cdot mol^{-1} \cdot s^{-1}$
k_B	Thermal initiation reaction rate constant	$L \cdot mol^{-1} \cdot s^{-1}$
k_C	Trimer rate constant	$L \cdot mol^{-1} \cdot s^{-1}$
k_{iR*}	Primary radicals attack rubber initiation reaction rate constant	$L \cdot mol^{-1} \cdot s^{-1}$
k_{iM*}	monomer radicals attack rubber initiation reaction rate constant	$L \cdot mol^{-1} \cdot s^{-1}$
k_{iGTR*}	Rubber radicals attack rubber initiation reaction rate constant	$L \cdot mol^{-1} \cdot s^{-1}$
k_p	Propagation rate constant	$L \cdot mol^{-1} \cdot s^{-1}$
k_{fM}	Chain transfer to monomer rate constant	$L \cdot mol^{-1} \cdot s^{-1}$
k_{fGTR}	Chain transfer to Rubber rate constant	$L \cdot mol^{-1} \cdot s^{-1}$
k_{fGTRMn}	Chain transfer to graft polymer rate constant	$L \cdot mol^{-1} \cdot s^{-1}$
k_{t1}	Termination by combination rate constant	$L \cdot mol^{-1} \cdot s^{-1}$
k_{t2}	Termination by disproportionation rate constant	$L \cdot mol^{-1} \cdot s^{-1}$

k_{t3}	Crossed termination rate constant	$L \cdot mol^{-1} \cdot s^{-1}$
k_{t4}	Rubber radicals termination rate constant	$L \cdot mol^{-1} \cdot s^{-1}$
K_{1a}	Apparent reaction rate constant at low conversion stage	$(L \cdot mol^{-1} \cdot s^{-1})^{1.5}$
K_{2a}	Apparent reaction rate constant at gel effect stage	$(L \cdot mol^{-1} \cdot s^{-1})^{1.5}$
K_{3a}	Apparent reaction rate constant at glass effect stage	$(L \cdot mol^{-1} \cdot s^{-1})^{1.5}$
K_1	Overall reaction rate constant at low conversion stage	$L \cdot mol^{-1} \cdot s^{-1}$
K_2	Overall reaction rate constant at gel effect stage	$L \cdot mol^{-1} \cdot s^{-1}$
K_3	Overall reaction rate constant at glass effect stage	$L \cdot mol^{-1} \cdot s^{-1}$
θ	time	s
ν	Kinetic chain length	-
C_M	Chain transfer constant to monomer	-
C_I	Chain transfer constant to initiator	-
C_s	Chain transfer constant to solvent	-
X_n	Number-average degree of polymerization	-
PR	Primary radical	$mol \cdot L^{-1}$
R_1	monomer radical of size 1	$mol \cdot L^{-1}$
R_n	monomer radical of size n	$mol \cdot L^{-1}$
D_3	trimpers	$mol \cdot L^{-1}$
G	GTR	$mol \cdot L^{-1}$
GPR	GTR radical	$mol \cdot L^{-1}$
GR_n	GTR-monomer radical of size n	$mol \cdot L^{-1}$
D_m	dead polymer of size m	$mol \cdot L^{-1}$
D_n	dead polymer of size n	$mol \cdot L^{-1}$
D_{n+m}	dead polymer of size n+m	$mol \cdot L^{-1}$
GD_m	dead GTR-polymer of size m	$mol \cdot L^{-1}$
GD_n	dead GTR-polymer of size n	$mol \cdot L^{-1}$
GD_{n+m}	dead GTR-polymer of size n+m	$mol \cdot L^{-1}$
k_{i1}	chemical initiation reaction rate constant	$L \cdot mol^{-1} \cdot s^{-1}$
k_{iG}	primary radicals attack GTR initiation reaction rate constant	$L \cdot mol^{-1} \cdot s^{-1}$
k_{i2}	GTR radicals initiation reaction rate constant	$L \cdot mol^{-1} \cdot s^{-1}$
k_{pG}	propagation rate constant of graft polymer	$L \cdot mol^{-1} \cdot s^{-1}$
k_{fg}	Chain transfer to GTR rate constant	$L \cdot mol^{-1} \cdot s^{-1}$
k_{fpg}	Chain transfer to graft polymer rate constant	$L \cdot mol^{-1} \cdot s^{-1}$
k_{fp}	Chain transfer to free polymer rate constant	$L \cdot mol^{-1} \cdot s^{-1}$

k_{tc}	Termination by combination rate constant of free polymer	$L \cdot mol^{-1} \cdot s^{-1}$
k_{tcG}	Termination by combination rate constant of graft polymer	$L \cdot mol^{-1} \cdot s^{-1}$
k_{td}	Termination by disproportionation rate constant of free polymer	$L \cdot mol^{-1} \cdot s^{-1}$
k_{tdG}	Termination by disproportionation rate constant of graft polymer	$L \cdot mol^{-1} \cdot s^{-1}$
k_{tpr}	Termination by primary radical rate constant	$L \cdot mol^{-1} \cdot s^{-1}$
k_{tprg}	Termination by GTR primary radical rate constant	$L \cdot mol^{-1} \cdot s^{-1}$
k_{da}	Deactivation reaction rate constant	$L \cdot mol^{-1} \cdot s^{-1}$
δ_c	Segmental diffusion parameter for styrene	$L \cdot g^{-1}$
C_p	Concentration of polymer in the system	$mol \cdot L^{-1}$
MW_m	Molecular mass of styrene	$kg \cdot mol^{-1}$
$k_{t,seg}$	Effective-segmental diffusion-limited termination rate coefficient	$L \cdot mol^{-1} s^{-1}$
T_{gp}	Glass transition point of polymer	K
T_{gm}	Glass transition point of monomer	K
k_B	Boltzmann constant	$m^2 \cdot kg \cdot s^{-2} \cdot K^{-1}$
α_m	Thermal expansion coefficient of monomer	K^{-1}
α_p	Thermal expansion coefficient of polymer	K^{-1}
d_m	Monomer density	$g \cdot L^{-1}$
d_P	Polymer density	$g \cdot L^{-1}$
d_I	Initiator density	$g \cdot L^{-1}$
K	Critical variable for the onset of the 2nd stage of diffusion control	$kg^{0.5} \cdot mol^{-0.5}$
K_{cr}	Critical constant for the onset of the 2nd stage of diffusion control	$kg^{0.5} \cdot mol^{-0.5}$
V_f	Total free volume	-
$V_{f,cr}$	Free volume at the onset point of the 2nd stage of diffusion control	-
A	Adjustable parameter for the onset of 2nd stage	-
A_{cr}	Pre-exponential factor of K_{cr}	$(g \cdot mol^{-1})^{0.5}$
R	Universal gas constant	$cal \cdot mol^{-1} \cdot K^{-1}$
N_{av}	Avogadro number	$1 \cdot mol^{-1}$
n	Coefficient for translational diffusion limited termination	cal/mol
E_{cr}	Activation factor of K_{cr}	$1 \cdot K^{-1}$
k_T	Effective translational diffusion-limited termination rate coefficient	$L \cdot mol^{-1} \cdot s^{-1}$
M_{wcr}	Weight-average molecular weight of dead polymer chains at the onset point of the 2nd stage of diffusion control	$kg \cdot mol^{-1}$

$k_{t,rd}$	Effective reactional diffusion-limited termination rate coefficient	$L \cdot mol^{-1} \cdot s^{-1}$
$k_{t,eff}$	Effective overall diffusion-limited termination rate coefficient	$L \cdot mol^{-1} \cdot s^{-1}$
σ	Lennard-Jones diameter for a styrene molecule	m
δ	Root-mean-squared end to end distance per square root of the number of monomer units	$m \cdot num^{-0.5}$
j_c	Number of monomer units between entanglements on a polymer chain	num
A_{crm}	Adjustable parameter for the onset of 3rd stage	-
$V_{f,crm}$	Free volume at the onset point of the 3rd stage of diffusion control	-
E_{crm}	Adjustable activation energy for the onset of 3rd stage	$cal \cdot mol^{-1}$
$k_{p,eff}$	Effective diffusion-limited propagation rate coefficient	$L \cdot mol^{-1} \cdot s^{-1}$
B	Adjustable parameter for 3rd stage	-
C_{rRatio}	Adjustable parameter for 4th stage	-
$V_{f,creff}$	Free volume at the onset point of the 4th stage of diffusion control	-
C	Adjustable parameter for the onset of 4th stage	-
f_{i0}	Efficiency factor for thermally induced radical initiation	-
$f_{i,eff}$	Effective diffusion-limited efficiency factor for thermally induced radical initiation	-

Subscripts

I Initiator

m Monomer

P Polymer

t Termination

0 Initial conditions

List of Figures

List of Tables

Résumé long

Le caoutchouc est une matière première très répandue, principalement utilisée dans l'industrie automobile, il existe en abondance dans les énormes décharges de pneus en caoutchouc produits chaque année. La structure réticulée de caoutchouc de pneus usés (également connue sous le nom de « Ground Tire Rubber » (GTR)) ajoutée à la présence de stabilisants et autres additifs, inhibe son processus de dégradation naturel, entraînant ainsi de graves problèmes environnementaux.

Une solution à ce problème est la réutilisation des particules GTR dans différentes applications, telles que l'incorporation dans des matières thermoplastiques, thermodurcissables et les élastomères. Cependant, la réalisation de cette idée a besoin de relever deux défis majeurs : (1) les PPU commerciales ont typiquement des diamètres de l'ordre de plusieurs centaines de micromètres. Or elles doivent être deux ordres de grandeur plus petits en taille pour pouvoir améliorer la résistance au choc des polymères fragiles. (2) L'adhésion interfaciale entre les polymères et les PPU est mauvaise et constitue donc des défauts mécaniques du matériau. Ces deux défis sont liés à la nature même des PPU qui sont intrinsèquement des réseaux réticulés chimiquement.

Il est possible d'améliorer l'adhérence inter-faciale entre la matrice de polymère (dans ce cas, le polystyrène PS) et GTR par la polymérisation par greffage radicalaire in situ de styrène sur les particules de caoutchouc. L'objectif de ce travail est d'étudier de manière expérimentale et par modélisation la polymérisation par greffage de radicaux libres du styrène avec les particules GTR réticulées.

Cette thèse est composée de deux parties :

Partie I : La polymérisation par greffage de styrène à l'intérieur des particules réticulées GTR a été étudiée expérimentalement en utilisant le BPO et DCP en tant qu'amorceurs de polymérisation. Tout d'abord, la polymérisatios de greffage de styrène à l'intérieur des particules GTR a été étudiée pour obtenir le taux de

conversion et l'efficacité du greffage greffe. Deuxièmement, on a augmenté la quantité de monomère pour étudier la polymérisation de greffage de styrène sur les particules GTR. Troisièmement, l'amélioration des propriétés d'impact des particules GTR-g- PS a été étudiée par l'extrudeuse bi-vis.

Partie II : Une approche couplée de modélisation phénoménologique / mécanistique est suivie pour une étude théorique de la cinétique complexe de polymérisation de greffage radicalaire. Initialement, un modèle de Réseaux de Neurones Artificiels est développé pour étudier l'influence des principales conditions de réaction (par exemple, la température et les quantités de monomère, GTR et amorceurs) sur la conversion du monomère et l'efficacité de greffage.

Dans un second temps, un modèle cinétique global est développé sur la base de la méthode de moments, qui affiche des capacités de prédiction étendues.

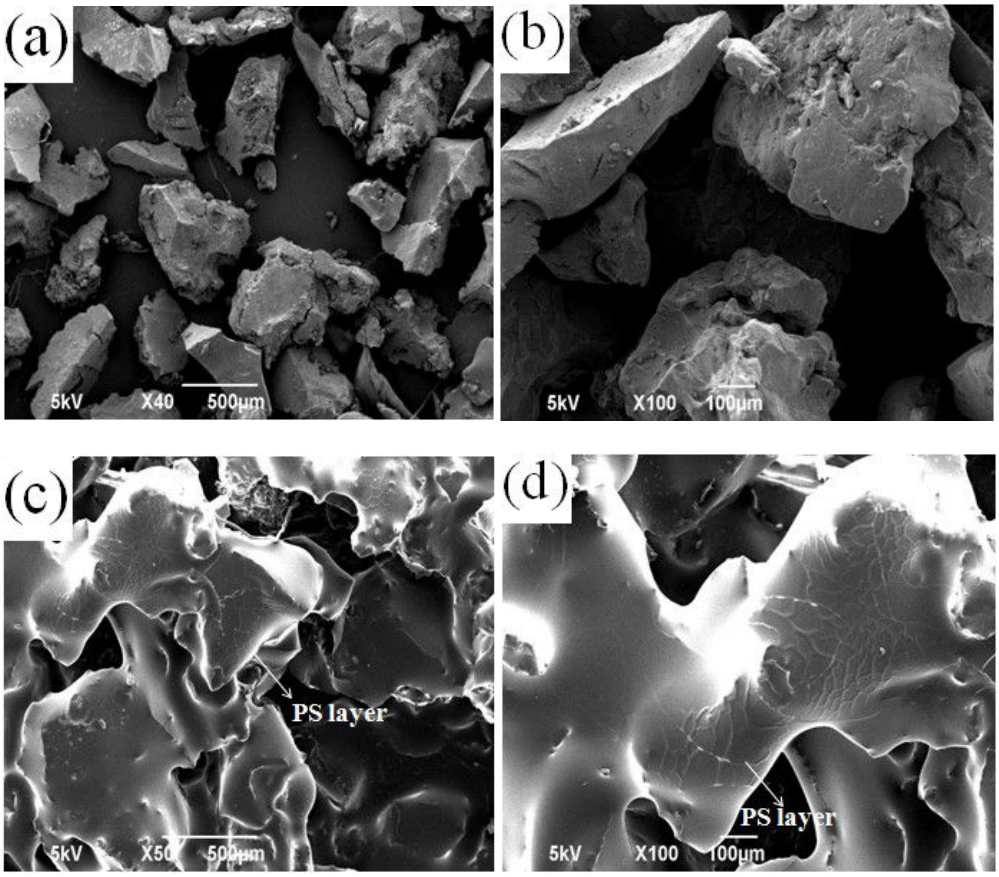

Figure 1- SEM Images SEM de (a) et (b) particules GTR d'origine, (c) et (d) particules GTR-g-PS.

Pour la Partie I, en tant que matière plastique typique ayant une faible résistance au choc, le polystyrène a été greffé avec succès à l'intérieur des poudres de GTR réticulés à l'aide de BPO et DCP comme amorceurs par un simple procédé de polymérisation radicalaire. Les résultats de la caractérisation de Microscopie à Balayage Electronique, a révélé que les particules GTR ont été greffées par des chaînes PS (Figure 1).

Dans ce travail, nous gardons le rapport styrène / GTR inférieur à 2 afin que le styrène soit complètement situé à l'intérieur des particules GTR. De cette façon, le styrène est polymérisé seulement à l'intérieur des particules GTR réticulées. Ceci est différent des travaux existants dans la littérature, dans lesquels le rapport styrène / GTR est tellement élevé que la quantité de styrène ne peut pas être complètement absorbée par le GTR. En tant que tel, la polymérisation du styrène a lieu à la fois à l'intérieur et à l'extérieur des particules GTR.

Lorsque le styrène est polymérisé à l'intérieur d'une particule GTR individuelle, il existe deux types de polymérisation. L'un est la polymérisation du styrène lui-même conduisant à des chaînes PS qui ne sont pas liées à la particule GTR. Ces chaînes de PS sont appelées PS libres. L'autre est la polymérisation du styrène à partir des chaînes de caoutchouc et les chaînes de PS résultantes sont fixées à celles du caoutchouc. Ces chaînes de PS sont désignées comme GTR-g-PS. Le matériau obtenu est des particules GTR à l'intérieur duquel il y a du PS libre et GTR-g-PS. Dans ce qui suit, ce matériau est désigné comme PS/GTR-g-PS.

L’un des principaux avantages de notre approche est qu'elle permet de minimiser la quantité de PS libre dans le PS/GTR-g-PS tout en maximisant la quantité de GTR-g-PS. Un autre avantage est qu'un minimum de PS libre présent dans le PS / GTR-g-PS avec un maximum de GTR-g-PS permet de recycler un maximum de GTR de meilleures propriétés, en particulier la résistance aux chocs. En effet, il est prévu que plus le rapport PS/GTR-g-PS diminue, plus la compatibilité entre le PS libre et le GTR-g-PS augmente, ainsi que la force d'impact.

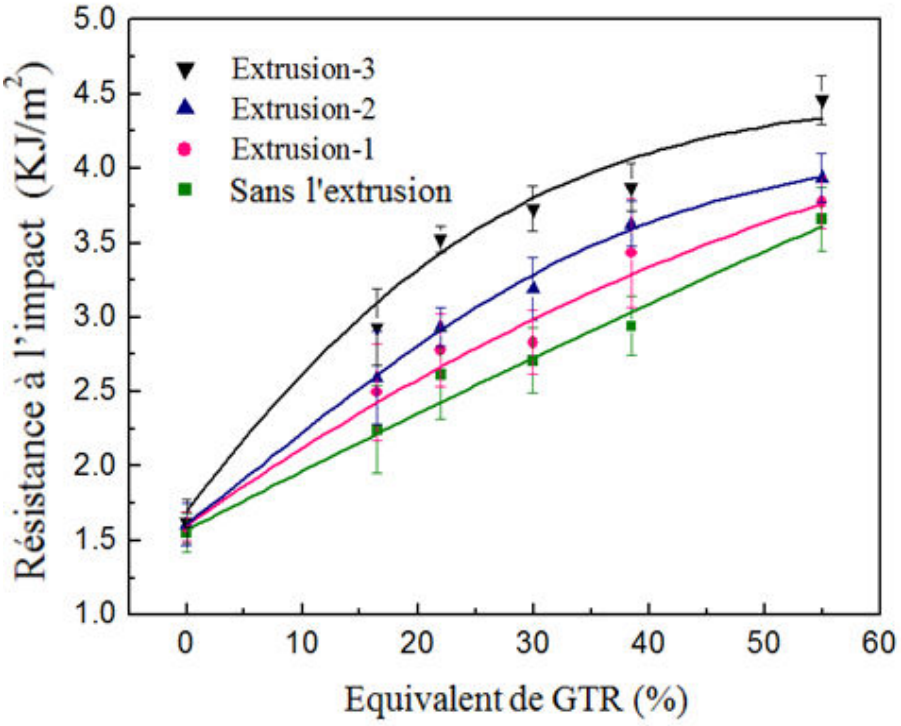

Figure 2 - Résistance à l'impact du GTR-g-PS/PS après l'extrusion.

La taille des particules de GTR-g-PS pourrait être réduite par extrusion. Il y avait peu d'influence sur la masse moléculaire du PS libre par extrusion. Les surfaces fracturées d'échantillons d'impact ont suggéré une meilleure dispersion de GTR en se greffant avec les chaînes PS dans la matrice PS et une adhérence inter-faciale supérieure entre les deux phases. Bien que la résistance à l'impact du PS commercial soit d'environ 1,5 KJ / m^2, elle s'élève à un niveau aussi haut que 4,5 KJ / m^2 par polymérisation in situ du styrène à l'intérieur de la GTR après l'extrusion (Figure 2). Ceci est une amélioration très significative.

Pour la Partie II, un modèle de réseau de neurones artificiel démontre la capacité d'un réseau neuronal à rétro-propagation à action directe pour prédire la performance de polymérisation par greffage de styrène. Le modèle a bien fonctionné dans la prédiction non seulement des données utilisées dans le processus de formation, mais aussi des données des tests qui étaient inconnues du réseau neuronal de conversion et GE de la polymérisation par greffage du styrène à particules GTR.

Un modèle mécanistique cinétique a été développé pour la polymérisation du styrène en masse avec le GTR. Le développement d'un modèle de polymérisation cinétique est fondamental pour la compréhension des différentes réactions chimiques. Ces réactions chimiques ont lieu dans la phase de monomère en masse et sur la surface des particules GTR, conduisant à la synthèse de deux populations de chaînes de polymère distinctes (à savoir le polymère libre et les chaînes de polymère greffé) ayant des caractéristiques et des propriétés distinctes. Lors de l'élaboration de ce modèle, les hypothèses d'homogénéité thermique et de limitations de transfert de masse négligeables ont été envisagées afin de simplifier cette première approche de modélisation cinétique de ce système complexe. Les phénomènes de diffusion, associés à l'approche et à la pénétration des radicaux au sein des particules GTR ont été pris en compte par l'examen des différentes constantes cinétiques pour les réactions de propagation et de terminaison qui se produisent à la surface ou à l'intérieur des particules GTR, concernant les mêmes réactions qui se produisent dans la phase St / PS.

Le modèle cinétique de polymérisation de greffage du styrène à l'intérieur / sur des particules GTR réticulées décrit non seulement la conversion du monomère, mais également l'efficacité de greffage. Les résultats des simulations ont montré que ce modèle est capable de prédire avec précision la conversion, le GE et la masse moléculaire de PS libre. Bien que ces hypothèses ne puissent pas tenir strictement dans des conditions différentes de celles mises en œuvre dans le présent travail et, par conséquent, limitent la généralité du modèle et des paramètres spécifiques proposés, en tout cas, elles n'affectent pas la validité du cadre de modélisation général développé qui peut être facilement modifié pour tenir compte des variations de concentration et/ou des conditions de température, sur la base de preuves

expérimentales pertinentes. Même sous ce prisme simplificateur et à la meilleure connaissance des auteurs, c'est la première fois qu'une telle étude approfondie de la modélisation cinétique est présentée pour la polymérisation de greffage radicalaire du styrène sur des particules GTR.

Chapter 1 Introduction

1.1 Introduction to Ground Tire Rubber (GTR)

Rubber is a commodity material, mainly used in the automotive and agricultural sectors. As a result, large amounts of waste tire rubber are produced every year. The cross-linked structure of this material along with the presence of stabilizers and other additives in the rubber formulation, inhibit its degradation process thus resulting in serious environmental issues [1]. A solution to this problem is the re-use of ground tire rubber (GTR) particles in different applications such as fillers in thermoplastics, elastomers and thermosets [2]–[5]. This recycling route has been implemented for many years but with limited success. The reason is that the incorporation of GTR particles into polymer matrices significantly impairs the mechanical properties of the resulting materials, even at low rubber content, due to poor adhesion between the GTR and the polymer and to the relatively large GTR particle size as well [6]–[8].

1.1.1 Waste tire and its reutilization

A car tire can travel at the average of 32,000 km over its lifetime, but when it reaches the end of its life, the waste tire could bright many serious environment problems [1]. Due to the cross-linked structure of rubbers and presence of stabilizers and other additives, the degradation of the waste tire rubber is very difficult. Therefore, the recycling and reutilization of waste tire rubber is a hot research topic in the past few years.

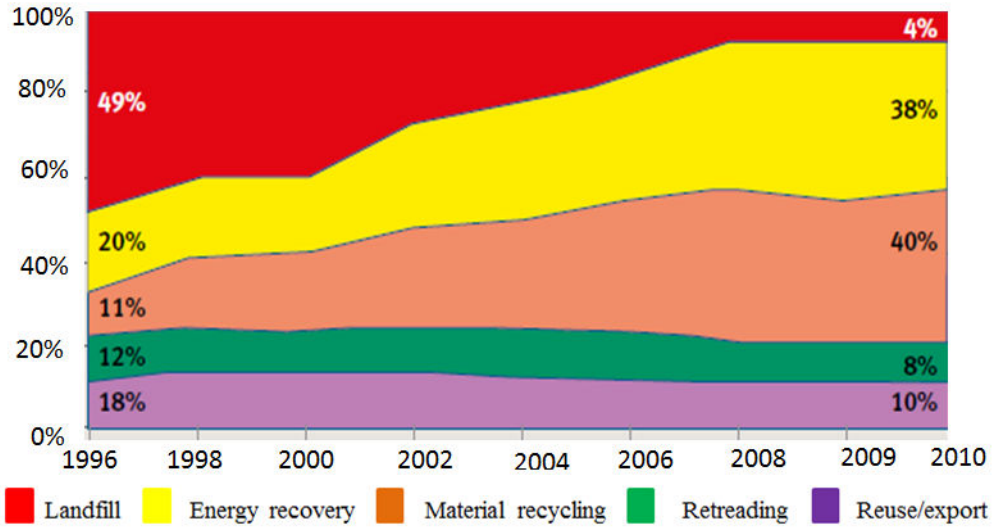

Figure 1.1 - Breakdown of waste tire utilization in EU from 1996 to 2010 [9].

Figure 1.1 shows the breakdown of waste tire utilization from year 1996 to 2010 in EU. In 1996, landfill is the main treatment for the waste tire. The landfill is an undesirable way for treating the waste tire, which can make many serious environmental problems. After the value of the waste tire was realized, recycling methods of waste tire was increased from 11% to 40% in EU from 1996 to 2010 [9].

France is a highly industrialized country with a large automotive market. There are some big automotive manufacturers, such as Renault, Citroen and Peugeot. This generates a huge amount of waste tire every year.

The scrap tire recycling industry in France is still in a nascent stage. According to statistics, waste tire generated in France has accounted for 390,000 tons of scrap tires in 2003 of which 52% were recycled. In 2004, the production of reclaimed rubber in France reached 265,530 tons of scrap tires, equal to 30.4 million tires. This number increased to 381,000 tons in 2010 in France. The number of scrap tires recycled is low with respect to the number of waste tires generated.

To utilize the reclaimed tire rubber, France is working to use it to replace part of its natural and synthetic rubber needs, and use it for other non-tire rubber products. This can alleviate the shortage of rubber resources and reduce the production cost. The majority of scrap tires generated in France are used in landfills and tire-derived fuel, while the rest are recycled and re-used. As shown in Figure 1.1, only about 52% of the scrap tires generated were recycled, 26% were reused and 22% were landfilled.

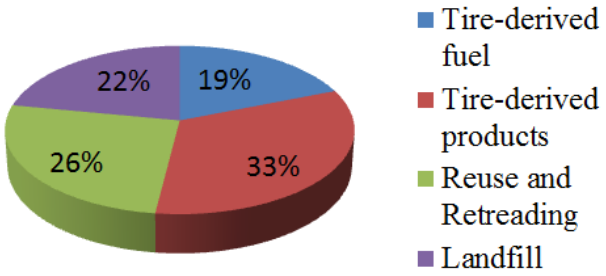

Figure 1.2 - Used tire destinations in France [10].

1.1.2 Surface modification of GTR

GTR particles (Figure 1.3) are commonly used as fillers in thermoplastics, elastomers and thermosets [5], [6], [11]. However, as pointed out above, the incorporation of GTR into polymer matrices can adversely affect the mechanical properties of product, even at low rubber content, due to the poor adhesion between GTR and polymer matrices [11].

Figure 1.3 - Waste tire and ground tire rubber (GTR).

Several techniques have been proposed in order to overcome this adhesion problem, such as the use of compatibilizers and the surface modification pre-treatment of the GTR. Among them, the surface modification of the GTR particles holds the lion's share since, in comparison with untreated GTR, the surface-treated GTR is expected to provide better compatibility and stronger interfacial interactions with the host materials. Consequently, it is possible to add a larger percentage of surface-

treated GTR into the matrix material. Among the different treatment technologies that are currently available, one can distinguish the redox method, grafting by gamma irradiation, plasma, corona and electron beam radiation and ozone induced surface grafting [12]–[16]. Fan et al. investigated the surface modification of PMMA onto waster tire rubber though ozonization [13]. Shuang et al. produced one kind of nano-powdered styrene-butadiene rubber though radiation and studied its toughening effect for polystyrene (PS) and high-impact polystyrene [17]. Feng et al. applied ultrasound to modify the surface of waste tire rubber particles [18]. Scuracchio et al. [19], Tyler and Cerny [20], reported the surface modification of waste tire rubber particles with microwave.

The use of in-situ radical polymerization techniques to directly "attach" polymer chains on the rubber particles via grafting reactions with a monomer is another efficient way to modify the surface characteristics of GTR and to create a natural compatibilizer (i.e., the grafted polymer chains) between the modified GTR and the matrix of the polymer of the same monomer. This method has been used to modify the surface of GTR to improve the miscibility and interfacial adhesion between polymer matrices and GTR [21].

1.1.3 Devulcanization of GTR

The purpose of devulcanization is to selectively break the sulfuric crosslinks in the vulcanized rubber such as C–S and S–S bonds. Devulcanization requires high energy to break the –C–S-C– (285 kJ/mol), –C–S–S–C– (268 kJ/mol) or –C–Sx–C– (251 kJ/mol) bonds [22]. There are some devulcanization methods for GTR. The themomechanical method, ultrasonic method and microwave method are introduced below.

1.1.3.1 Themomechanical method

The themomechanical method can be used to break the sulfur bonds of cross-linked rubber with the shearing force [1]. Recent researches report the use of a twin screw extruder for the ground rubber devulcanization [23]. During the themomechanical process, the shearing action is applied to the material that tears the

rubber network. Continuity and higher efficiency are the advantages of this approach compared to other devulcanization methods such as themochemical process and microwave method. The quality of devulcanized rubber which is obtained through this method is affected by processing conditions such as temperature profile and screw rotation speed [24]–[26]. In the mechanical process, the devulcanization rate of GTR can be increased by increasing the reaction temperature and rotational speed. Temperatures should not be too low. For instance, a temperature lowers than 50℃ slows down the devulcanization rate of the waste vulcanized rubber. Temperatures should also not be higher than 400℃ either. Otherwise the rubber degrades.

Some conditions of the mechanical process are summarized as follows. Sipahi-Saglam et al. (2001) modified epoxy with recycled rubber in a continuous twin-screw devulcanizer [24]. The rubber was subjected to high shearing action between the screw and the wall of the extruder barrel. Temperatures between 175-205℃ were applied and the residence time was between 1 and 3 minutes [24], [27]. Kumar et al. (2002) illustrated this continuous process to blend the rubber and LDPE with a twin screw extruder [26]. Rubber was fed at about 10 kg/h, extruded and cooled in a water bath. Screw rotation speeds of 100-400 rpm and temperatures between 50-400℃ were applied. Maridass et al. (2008) used a counter-rotating twin screw extruder to devulcanize waste ground rubber tire for recycling [23]. In this process, breakage of crosslinking points in the three dimensionally crosslinked vulcanizate occured selectively under the controlled temperature and shearing action. They found that the optimum properties were predicted at temperature 180℃ and screw speed 27 rpm by the central composite rotatable design, which was confirmed experimentally.

1.1.3.2 Ultrasonic method

A devulcanation process of GTR by ultrasound is a process where ground rubber particles are extruded and then flow through the die, where a horn gives ultrasonic energy to the material. The devulcanization takes place in the gap between the die and the horn. The material turns soft and is able to flow again. The carbon black filled rubbers may influence the devulcanization of rubber with the ultrasonic method. This is because a certain portion of ultrasonic energy can be spent on breaking physical and chemical bonds between rubbers and carbon black, which

possibly displays a lower bond energy than chemical bonds in polymer chains and cross-links. This decreases devulcanization of rubber [28].

Isayev et al. (2004) studied devulcanization of PS/SBR blends by an ultrasonic method in a twin screw extruder. A horn vibrated longitudinally at a frequency of 20 kHz and an amplitude of between 5 and 10 microns, which was provided by a 3000W ultrasonic power supply equipped with a converter and a booster. Higher devulcanization was achieved at a higher amplitude [29].

1.1.3.3 Microwave method

Microwave technology is extensively used for breaking sulfur-sulfur or carbon–carbon bonds with a controlled dose of microwave energy at specified frequency and energy level. Microwaves are especially suitable for this use since they are more easily focused into narrower beams than radio waves. Therefore, this method could be used in the devulcanization of waste tire rubber.

Tyler et al. (1984) proved that their microwave devulcanization method could be used for controlling pollution by passing a sulfur cross-linked elastomer through a microwave energy devulcanization device. The microwave energy devulcanization device was implanted in the extruder die whose temperature was maintained at about 90 to 125℃. The heat generated by the microwave raised the melt temperature to over 260℃. The extrudate could be used per se as a compounding stock [20]. Wicks et al. (2002) showed that vulcanized crumb rubber had selected chemical bonds broken by microwave radiation to be used in new rubber formulations [30]. They concluded that the rubber mixture has better properties with the higher power of microwave to treat the crumb rubber. Zanchet et al. (2009) studied styrene-butadiene rubber composites containing only industrial rubber scraps devulcanized by microwave for 3 to 4 min. The tensile strength and tear strength of the compositions were ~25% and 41% of those of the control sample, respectively. The tensile strength and tear strength of the SBR/ industrial rubber scraps blends were ~25% and 41% of those with devulcanized by microwave, respectively.

1.1.4 Plastics/GTR blends

Plastics/devulcanized rubber blends are a straightforward option to use the rubber to toughen plastics. The use of the devulcanized rubber as a toughening agent in thermoplastics would reduce the cost of the final blend. Several studies have reported the use of recycled rubbers as toughening agents in thermoplastics, such as polyethylene (PE), polypropylene (PP) and PS.

1.1.4.1Polyethylene (PE)/GTR blends

Sonnier et al. (2007) reported that GTR showed poor adhesion to a high density PE and worsened the tensile properties of the latter. The size of the GTR was 0.6-0.7mm and the PE/GTR ratio was from 100/0 to 30/70. The GTR was treated by oxidation method ($KMnO_4$) [31].

Scaffaro et al. (2005) used the GTR of 0.4-0.7mm in size and the PE/GTR ratio was from 75/25 to 25/75. The blends were processed in a twin screw extruder. The injection molded samples showed better performance than compression molded ones [32].

Shojaei et al. (2007) blended the PE and GTR in a twin screw extruder. They found that with increasing GTR content, the yield stress and impact strength decreased. The size of the GTR was below 0.4mm and the PE/GTR ratio was from 75/25 to 25/75 [33].

1.1.4.2 Polypropylene (PP)/GTR blends

PP has good performance. However its toughness is poor, limiting its applications. Therefore, numerous methods have been proposed to overcome this shortcoming. One of them is to use the GTR as an impact modifier. Fuhrmann et al. (1999) studied PP/GTR blends in a twin screw extruder. The size of the GTR was 0.4-0.7mm and the PP/GTR ratio was from 100/0 to 40/60.The specimen was produced by injection molding. They showed that the notched charpy impact strength at room temperature increased with increasing GTR content [34].

Kuznetsova et al. (2004) studied rubber devulcanization by a themomechenial method in a twin screw extruder. The sizes of the GTR were below 0.4mm and 0.4-

0.7mm, respectively. The PP/GTR was from 100/0 to 50/50.They found that smaller GTR particles resulted in slightly better mechanical properties [35].

Awang et al. showed that tensile properties of PP/modified-GTR blends were better than those of PP/unmodified-GTR ones [2]. An improved dispersion and a size reduction of particles were observed in the micrographs of tensile fracture surfaces. It indicated that the modifications of GTR were capable of offering an improved interfacial adhesion which should lead to improved properties.

1.1.4.3 Polyvinyl chloride (PVC)/GTR blends

Naskar et al. (2002) used chlorinated ground rubber tire (Cl-GRT) particles as fillers for a plasticized PVC. The physical properties of the Cl-GRT-filled PVC compound were improved compared with those of the non-chlorinated counterpart. Moreover, the Cl-GRT-filled composite was found to be re-processable like the unfilled PVC compound [5]. Stelescu et al. (2013) focused on the polymer composites based on plasticized PVC and rubber powder from vulcanized nitrile rubber waste. Lower hardness, higher elongation at break, a better tensile strength, and better ozone resistance were the good properties of the new polymer composites. Moreover, the polymer composites had good fluidity that could be processed by injection, extrusion, and compression molding [36].

1.2 Introduction to polystyrene (PS)

PS is one of the most widely used plastics, with applications in industries of packaging, buildings and construction appliances. A major limitation of the commercial production of PS is the heat transport in the highly viscous system during the polymerization of styrene. A huge amount of heat is generated. Therefore, the control of temperature of polymerization of styrene is a key factor.

1.2.1 Polystyrene structure

The brittleness of polystyrene is depended on its structure. The polystyrene

structure is the phenyl alternately connected on the side of the molecular chain of polystyrene. The bigger volume of phenyl results in the larger steric hindrance effect, and makes the polystyrene chains become hardened, therefore, the glass transition temperature is higher than polyethylene, polypropylene. Due to the phenyl on the side of the main chain of polystyrene is random arranged, the polystyrene is one kind of amorphous polymers, has the very high transparency.

1.2.2 General Purpose Polystyrene (GPPS)

The most common type of commercial PS is the so-called general purpose polystyrene (GPPS). It is a linear polyethylene chain with laterally attached phenyl rings, being responsible for the enhanced glass transition temperature and high refractive index [37]. It is a hard, rigid thermoplastic with excellent thermal properties but its brittle nature along with its low impact strength and increased stress-cracking tendency inhibit its application [21]. It is used for family and aviation supplies (tableware, tray, etc.), electrical (transparent container, light scattering, insulation film), etc.

1.2.3 High Impact-Modified Polystyrene (HIPS)

The incorporation of polybutadiene is an earliest way to overcome the brittleness of GPPS. Ostromislensky [38] invented the high impact-modified HIPS, which has been commercialized since the 1950s. He used the cellular rubber particles to toughen PS during the manufacturing process and the rubber particles were embedded into the PS matrix. However, the transparency of PS was lost by using the rubber toughening. As the research continued, core/shell particles were used to toughen PS, such as styrene—butadiene block copolymers. Due to the small domains of this copolymer in the PS, the resulting material is translucent impact polystyrene [37].

1.2.4 PS/plastics blends

In general, PS can be modified through physical and chemical means. Physical means include extrusion, blending of polymers and additives. Chemical means include grafting reactions, copolymerization.

Polymers such as polyamide (PA), PE and PP could be used to improve the mechanical properties of PS by physical blending. Won et al. (1996) studied the grafting of maleic anhydride (MAH) onto PS through reactive extrusion and its blending with polyamide 6(PA6) by melt mixing [39]. They investigated the effect of MAH units incorporated in PS on the compatibility with PA6. The blending parameters in a twin-screw extruder were: the screw speed was 30rpm, the mixing temperature was 230℃, and the residence time was 3min. The mechanical properties of PA6/PS blends showed increased strength and elongation from 47.8 to 57.5 MPa and 187 to 238%, respectively, when MAH-PS were added [39]. PE/PS alloy foams were produced by Zhe et al. using supercritical carbon dioxide foaming method. They used styrene–ethylene–butylene–styrene (SEBS) copolymer as a compatibilizer of PS and PE to improve the cell morphology. The PS/PE/SEBS alloy foams had a smaller mean cell diameter and higher cell density than those without SEBS [40]. Asha Krishnan et al. (2015) studied the effect of cellulose nanofibers on the mechanical and morphological properties of PP/PS blends. They announced that the strength and modulus of PP/PS blends could be improved with addition of cellulose nanofibers [41].

From the articles above, adding an appropriate polymer to PS could improve its properties, provided that a compatibilizer be added. To overcome the low compatibility between PS and the modifier, it is better to use chemical means. The most important way is to use the rubber to toughen PS via the copolymerization or graft polymerization. It will be further described in the next section.

1.2.5 Rubber modified PS

Since the mechanical properties of PS are known to improve via the incorporation of rubber into its matrix during the manufacturing process, a significant number of studies have been focused on the blending of rubber with PS towards an improvement of its properties [42]–[45]. PS can be toughened by co-polymerization of polybutadiene (PB) rubber to extend its applications. The size of rubber particles is a key factor to toughen PS.

A wide variety of morphological structures can be formed during phase separation induced by polymerization [46] [47] [48] . Salami structure of high-impact

polystyrene (Figure 1.4) is especially interesting because of duality of the structure [47] [48]. Salami structure is that each rubber particle containing a high volume fraction of polystyrene subinclusions. It has been experimentally revealed that production of graft polymers by attacking of polystyrene radicals onto double bonds of polybutadiene and stirring of reacting mixture play essential roles in its formation [47]. However, detailed mechanism of the salami structure formation in high-impact polystyrene has not been fully understood because of its complexity [47].

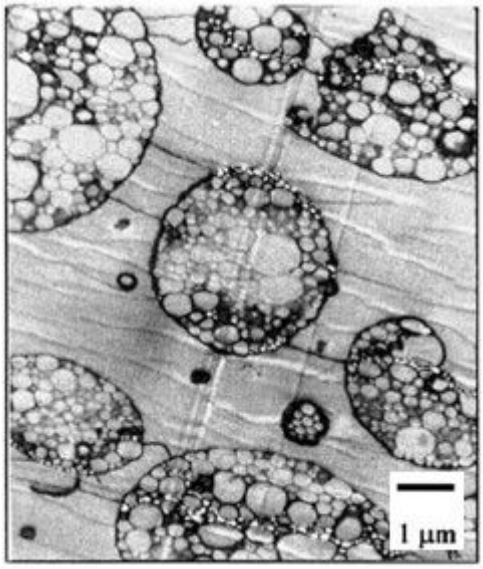

Figure 1.4 - Salami structure of high-impact polystyrene [48].

Some articles reported on the toughening of PS using rubber [1], [3], [49]. Moore (1971) studied rubber-reinforced PS using various butadiene polymers and copolymers [50]. A particle size of 2μm was required to obtain reasonable improvements in impact strength. Rubber type and concentration, and pre-polymerization temperature were changed to vary the rubber particle size. Silberberg and Han (1978) reported that the agitation rate affected the different rubber particle sizes [51]. They indicated that the particle size dependence of energy absorption in impact and tensile testing appears to be opposite in nature. Piorkowska (1990) studied the morphological transformation by PS blends containing concentric spherical shell particles of 0.32 and 2.3μm [52]. It was found that at a constant particle size, the craze flow stress increased systematically with decreasing particle volume fraction. From the above articles, rubber particles of around 1–3μm in diameter are best at toughening PS.

Recently, Gao (2006) prepared core-shell polybutadiene-graft-polystyrene (PB-g-PS) rubber particles with different ratios of polybutadiene to PS by emulsion polymerization through grafting styrene onto polybutadiene latex [43]. It was generally accepted that PS could only be toughened effectively by 1-3μm rubber particles through a toughening mechanism of multiple crazing. However, their experimental results showed that PS could be toughened efficiently by monodisperse sub-micrometer core–shell PB-g-PS rubber particles. They (2009, 2010) continued the study to show that a specimen with a 'cluster' dispersion state of rubber particles in the PS matrix displayed better mechanical properties [53], [54]. They explained that the dispersion of rubber particles in a 'cluster' state leads to better impact resistance.

1.2.6 GTR toughened PS

There are publications on the free radical grafting of styrene onto GTR by using free radical initiators such as peroxides and diazocompounds [55] [56] [43]. It should be considered the presence of carbon black (CB) in the ground tire rubber, it can influence the polymerization. The surface of CB can be bonded with free radicals [57]. The radicals formed on the CB surface are stabilized by the polycondensed aromatic rings, which act as strong radical trapping-agents [55]. Therefore, the free radical polymerization might be inhibited by the CB.

Coiai et al. (2006) studied on the synthesis of PS chains covalently bound to the surface of cross-linked rubber particles from recycled tires GTR via free radical polymerization [55] [56]. The polymerization temperature was 70℃ for AIBN and 85℃ for BPO [55]. They concluded that free radicals can attack both the monomer and double bonds of the rubber thus creating conditions for homo-polymerization of the monomer and graft polymerization of the monomer onto the rubber. The polymerization time was 24 hours which was very long. They did not mention mechanical properties of materials. Zhang et al. studied the effect of polymerization conditions of styrene on the surface of waste tire rubber. However, they did not investigate mechanical properties [21].

Wang et al. (2011) prepared PS/GTR blends in a batch mixer. They found that GTR improved the impact resistance of the PS but deteriorated its tensile properties. The effect of the GTR particle size (75, 105 and 200μm) on the mechanical properties

of PS/GTR blend was investigated. Their tensile strength, notched impact strength and elongation at break were increased from 18.9 to 20.2 MPa, 2.13 to 2.51KJ·m^{-2} and 1.7 to 2.5 %, respectively, with the GTR particle size was decreased from 200 to 75μm. Glycidyl methacrylate (GMA), styrene-butadiene triblock copolymer (SBS), and maleic anhydride grafted polypropylene (PP-g-MAH) were used as compatibilizers to improve the compatibility between the PS and GTR. GMA and SBS could improve the impact resistance of the PS/GTR blend, while PP-g-MAH had only a little effect. When the PS/GTR(75μm)/SBS ratio was 100/40/10, the blend had excellent comprehensive properties, and its notched impact strength reached 4.87 kJ·m^{-2} [58].

Pittolo et al. (1986) reported the polymerization of styrene in the presence of rubber-crumb using BPO or AIBN as a free radical initiator) and mechanical properties of the blend. The rubber-crumb size was 0.3mm and the PS/rubber-crumb mass ration was from 100/0 to 80/20. Blends containing either untreated or modified rubber-crumb were prepared in a Haake internal mixer. The procedure was to melt PS pellets at 150℃ and then add the rubber-crumb. When the untreated-GTR content is increased from 0 to 20%, the tensile strength and energy to break strongly decreased from 38.83 to 15.23MPa and 297 to 108 kJ·m^{-3}, respectively, while the elongation at break slightly increased from 1.48 to 1.57%. Styrene grafting of GTR enhanced the elongation at break from 1.25 to 1.94% and the energy to break from 108 to 249 kJ·m^{-3}, respectively, compared with the PS/untreated-GTR (80/20) blend [59].

The above articles show that there is a great interest in compounding GTR with thermoplastics such as PP, PE and PS. However, mechanical properties of the resulting blends are poor due to the large GTR particle size, on the one hand, and poor interfacial adhesion between the GTR and polymers, on the other hand. The compatibilization methods developed remain inefficient.

1.3 Introduction to GTR/PS blends using a twin screw extruder

The aim of this part is to describe the blending process of a polymer with GTR in a twin screw extruder. Mechanical properties of the blends depend on their morphologies which depend on processing parameters such as screw profile, barrel temperature and screw speed.

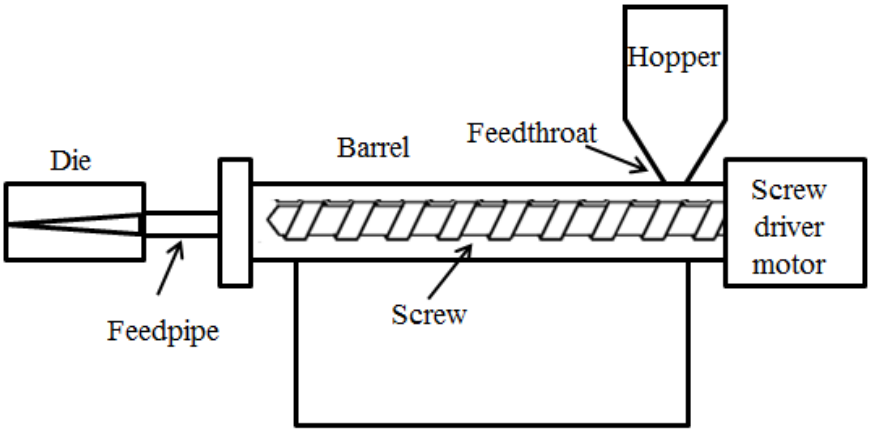

Figure 1.5 - A scheme of a screw extruder.

The main components of a screw extruder include a hopper, a barrel, a screw a screw driver motor and a die, as shown in Figure 1.5. Polymer pellets are fed from the hopper. As the pellets travel along the screw, it is subjected to friction, compression, and heated zones. Extra heat is contributed by friction taking place inside the barrel to mix the melt homogeneously. The melt enters and then exits from a die [60].

1.3.1 Screw profile

There are three possible zones in a thermoplastic screw, such as feed zone, melting zone and metering zone. It is very important to fit the screw profile to a specific system. Villmow et al. (2010) provided extrusion screws with a modular assembly of individual screw elements [61], like conveying (1 and 2), back-conveying (3), kneading (4–6), and mixing elements (7 and 8). They are shown in Figure 1.6.

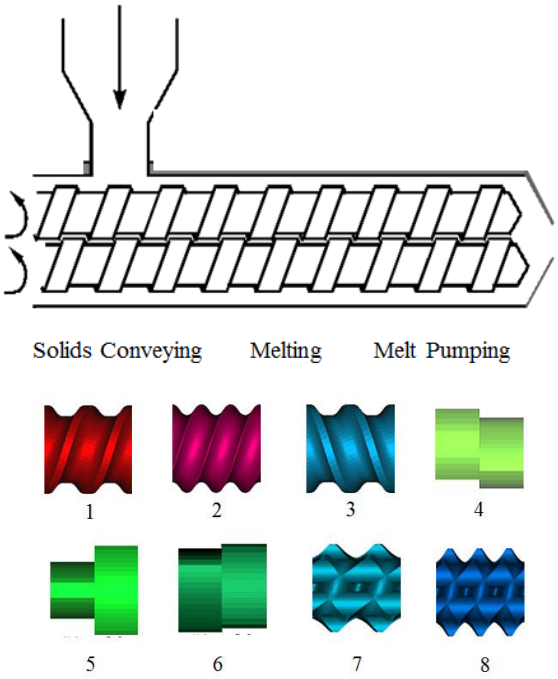

Figure 1.6 - A twin-screw extruder and screw elements [62]. Conveying elements (1 and 2), back-conveying element (3), kneading elements (4–6), mixing elements (7 and 8).

Yazdani et al. (2011) used a laboratory intermeshing co-rotating twin screw extruder to devulcanize GTR. The extruder had five heating/cooling zones and a screw diameter of 20 mm with an L/D ratio of 40. The feed rate was constant (1 kg/h) for all samples. The barrel temperature was set at three levels: 220, 250, and 280℃. The screw speeds were 30, 60, 90, and 120 rpm [62].

1.3.2 Screw speed

Shearing and stress of a twin screw extruder can influence the mechanical properties of plastic/rubber blends [60]. It can accelerate the dispersion and/or distribution of rubber particles in the plastic matrix and enhance the interfacial bonding strength between them. Furthermore, increasing screw rotation speed can not only destroy the crosslinks of rubber, but also improve the compatibility between rubber and plastic. However, a further increase in screw rotation speed may degrade PS too [63].

1.3.3 Barrel temperature

Maintaining a correct temperature level is an important consideration when blending rubber and plastics. Some variables such as pressure and friction that build up in the screw may raise the material temperature. Therefore, the heat must be monitored carefully. The cooling system like fans and water cooling can help maintain proper extrusion temperature. In general, the range of barrel temperature depends on the nature of the plastic and rubber [60]. For instance, the barrel temperature for the blending of PS and rubber ranges from 180 to 210℃. Temperatures above 240℃ can cause a loss in desired physical properties of the blends due to degradation. Temperatures below 100℃ can cause high extruded-in stress and a loss in desirable physical properties of the extruded part. Therefore, it is important to control the actual temperature of the material in the extruder [60].

1.4 Introduction to the free radical polymerization kinetics of styrene

1.4.1 Free radical polymerization mechanism of styrene

Before a kinetic model is established, the mechanism of free radical polymerization of styrene should be described first. There are four significant reactions that take place in free radical polymerization of styrene: initiation, propagation , termination and transfer.

1.4.1.1 Initiation reaction

Initiation reaction of styrene polymerization often includes the chemical initiation by the initiator and thermal initiation of styrene, the latter becoming important at temperatures above 100℃. For the chemical initiation of the free radical polymerization of styrene, Villalobos et al. (1993) [64] and Kotoulas (2003) [65] studied the polymerization of styrene using the benzoyl peroxide (BPO) and dicumyl peroxide (DCP), respectively. They measured the conversion, number and weight average molecular weights at different polymerization temperature (60-200℃), the temperature control was achieved using an oil bath. Yamazoe et al. (2001) used Near-

Infrared Spectroscopic to study the entire conversion range of free radical bulk polymerization of styrene [66]. The polymerization was maintained at 70℃for a initiator, dimethyl 2,2'azobis (isobutyrate).

For the thermal initiation of styrene, there are two kinds of initiation mechanisms. One involves two styrene molecules, first put forward by Flory et al. (1937) [67]. Bengough et al. (1978) supported Flory's theory by thermal initiation of the polymerization of styrene from 60–140℃. Mayo et al. (1943-1953) [68]–[70] and Russell et al. (1953) [71] proposed a thermal initiation mechanisms involving three styrene molecules. They deduced this mechanism from the fact that the thermal initiation rate is proportional to the monomer concentration to the power of 2.5. Pryor et al. (1970) continued to investigate the thermal free radical polymerization of styrene by computer simulations [72].

A generalized thermal initiation mechanism is described below [65]. A reversible Diels-Alder dimerization of styrene leads to 1-phenyl-1, 2, 3, 9-tetrahydronaphtalene (AH). AH with one styrene forms one styryl (MR) and one 1-phenyltetralyl radical (AR). MR and AR could further produce polymer chains. The reaction of AH with styrene makes a 'dead' trimmer (D_3).

$$2M \underset{k_{-1}}{\overset{k_1}{\rightleftharpoons}} AH \qquad (1.1)$$

$$AH + M \xrightarrow{k_2} AR + MR \qquad (1.2)$$

$$AR + M \xrightarrow{k_A} R_3 \qquad (1.3)$$

$$MR + M \xrightarrow{k_B} R_2 \qquad (1.4)$$

$$AH + M \xrightarrow{k_C} D_3 \qquad (1.5)$$

1.4.1.2 Propagation reaction

Propagation steps involve addition of a radical to a double bond. The successive additions may be represented by

$$R_1 + M \xrightarrow{k_p} R_2 \qquad (1.6)$$

$$R_n + M \xrightarrow{k_p} R_{n+1} \quad (1.7)$$

where k_p is the rate constant for propagation. Propagation with chain growth to high polymer proportions takes place very rapidly.

1.4.1.3 Termination reaction

Termination reactions can be combination termination or disproportionation termination or both. Kotoulas et al. (2003) [65] and Manaresi et al. (1975) [73] established the kinetic model without using the disproportionation termination. Huang et al. (1995) [74] ignored the termination reaction including primary radical, CTA radical, monomer radical, backbone polymer radical and initiator radical. This is because each of these concentrations is several orders of magnitude lower than the polymeric radical species [74].

1.4.1.4 Chain Transfer reaction

Chain transfer is a polymerization reaction by which the activity of a growing polymer chain is transferred to another molecule. The average molecular weight of the final polymer can be reduced by chain transfer reactions. In general, the chain transfer reactions can be divided into transfer to monomer, polymer, chain transfer agent (CTA) and solvent. The chain-transfer constants for initiator, monomer and solvent are abbreviated by CI, CM and CS. Ignoring chain transfer to polymer does not present a difficulty in obtaining precise values of CI, CM, and CS, since these are determined from data at low conversions [75].

1.4.2 Model of the polymerization kinetics of styrene

1.4.2.1 The development of kinetics model of polymerization of styrene

Prior to the 1970s, some of the basic works of modeling of radical polymerization of styrene were done by Hamielec (1967) [71] and Hui (1972) [72]. They found that a model of third order of the initiation rate respect to the monomer concentration was better than that of second order. Kotoulas (2003) [65] and Kiparissides et al. (1992) [78] showed that a mathematical model accounting for both chemical and thermal radical initiation could be used for temperatures ranging from

60 to 200℃. When the system becomes viscous, the diffusion-controlled phenomena may come into play in the polymerization process. The diffusion-controlled phenomena of the cage, glass and gel effects have been related to the initiation, propagation and termination reactions [65]. Diffusion controlled reactions of termination, propagation and initiation were described. However, they did show the critical points of different diffusion effects (gel effect, glass effect). O'Neil et al. (1998) [79] established a model with focus on the description of the onset of the gel effect. Huang et al. (1990) [80] developed a kinetic model which took into account the gel and glass effects via DSC measurements. Cavin et al. (2000) [81] proposed a model to describe the conversion, gel effect and the number average molecular weight.

More recently, Woloszyn et al. (2013) [82], [83] developed a mathematical model of thermal radical polymerization of styrene. They studied the chemically initiated free radical polymerization of styrene using DCP, at the temperatures ranging from 100 to 150℃ as well as using BPO, at temperatures ranging from 70 to 90℃. A generation and consumption of styrene adduct could be calculated by their model.

This section deals specifically with kinetic models for the graft polymerization of styrene onto rubber. Manaresi et al. (1975) [73] showed the graft polymerization of styrene solutions of polybutadiene (2-9 wt%) containing dicumyl peroxide (0.1-0.3 wt%) as initiator at 100℃. Graft efficiency was found to be independent of the peroxide concentration, but increased with the rubber content. The graft efficiency was given by Eq 1.8.

$$E = \frac{10^4 \times PR}{C(100-P)(100-R)} \tag{1.8}$$

where P was the PS (wt%) in the grafted fraction. R was the polybutadiene (wt%) in the initial solution.

Capek et al. (1992) [84] studied the copolymerization of styrene terminated poly(oxyethy1ene) (St-PEG) macromonomers and styrene, initiated by BPO at 60℃. The ratios of the rate constants for propagation and termination (k_p/k_t=0.5) for polymerization and copolymerization of St-PEG were one order of magnitude higher than that for styrene. Yenal'ev et al. (1974) [85] worked on the mechanism of styrene-rubber graft copolymerization by the bulk suspension method using BPO and tert-

butyl perbenzoate (TBPB) as an initiator. Three stages were found when styrene was graft-copolymerized with rubber, i.e. up to 40-55% polymerization in which there is a continuous increase in the quantity of graft copolymer, from 40-55% to 94-98% in which there is hardly any grafting, and the final stage in which there is a 1.7-2.3 fold increase of the amount of graft copolymer.

The whole polymerization process can be described by several stages using a free volume theory [82], [83]. In the first stage the viscosity is low, the free volume is large and molecules diffuse fast. Thus the reaction rate is chemically controlled. The second stage is the termination diffusion controlled. Increasing the monomer conversion and decreasing the free volume significantly reduce the termination rate. As a result, the polymerization rate increases dramatically. In the third stage, small molecules diffuse in a significantly reduced pace, and the propagation becomes diffusion controlled. The polymerization rate decreases. In the final stage, the initiator efficiency is reduced, when the viscosity is increased to a high enough level to inhibit diffusion of initiator radicals.

1.4.2.2 Three Stage Polymerization Model

A Three Stage Polymerization Model (TSPM) was developed by Qin et al. (2002) [86]–[88]. The model divides the polymerization process into three stages: low conversion stage, gel effect stage and glass effect stage. However, they did not provide experimental details and molecular weights. They also studied the kinetics of bulk thermal polymerization of styrene and found that the critical conversion between low conversion stage and gel effect stage is equal to 0.5.

An analytical description of the equations of this model are given in Appendix I.

1.4.2.3 Values of constants of k_d ,k_p and k_t.

(1) Values of constant k_d

Various initiators are used at different temperatures, depending on their rates of decomposition [75]. Most initiators are used at temperatures where k_d is usually 10^-

^{4}-10^{-6} s^{-1}. For example, azobisisobutyronitrile (AIBN) is commonly used at 50-70℃, benzoyl peroxide at 80-95℃, and dicumyl or di-t-butyl peroxide at 120-140℃ [75]. The differences in the decomposition rates of various initiators can be conveniently expressed in terms of the initiator half-life ($t_{1/2}$) defined as the time for the concentration of I to decrease to one half its original value [75]. The half-life of the initiator is an important parameter to choose the appropriate initiator for the polymerization. To calculate the half-life of initiator, we should use the formula below:

$$t_{1/2} = \frac{\ln 2}{k_d} = 0.693/\ k_d \qquad (1.9)$$

by setting $\frac{[I]}{[I]_0} = 0.5$

Table 1.1 lists the initiator half-lives for several common initiators at various temperatures [89].

Table 1.1 - Lists of the initiator half-lives for AIBN, BPO and DCP at various temperatures calculated by the formula (1.9).

	Half-life at									
Initiator	70℃	80℃	85℃	90℃	95℃	100℃	120℃	125℃	130℃	135℃
AIBN	4.5h	1.3h	—	22min	—	7.2min	—	—	—	—
BPO	—	3.3h	1.8h	1.0h	36min	—	—	—	—	—
DCP	—	—	—	—	—	—	5.8h	3.1h	1.7h	1.0h

From Table 1.1, we can obtain the $[I]/[I]_0$ as a function of reaction time at different temperatures for AIBN, BPO and DCP (see Figure 1.7).

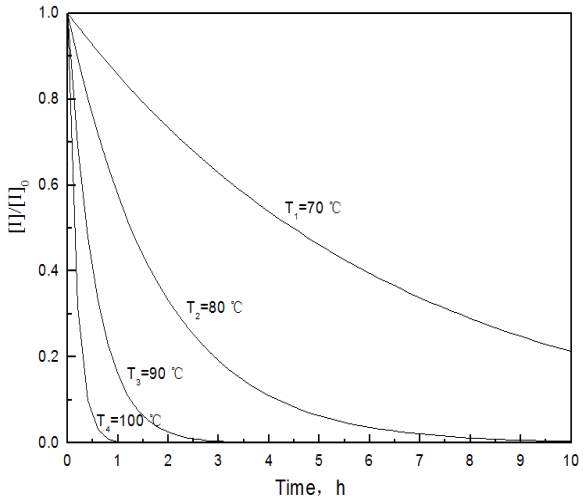

(AIBN)

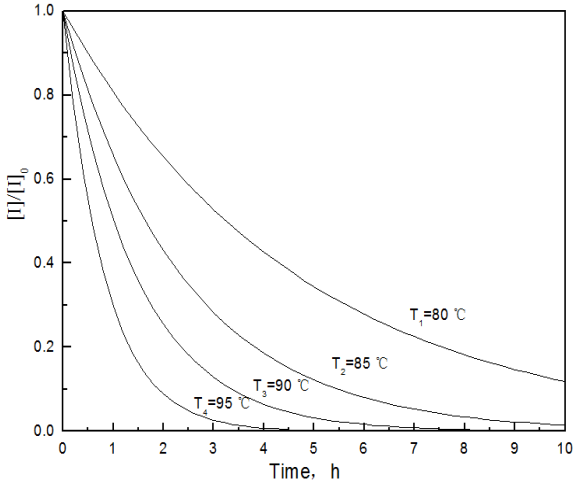

(BPO)

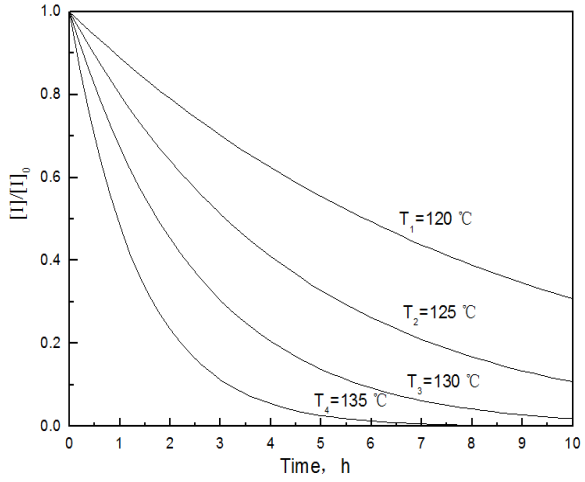

(DCP)

Figure 1.7 - $[I]/[I]_0$ as a function of reaction time at different temperatures for AIBN, BPO and DCP.

In order to reduce the reaction time of the graft polymerization of styrene onto GTR, we use a mixture of free radical initiators. In this work, we use a mixture of BPO and DCP. BPO is favored over AIBN because it was reported that the former has a higher grafting efficiency of styrene onto GTR than the latter [16, 19]. This is because of a competition between the homo and grafted PS reactions. The competition was determined by the ratio of free radical and GTR radical which was lower in the case of BPO compared to AIBN. DCP has a higher decomposition temperature than BPO. The polymerization can be carried out at a temperature ranging from 70 to 90℃ for a certain period of time and then the temperature is raised to a higher value at which DCP starts to decompose [20].

(2) Values of constants k_p and k_t

The accuracy of the constants k_p and k_t is very important for the kinetic model. Techniques have been developed in order to acquire accurate measurements of the values of k_p and k_t. Buback et al. (1995) [90] and Beuermann et al. (2002) [91] compared the values of k_p between different methods (electron spin resonance spectroscopy method, pulsed-laser-initiated polymerization). Pulsed-laser-initiated polymerization turned out to be the most accurate technique for measuring k_p. Yamazoe et al. (2001) [92] used electron spin resonance and near-infrared spectroscopy and found that the propagation rate constant as a function of monomer conversion exhibited a marked dependence on the initiator concentration at high monomer conversion.

Zetterlund et al. (2001) [93] concluded that the k_t exhibits a significant dependence on the initiator concentration, a higher initiator concentration resulting in a higher k_t. They observed that k_t increased rapidly above a conversion of about 0.6 and started decreasing above a conversion of about 0.9. Tokareva et al. (1990) [94] studied the polymerization of vinyl monomers in three-dimensional networks. The chain propagation rate constants for the bulk polymerization of styrene and for the polymerization in the three-dimensional network were identical. Moreover, the rate constants for the termination of macroradicals in the three-dimensional network were 3-4 orders less than those for the bulk polymerization.

Table 1.2 - Literature results for k_d, k_p and k_t.

Rate constant	Value of constant	k_0	E	Temp	Ref.
k_{dBPO}		1×10^{13}	28.4	100	[80]
		6.37×10^{13}	29.7		[95]
		4.59×10^{13}	29.25		[96]
		2.88×10^{12}	30.39		[82]
		6.94×10^{13}	29.2		[82]
		1.7×10^{15}	29.995		[82]
		2.29×10^{14}	27.22		[82]
		1.44×10^{13}	29.21		[82]
		3.8×10^{12}	27.2		[64]
k_{dDCP}		9.24×10^{15}	36.54		[82]
		3.06×10^{12}	30.01		[82]
		1.0×10^{16}	36.567	30–100	[97]
		9.2×10^{15}	36.6	120-150	[65]
k_1/k_{-1}		6.4×10^{4}	12.9		[65]
k_{-1}	7.3×10^{-7}		22.3	101	[82]
k_2	8.46×10^{-5}		22.3	120	[82]
		1.63×10^{6}			[65]
k_A		1.1×10^{7}	7.1		[65]
k_B		1.1×10^{7}	7.1		[65]
k_C		3.93×10^{4}	21.346		[65]
k_p	160		7.528	40	[91]
	106		6.573	30	[91]
		7.138×10^{9}	11.159	60-80	[80]
		1.09×10^{7}	7.051		[79]
		4.26×10^{7}	7.74		[95]
		7.47×10^{7}	8.236		[96]
		1.1×10^{8}	6.568		[96]
	344		7.767	60	[82]
		1.02×10^{7}	7.068		[64]
		1.62×10^{8}	8.628	100-200	[98]
		1.05×10^{7}	7.051		[77]
		1.05×10^{7}	7.07	90-100	[99]
		1.1×10^{7}	7.1		[65]
k_{fm}		1.02×10^{7}	13.45		[64]
		7.67×10^{7}	14.435		[98]
		2.31×10^{6}	12.67	100-200	[77]
		3.86×10^{6}	11.45	90-100	[99]
		2.31×10^{6}	12.6		[65]
k_{fa}	2.31×10^{2}		23.3	60	[82]
		1.22×10^{7}	30.8		[65]
k_S	69.9		30.1	155	[82]
k_{tc}		1.25×10^{9}			[95]
		2.67×10^{8}	2.084		[96]
		1.26×10^{9}	1.67		[64]
		1.02×10^{11}	4.46		[98]
		1.25×10^{9}	1.67×10^{3}	100-200	[77]

		1.25×10^{9}	1.68×10^{3}	90-100	[99]
k_{td}	1.59×10^{7}		1.496	60	[82]
k_{tpr}	1.11×10^{8}		1.496	60	[82]

Units (*kcal, mol, °C, L, s*)

1.4.3 Literature on the graft polymerization of styrene onto rubber

In the following Table 1.3, an overview of the different kinetic schemes that have been adopted by several authors, in terms of their model developments, is presented.

Table 1. 3 - Kinetic models from the literature. (+) reactions are taken into account, (–) reactions are not taken into account.

Kinetic model scheme	Manaresi 1975[73]	Huang 1995 [74]	Kiparissides 2003[65]	Woloszyn 2013[82]
Initiation				
Chemical Initiation:	+	+	+	+
Decomposition of Initiator:				
$I \xrightarrow{k_d * f} 2\,R^*$				
$R^* + M \xrightarrow{k_I} RM_1^*$				
Thermal Initiation:	+	–	+	+
$2M \underset{k_{-1}}{\overset{k_1}{\leftrightarrow}} AH$				
$AH + M \xrightarrow{k_2} \dot{A} + \dot{M}$				
$\dot{A} + M \xrightarrow{k_A} RM_1^*$				
$\dot{M} + M \xrightarrow{k_B} RM_1^*$				
$AH + M \xrightarrow{k_C}$ trimmers				
Graft site initiation :	+	+	–	–
GTR radical production:				
$R^* + GTR \xrightarrow{ki_{R*}} GTR_1^* + RH$				
$RM^* + GTR \xrightarrow{ki_{M*}} GTR_1^* + MH$				
$GTR^* + GTR \xrightarrow{ki_{GTR*}} GTR_1^* + GTRH$				
Initiation:				
$GTR_1^* + M \xrightarrow{k_I} GTRM_1^*$				

Initiator Mid-Chain β-Scission:	−	−	−	+
$R^* + M_{n+m} \xrightarrow{k_I} M_n + M_m^*$				
$GTR_1^* + M \xrightarrow{k_I} GTRM_1^*$				
Propagation				
Propagation of homo-polymerization:	+	+	+	+
$RM_1^* + M \xrightarrow{kp} RM_2^*$				
$RM_n^* + M \xrightarrow{kp} RM_{n+1}^*$				
Propagation of graft-polymerization:	+	+	−	−
$GTRM_1^* + M \xrightarrow{kp} GTRM_2^*$				
$GTRM_n^* + M \xrightarrow{kp} GTRM_{n+1}^*$				
Chain Transfer Reactions	+	+	+	−
Chain transfer to monomer:	+	−	+	+
$RM_n^* + M \xrightarrow{k_{fM}} M_nH + RM_1^*$				
$GTRM_n^* + M \xrightarrow{k_{fM}} GTRM_n + RM_1^*$				
Chain transfer to GTR：	+	+	−	−
$RM_n^* + GTR \xrightarrow{k_{fGTR}} M_nH + GTR_1^*$				
$GTRM_n^* + GTR \xrightarrow{k_{fGTR}} GTRM_n + GTR_1^*$				
Chain transfer to graft-polymer:	−	+	−	−
$RM_n^* + GTRM_n \xrightarrow{k_{fGTRMn}} M_nH + GTRM_n^*$				
$GTRM_n^* + GTRM_n \xrightarrow{K_{fGTRMn}} GTRM_n + GTRM_n^*$				
Chain transfer to AH (adduct):	−	−	−	+
$RM_n^* + AH \xrightarrow{k_{fAH}} RM_n + \dot{A}$				
$GTRM_n^* + AH \xrightarrow{k_{fAH}} GTRM_n + \dot{A}$				
Termination				
Termination by combination:	+	+	+	+
$RM_n^* + RM_m^* \xrightarrow{k_{tl}} M_{n+m}$				
$GTRM_n^* + GTRM_m^* \xrightarrow{k_{tl}} GTRM_{n+m}GTR$				
$GTRM_n^* + RM_m^* \xrightarrow{k_{tl}} GTRM_{n+m}$				

Termination by disproportionation:		−	−	−	+
$RM_n^* + RM_m^* \xrightarrow{k_{t2}} M_n + M_m$					
$GTRM_n^* + GTRM_m^* \xrightarrow{k_{t2}} GTRM_n + GTRM_m$					
$GTRM_n^* + RM_m^* \xrightarrow{k_{t2}} GTRM_n + M_m$					
Cross-terminations:		+	−	−	−
$GTR^* + GTRM_n^* \xrightarrow{k_{t3}} GTRM_nGTR$					
$GTR^* + RM_n^* \xrightarrow{k_{t3}} GTRM_n$					
Terminations between GTR radicals:		+	−	−	−
$GTR^* + GTR^* \xrightarrow{k_{t4}} GTR\text{-}GTR$					
Terminations by primary radicals:		−	−	−	+
$RM_n^* + R^* \xrightarrow{k_{t5}} RM_n$					
$GTRM_n^* + R^* \xrightarrow{k_{t5}} GTRM_n$					

Although many articles have been published concerning the modeling of bulk or suspension polymerization of styrene (Table 1.3), to the best of our knowledge there is no theoretical study on the bulk polymerization of styrene onto GTR. The presence of GTR in the growing and dead polymers can influence the initiation, propagation, chain transfer and termination reaction during the course of polymerization. Thus, the presence of the GTR further complicates the polymerization kinetics.

1.5 Introduction Artificial Neural Networks (ANNs)

1.5.1 Artificial Neural Networks (ANNs)

An Artificial Neural Network (ANN) is a highly complicated nonlinear dynamics system, consisting of processors (called nodes) which widely connect to others to form a complex network system [100]. The nodes, containing a small

amount of local memory, are connected by interconnections. The strength of these interconnections is determined by the weight associated with the neurons. An ANN can be properly trained, on the basis of a series of measured inputs and their respective responses, in order to provide accurate simulated (i.e., theoretical) responses within the range of the input measurements domain.

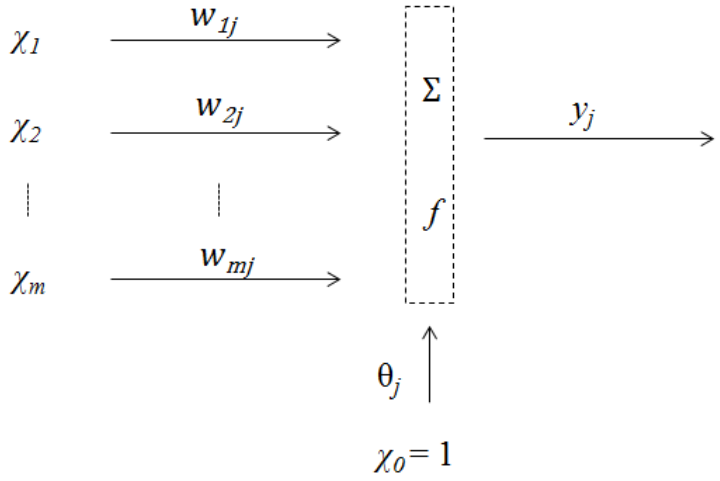

Figure 1.8 - Diagram of one neuron (node).

In general, the net input to each node (Figure 1.8) is calculated as shown in Eq 1.10 and Eq 1.11 [101]:

$$s_j = \sum_{i=1}^{m} w_{ij}\, x_i - \theta_j \tag{1.10}$$

$$y_j = f(s_j) \tag{1.11}$$

where s_j is the net input of layer j, w_{ij} is the weight corresponding to the node i of layer j, m is the total number of nodes in the layer j, θ_j is a threshold value (bias) assigned to layer j, and x_i is the input of node i, y_j is the net output of the layer. f is a nonlinear transfer function assigned to each layer in the network.

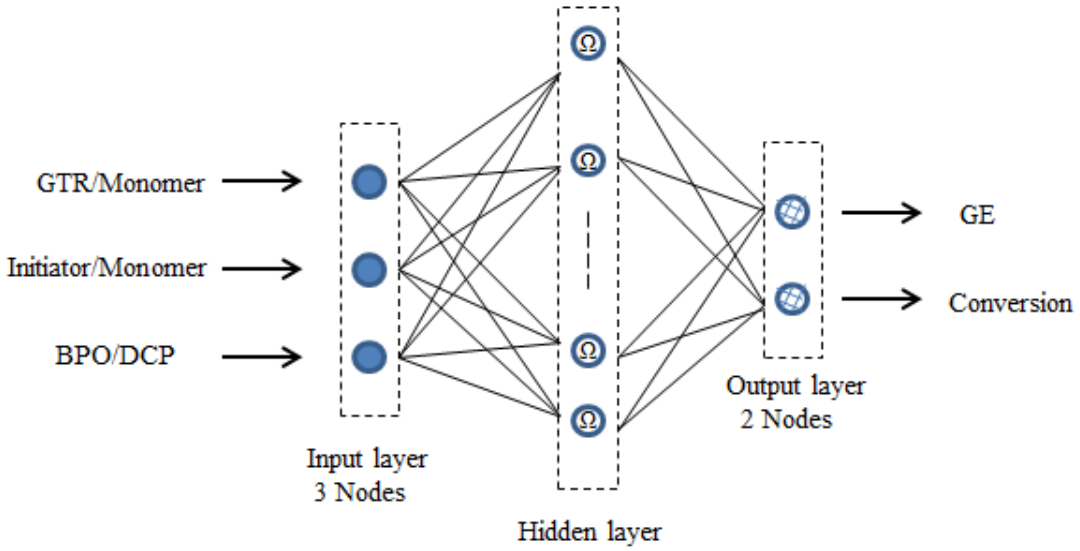

Figure 1.9- Architecture of neural network model.

The topology of an ANN is specified by the number of layers, number of neurons in the hidden layer(s) and the nature of the transfer functions (Figure 1.9). In this work, a three-layered feed-forward back propagation ANN was developed containing (3 : N : 1) neurons in the input, hidden and an output layers, respectively. The number of neurons of the input layer (independent variables) correspond to the number of operational parameters of the process, namely the molar ratios of GTR to monomer, initiator to monomer and BPO to DCP. The number of neurons in the output layer (dependent variable) corresponds always to the response of the model. In the present work, to different ANN models where developed to simulate the graft efficiency and conversion of the process. The hidden layer(s) of each model can contain a large number of neurons [102]. The number of hidden layers and neurons of a network largely affect the accuracy of the developed model. Their number must be sufficient to allow a required "flexibility" of the model but not too high in order to avoid "overfitting" phenomena [103].

There are four important aspects that must be determined in the design procedure of ANN model as follows: [104]

-Selection of database,

- Selection of model architecture,

- Model training and testing

- Model validation

1.5.2 Back Propagation network

Back propagation (BP) networks have the preliminary ability of adaptive and self–organization. The network can have different functions with a different learning style. It even has the ability to innovate. A feed-forward back propagation network uses a learning mechanism that transfers the feed signal forward from the input layer to the output layer. The output signal is then compared to the error with the known targets, reversed and sent back to the input layer in order to adjust the weights and biases until the output error reduces to an acceptable level [105].

Learning Rate (LR) is the training parameter that controls the size of weight and bias changes in learning of the training algorithm. For nonlinear system, select the appropriate learning rate is very important. The learning rate, applies a greater or lesser portion of the respective adjustment to the old weight. If the learning rate is set to a large value, then it may lead to the training process is not stable. However, if the learning rate is too small, it will cause the training time to become too long.

Conclusions

Rubber is a common material, mainly used in the automotive industry, which exists in abundance in the large quantities of waste tire rubber being produced every year. The cross-linked structure of waste tire rubber (also known as ground tire rubber, GTR) along with the presence of stabilizers and other additives, inhibit its degradation process thus resulting in serious environment issues.

A solution to this problem is the re-use of GTR particles in different applications, such as fillers in thermoplastics, elastomers and thermosets. However, the incorporation of GTR particles into a number of polymer matrices significantly impairs the mechanical properties of the resulting material, even at low rubber content, due to poor adhesion issues between the two materials as well as to the relatively large particle size of GTR. It can be improved the interfacial adhesion between the polymer matrix (in this case polystyrene, PS) and GTR via in-situ free-radical grafting polymerization of styrene onto the rubber particles. The objective of this work is to study both experimentally and by modeling the free-radical grafting polymerization of styrene inside /onto the cross-linked GTR particles.

Chapter 2 Experimental

GTR particles have to be modified when they are used as fillers in thermoplastics, elastomers and thermosets. Both the big size of the GTR particles and their bad adhesion with polymer matrices pose a big problem, as outlined in the introduction.

When styrene is added to GTR particles, it can be located inside and/or outside them, depending on the styrene/GTR ratio. In fact, GTR particles are able to absorb a certain amount of styrene. As such, when the styrene/GTR ratio is less than a critical threshold (it is approximately 2, namely, GTR particles are able to absorb twice their mass), styrene is only located in GTR particles, namely, GTR particles are swollen by styrene but remain relatively "dry". When the styrene/GTR ratio exceeds that critical threshold, the excess of styrene will stay outside GTR particles.

In this work, we keep the styrene/GTR ratio below 2 so that styrene is completely located inside GTR particles. This way, styrene is polymerized only inside individual three-dimensionally crosslinked GTR particles only. This is different from the literature works in which the styrene/GTR ratio is so big that the amount of styrene cannot be completely absorbed by GTR. As such, the polymerization of styrene takes place both inside and outside GTR particles.

When styrene is polymerized inside an individual GTR particle, there are two types of polymerization. One is the polymerization of styrene itself leading to PS chains which are not linked to the GTR particle. These PS chains are called free PS. The other is the polymerization of styrene from the rubber chains and the resulting PS chains are attached to the rubber ones. These PS chains are designated as GTR-g-PS. The resulting material is GTR particles inside which there are free PS and GTR-g-PS. In what follows, this material is designated as PS/GTR-g-PS.

One of the main advantages of our approach is that it allows minimizing the amount of free PS in the PS/GTR-g-PS while maximizing the amount of GTR-g-PS. Another advantage is that a minimum of free PS present in the PS/GTR-g-PS together with a maximum of GTR-g-PS allows recycling a maximum of GTR with best

properties, especially impact strength. As a matter of fact, it is expected that the lower the PS/GTR-g-PS ratio, the higher the compatibility between the free PS and the GTR-g-PS, and the higher the impact strength.

This work attempts to search for optimal conditions under which the polymerization of styrene inside GTR particles leads to a minimum of free PS and a maximum of GTR-g-PS while maximizing the conversion of styrene into polymers.

2.1 Experimental Procedure

2.1.1 Materials

GTR particles were kindly supplied by REGENE Company. They were obtained by a cryogenic grinding process. According to the supplier, the maximum particle diameter was 0.8mm or 800μm. Compositions of GTR and elastomers were shown in Table 2.1 and Table 2.2, respectively. Styrene was purchased from Sigma-Aldrich, with a purity of ≥ 99 %. Benzoyl peroxide (BPO), dicumyl peroxide (DCP) and Hydroquinone (HQ) were purchased from Sigma-Aldrich, with a purity of 99 %. Chloroform was the experimental grade and was purchased from Carlo Erra Reagents Company. Commercial-PS (N1840 GPPS) was purchased from EDISTIR.

Table 2.1 - Compositions of GTR (% by weight).

GTR	
charge	36%
organic	64%
elastomer	56%

Table 2.2 - Compositions of elastomers (% by weight).

Elastomers	
NR(Natural rubber)	30%
SBR(styrene-butadiene rubber)	40%
BR (butadiene rubber)	20%
IIR/NBR (butyl-and nitrile butadiene rubber)	10%

2.1.2 Experimental steps

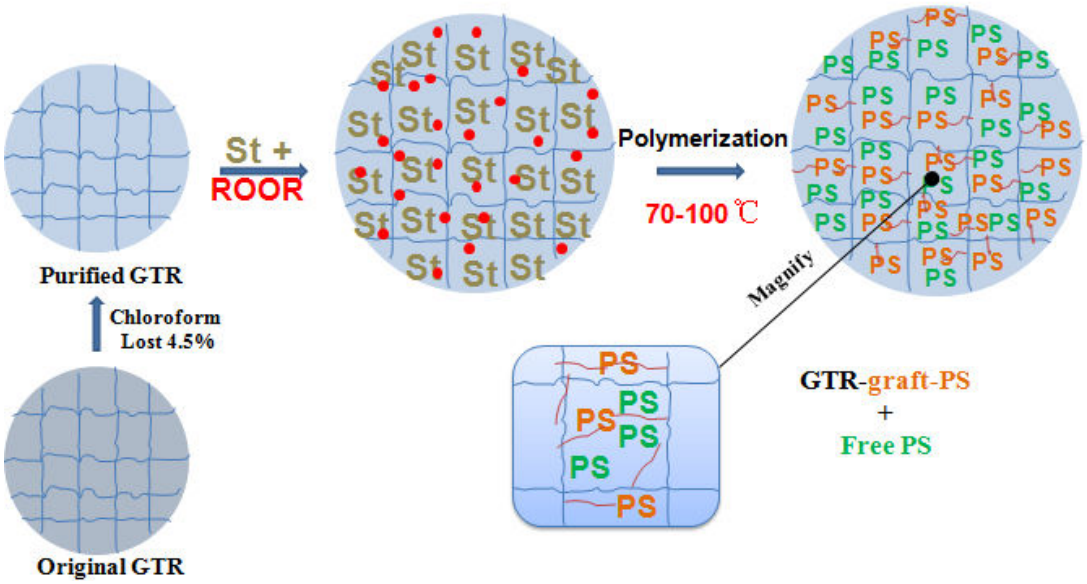

Figure 2.1- A scheme of the polymerization of styrene inside a single GTR particle.

The polymerization of styrene inside cross-linked GTR particles was carried out following the following steps (see Figure 2.1):

1. The original GTR particles were added to a beaker with chloroform in order to extract from the GTR particles plasticizing oils and other types of additives used during the rubber vulcanizing process for tire production. Then, they were stirred under a magnetic bar for about 6 days. Chloroform was changed every 2 days. Finally, they were filtered and dried by a rotary evaporator till a constant weight. The loss in weight was of the order of 4 to 5%.

2. A free radical initiator was added to styrene in a beaker and the solution was stirred for about 30min at the room temperature.

3. Purified GTR particles in step 1 were charged to a stainless steel reactor of 1 liter, 19 cm high, 15 cm diameter and 0.1143m^2 surface area (see Figure 2.3), followed by the solution of styrene and the initiator in a drop-wise manner in order to ensure homogeneous absorption of the styrene and initiator solution by the GTR particles. The heating and cooling of the reactor were controlled by an oil bath.

4. The system was brought to a given temperature (between 70 to 100℃) and the polymerization of styrene inside the GTR particles proceeded for a chosen period of time. More specifically, the polymerization system was stirred and purged with nitrogen. The temperature was 70℃for 3h, 80℃for 3h, 90℃for2h and 100℃ for 2h.

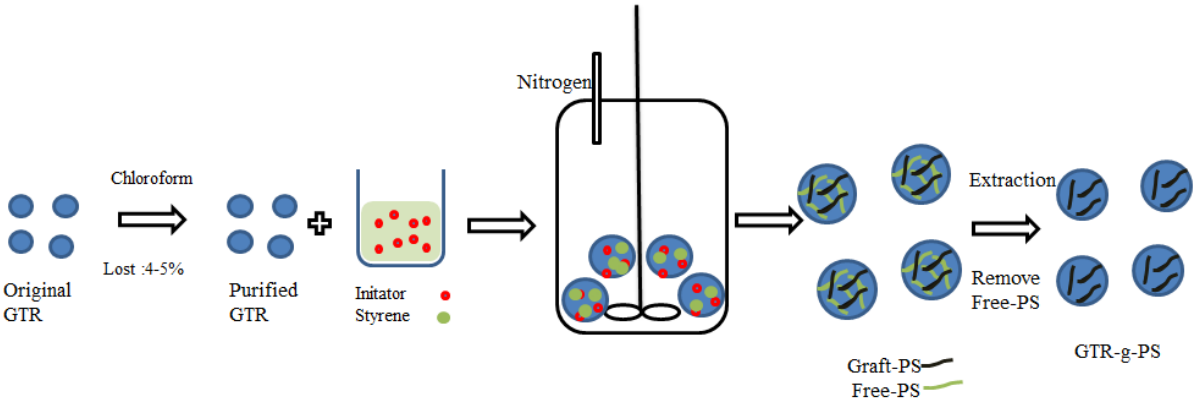

Figure 2.2 - A process of the polymerization of styrene inside GTR particles.

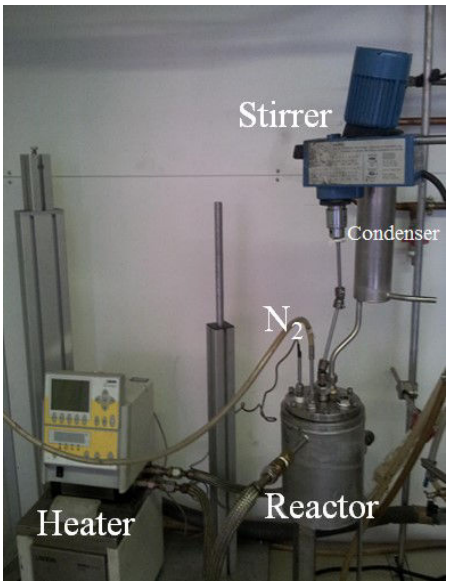

Figure 2.3 - Photo of reactor equipment of graft polymerization of styrene inside GTR particles

The polymerization of styrene onto GTR particles was also studied. The experimental steps were mostly similar with the polymerization of styrene inside cross-linked GTR particles. The only differences were the temperature and reaction time. The temperature of the polymerization of styrene onto GTR particles was 90℃

for 2.5 hours and was then increased to 120℃ with a speed of (2℃/min). The polymerization ended after 2.5 hours at 120℃.

2.1.3 Soxhlet extraction procedure

The Soxhlet extractor is shown in Figure 2.4. Chloroform was used for the extraction. The extraction lasted 6 hours under reflux. What is extracted is free PS and what remains in the thimble is GTR or GTR-g-PS.

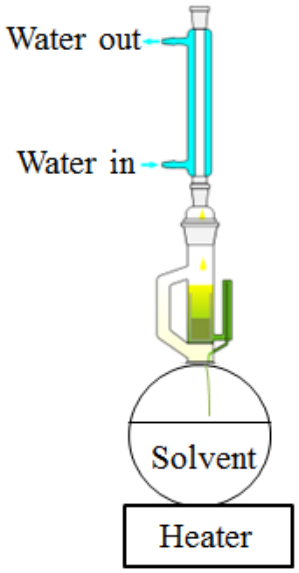

Figure 2.4 - Schematic diagram.

2.1.4 Solvent selection for GTR particle swelling

In order to increase the amount of the initiator inside the GTR particles, it is important to select a suitable solvent to swell them. Two solvents (xylene and chloroform were tested.

The GTR were put into one of the solvents (xylene or chloroform) in a beaker. The swelling process lasted 7 days at the room temperature. It was observed that the GTR did not swell much in xylene but swelled significantly in chloroform. This indicates that chloroform is a better solvent for GTR particles.

2.1.5 GTR particle size measurement procedure

In order to understand how much styrene may swell GTR particles, the size of GTR particles in different amounts of styrene was measured. For that purpose, purified GTR particles were vacuum dried at room temperature for at least 24h. They were dropped in different amounts of styrene taken in diffusion bottles and kept in a thermostatically controlled oven for 12h. Styrene swollen samples were taken out at constant time intervals and quickly put onto a microscope slide and took photos on an electronic microscope in 30s for repeating several times. The error associated with the evaporation of styrene was negligible. For each sample, the diameters of at least 150 GTR particles were measured.

Table 2.3 - Particle sizes of the original GTR, purified GTR and GTR/styrene particles by an optical microscope (mm).

Original GTR	Purified GTR	GTR/St		
		1/1	1/2	1/4
0.551±0.087	0.546±0.098	0.699±0.122	1.031±0.127	1.036±0.101

Table 2.3 shows the diameters of the original GTR, purified GTR and GTR/styrene. As expected, the diameter of the GTR particles increases with increasing amount of styrene. Those of GTR/styrene for 1/2 and 1/4 are similar, indicating that GTR/styrene (1/2) already reaches the upper absorption limit of GTR toward styrene. In other words, GTR particles are able to absorb styrene twice their weight. This is the basis on which we change the GTR/styrene ratio for the polymerization of styrene inside GTR particles.

2.1.6 Conversion measurement procedure

The conversion of monomer was measured by a gravimetric method. Samples were taken from the reactor and weighed. A known amount of hydroquinone (HQ)

was added in to stop the polymerization. Then they were put into a Halogen Moisture Analyzer and the temperature was raised to 170℃ and were kept at this temperature for 10 min. The residual monomer could completely evaporate and the remaining material was composed of free PS, GTR-g-PS and HQ. At least three samples were taken at each measurement point.

2.1.7 Grafting extent measurement procedure

The grafting efficiency (GE) is defined as the ratio between the amount of grafted PS and that of the total PS (grafted PS + free PS). Samples taken from the reactor were put in chloroform to measure the grafting efficiency of the polymerization of styrene inside GTR particles. Free PS and HQ are soluble in chloroform, while GTR and/or GTR-g-PS are not soluble in it. After at least four days during which the samples were shaken many times, the solvent was removed using filter paper. The free PS and HQ were in the solvent, and the non-soluble portion of in the filer paper was GTR or GTR-g-PS.

2.2 Characterization Methods

2.2.1 Scanning Electron Microscopy (SEM)

A scanning electron microscope of type JEOL 6490LV was used to observe the morphologies of GTR or GTR-g-PS particles and to analyze their elements by energy dispersive spectrometer (EDS). Prior to the SEM observation, samples were fractured in liquid nitrogen and fractured surfaces were sputtered with gold. During the experiment, the acceleration voltage of electrons was 8kV.

2.2.2 Fourier Transform Infrared Spectroscopy (FTIR)

GTR or GTR-g-PS samples were mixed with KBr power and grinded together. They were then pressed into disks using a hydraulic press. Infrared spectra of the

disks were recorded by transmission using Bruker Tensor 27. The number of scans was 64 and the wavelength ranged from 600 to 4000cm^{-1}.

2.2.3 Gel Permeation Chromatography (GPC)

GPC of type Viscotek GPC was employed to measure the number average molecular masses (M_n) and mass average ones (M_w) using PS standards. The polydispersity index (PDI) is defined as M_w/M_n.

Polymer samples were dissolved in 0.5% solutions in THF and filtered through 0.45 mm filters prior to injection. THF was used as the eluent at a flow rate of 1.0 mL/min.

2.2.4 Differential Scanning Calorimetry analysis (DSC)

The DSC of type DSC 1 Mettler Toledo STAR System was used. [18] Samples were inserted in the apparatus at room temperature and immediately heated to 200℃ at a rate of 40℃ min^{-1} and kept for 1 min at this temperature in order to remove the volatile impurities. The samples were quenched to -60℃ at a rate of 20℃ min^{-1}, and then, were quenched to -90℃ at a rate of 5℃ min^{-1} and kept for 4 min at this temperature in order to stabilize the test. The glass transition temperature of each sample was taken as the midpoint of the step in the DSC trace [19].

2.2.5 Thermogravimetric analysis (TGA)

The thermogravimetric analysis (TGA) can track the degradation of a product according to the variation of temperature in a given atmosphere. A nacelle containing a sample is placed in an oven that can be maintained under vacuum or be swept away by a carrier gas and control the total flow rate. The experiment conditions for TG (TGA Mettler Toledo STAR System) were as follows: temperature range room

temperature to 750℃ [14]; heating rate, 15℃ min^{-1}. The thermal degradation of the powder was under nitrogen flow, the flow rate was 50 ml min^{-1} of nitrogen [20-21].

2.2.6 Particle Size Distribution (PSD) by Malvern Mastersizer

The size of the GTR or GTR-g-PS particles obtained after polymerization and extrusion was measured directly using the light diffraction with a Mastersizer 2000 from Malvern Instruments. This device was responsive to the volume of the particles and could determine the size distribution of particles between 0.02 microns to 2000 microns.

2.2.7 Mechanical Testing

A mini-injection molding machine DSM (Figure 2.5) was used to mold specimens for impact testing. A polymer in the molten state is pushed into a mold where it is cooled to the desired shape. The sleeve of the injection molding machine can be fed directly from the microcompounder DSM to inject specimens from molten polymer.

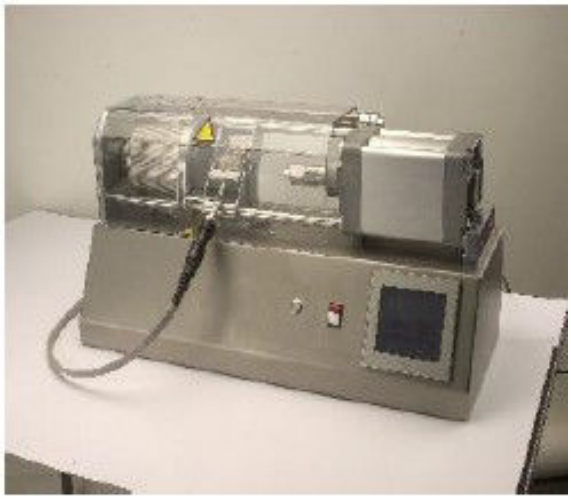

Figure 2.5 - Mini-injection molding.

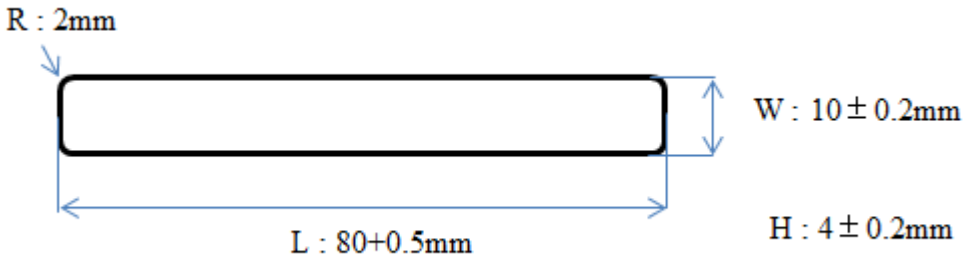

Figure 2.6 - Injection molding of specimens for impact testing.

Izod impact tests were performed at room temperature with an instrument CEAST Resil Impactor 6967. First, samples were mixed in a microcompounder (DSM Explore) for 30 min at 180℃. Secondly, they were injection molded into specimens (length=80+0.5mm, width =10±0.2mm and height= 4±0.2mm) (Figure 2.6) The pressure of this inject machine was 7.0 bar and a holding time was 30 seconds. The temperature profile was 80-170-160-150-70℃ and the mold temperature was 60°C. At least five specimens were tested for each sample to get an average value.

2.3 Extrusion of PS/GTR blends

2.3.1 Screw profile

The twin screw extruder used was of type PTW 24 (Figure 2.7) with a screw diameter of 24cm and a length-to-diameter ratio of 40 (Figure 2.8). The goal was to decrease the size of the GTR particles as much as possible, requiring therefore many kneading zones, each with several kneading elements. More specifically, the screw was composed of 4 kneading zones and each consisted of 5 kneading discs with a positive (90°) staggering angle, 2 kneading discs with a negative (-30°) staggering angle, 1 reverse conveying element, and 3 kneading discs with a negative (-60°) staggering angle.

Figure 2.7 – PTW 24 extruder.

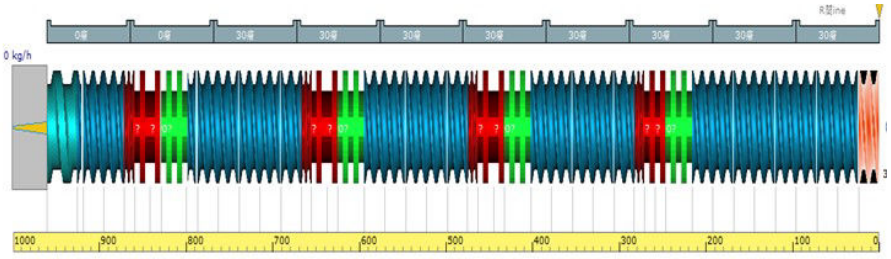

Figure 2.8 - Schematic view of screw profile.

2.3.2 Barrel temperature and screw speed

In order to obtain highest shear stress possible in the extruder, the extruder worked under the condition that its torque was very close to its upper limit. This the barrel temperatures were as low as possible, especially in the first part of the barrel and the screw speed as high as possible (see Table 2.4). GTR-g-PS/PS blends with various compositions were prepared (see Table 2.5). As a control experiment, the GTR/PS blends were produced by the same twin screw extruder with the same content of GTR.

Table 2.4 - Temperature along the extruder.

Extrusion	Zone1 (℃)	Zone2 (℃)	Zone3 (℃)	Zone4 (℃)	Zone5 (℃)	Zone6 (℃)	Zone7 (℃)	Zone8 (℃)	Zone9 (℃)	Zone10 (℃)	Speed (rpm)	Torque (Nm)
1	20	20	125	125	125	140	140	155	160	165	200	130
2	20	20	110	110	115	125	130	140	160	165	200	140
3	20	20	100	100	105	105	130	130	160	165	200	155

Table 2.5 - Compositions of GTR-g-PS/PS blends (% by weight).

GTR-g-PS(%)	Free-PS(%)	Commercial-PS(%)
22.5	7.5	70
30.4	9.6	60
41.8	13.2	45
53	17	30
76	24	0

Chapter 3 A Comprehensive Kinetic Model for Polymerization of Styrene with Ground Tire Rubber

3.1 Overall kinetic scheme

In the present study, a mechanistic kinetic model was developed for the bulk polymerization of styrene with ground tire rubber. In this respect, a generalized kinetic scheme was adopted comprising of the following chemical reactions:

3.1.1 Initiation Reactions

Chemical Initiation

$$I \xrightarrow{k_d * f} 2\,PR \quad (3.1)$$

$$PR + M \xrightarrow{k_{i1}} R_1 \quad (3.2)$$

Thermal Initiation

$$2M \underset{k_{-1}}{\overset{k_1}{\longleftrightarrow}} AH \quad (3.3)$$

$$AH + M \xrightarrow{k_2} AR + MR \quad (3.4)$$

$$AR + M \xrightarrow{k_A} R_3 \quad (3.5)$$

$$MR + M \xrightarrow{k_B} R_2 \quad (3.6)$$

$$AH + M \xrightarrow{k_C} D_3 \quad (3.7)$$

GTR Initiation

$$PR + G \xrightarrow{k_{iG}} GPR + PRH \quad (3.8)$$

$$GPR + M \xrightarrow{k_{i2}} GR_1 \quad (3.9)$$

3.1.2 Propagation Reactions

Propagation of homo-polymerization

$$R_1 + M \xrightarrow{k_p} R_2 \quad (3.10)$$

$$R_n + M \xrightarrow{k_p} R_{n+1} \quad (3.11)$$

Propagation of graft-polymerization

$$GR_1 + M \xrightarrow{k_{pG}} GR_2 \quad (3.12)$$

$$GR_n + M \xrightarrow{k_{pG}} GR_{n+1} \quad (3.13)$$

3.1.3 Chain Transfer Reaction

Chain transfers to monomer

$$R_n + M \xrightarrow{k_{fm}} D_n + R_1 \quad (3.14)$$

$$GR_n + M \xrightarrow{k_{fm}} GD_n + R_1 \quad (3.15)$$

Chain transfers to GTR

$$R_n + G \xrightarrow{k_{fg}} D_n + GPR \quad (3.16)$$

$$GR_n + G \xrightarrow{k_{fg}} GD_n + GPR \quad (3.17)$$

Chain transfers to AH(adduct)

$$R_n + AH \xrightarrow{k_{fa}} D_n + AR \quad (3.18)$$

$$GR_n + AH \xrightarrow{k_{fa}} GD_n + AR \quad (3.19)$$

Chain transfers to free polymer

$$R_n + D_m \xrightarrow{k_{fp}} R_m + D_n \quad (3.20)$$

$$GR_n + D_m \xrightarrow{k_{fp}} R_m + GD_n \quad (3.21)$$

Chain transfers to graft polymer

$$R_n + GD_m \xrightarrow{k_{fgp}} D_n + GR_m \quad (3.22)$$

$$GR_n + GD_m \xrightarrow{k_{fgp}} GD_n + GR_m \quad (3.23)$$

Scission Reaction

$$PR + D_n \xrightarrow{k_S} D_{n-m} + R_m \quad (3.24)$$

Chain transfer reactions play an important role in the molecular weight developments of the produced polymer and should, thus, be taken into account in the kinetic modeling developments. Chain transfer to monomer is an ambiguous reaction for the polymerization of styrene since certain authors have questioned its validity for the present system, but finally included it in their developed model [82]. In the present work, only the chain transfer to polymer reactions have been considered negligible since indication of their occurrence (i.e., chain branching phenomena) has been reported for the system of free-radical polymerization of styrene.

3.1.4 Termination Reactions

Termination by combination

$$R_n + R_m \xrightarrow{k_{tc}} D_{n+m} \quad (3.25)$$

$$GR_n + GR_m \xrightarrow{k_{tcG}} GD_{n+m} \quad (3.26)$$

$$R_n + GR_m \xrightarrow{k_{tc}} GD_{n+m} \quad (3.27)$$

Termination by disproportionation

$$R_n + R_m \xrightarrow{k_{td}} D_n + D_m \quad (3.28)$$

$$GR_n + GR_m \xrightarrow{k_{tdG}} GD_n + GD_m \quad (3.29)$$

$$GR_n + R_m \xrightarrow{k_{td}} GD_n + D_m \quad (3.30)$$

Terminations by primary radicals

$$R_n + PR \xrightarrow{k_{tpr}} Dn \quad (3.31)$$

$$GR_n + PR \xrightarrow{k_{tpr}} GD_n \quad (3.32)$$

$$GR_n + GPR \xrightarrow{k_{tprg}} GD_n \quad (3.33)$$

$$R_n + GPR \xrightarrow{k_{tprg}} GD_n \quad (3.34)$$

Huang et al. ignored the termination reaction including primary radicals, due to their very low concentration. In the present work, the only termination reaction that was neglected is that of termination with GTR primary radicals [74].

3.2 Polymerization rate functions

On the basis of the postulated kinetic scheme, the net production/consumption rate functions of the participating macromolecular species can be established. The rate function of the 'live' free (i.e., non-grafted) polymer chains is shown here as example, while the analytical expressions of the rate functions of all the participating species in the polymerization are shown in Appendix II.

In order to reduce the infinite-order system, with respect to the chain lengths of the different polymer chain species present in the system, and its associated numerical problem, the method of moments is applied to the developed set of rate functions. The method of moments describes the moments of the number-chain-length distributions of the 'live' and 'dead' polymer chains on the basis of the statistical representation of the average molecular properties [65]. Hence, the moments for the 'live' and 'dead'free polymer/ graft polymer chains can be defined as:

$$\lambda_k = \sum_{m=1}^{\infty} n^k \mathrm{R}_n \tag{3.35}$$

$$\mu_k = \sum_{m=1}^{\infty} n^k \mathrm{D}_n \tag{3.36}$$

$$\nu_k = \sum_{m=1}^{\infty} n^k \mathrm{GR}_n \tag{3.37}$$

$$\xi_k = \sum_{m=1}^{\infty} n^k \mathrm{GD}_n \tag{3.38}$$

The moment rate functions for the polymer chains can be derived from the equations (3.35-3.38) by multiplying all terms by n^k and summing over all values of m. The corresponding expression of the moment rate function of the 'live' free polymer chains is shown below, while the respective rate functions of all the species are presented in Appendix II:

3.3 Reactor design equations

The design equations for a batch polymerization reactor can be derived after obtaining the moment rates of the polymer chains. The net production/consumption rate of initiator, monomer, primary radical, rubber primary radical, Diels-Alder adduct, styryl radical and 1-Phenyl tetraryl radical can be obtained by the elementary reactions. In addition, the assumption of no consumption of GTR in the reaction is also considered.

3.3.1 Initiator, I

$$\frac{1}{V}\frac{d(V \cdot I)}{dt} = - k_d \cdot I \tag{3.39}$$

3.3.2 Monomer, M

$$\begin{aligned}\frac{1}{V}\frac{d(V \cdot M)}{dt} = r_M = & 2 \cdot k_{-1} \cdot AH - 2 \cdot k_1 \cdot M^2 \\ & - (k_{i1} \cdot PR + k_2 \cdot AH + k_A \cdot AR + k_B \cdot MR + k_C \cdot AH \\ & + k_{i2} \cdot GPR + k_{fm} \cdot (\lambda_0 + v_0) + k_p \cdot \lambda_0 + k_{pG} \cdot v_0) \cdot M\end{aligned} \tag{3.40}$$

3.3.3 Primary radical, PR

$$\frac{1}{V}\frac{d(V \cdot PR)}{dt} = 2 \cdot f \cdot k_d \cdot I - (k_{i1} \cdot M + k_{iG} \cdot G + k_S \cdot \mu_0 + k_{tpr} \cdot (\lambda_0 + v_0)) \cdot PR \tag{3.41}$$

3.3.4 Rubber primary radical, GPR

$$\begin{aligned}\frac{1}{V}\frac{d(V \cdot GPR)}{dt} = & k_{iG} \cdot PR \cdot G - k_{i2} \cdot GTR \cdot M + k_{fg} \cdot (\lambda_0 + v_0) \cdot G \\ & - k_{tprg} \cdot (\lambda_0 + v_0) \cdot GPR\end{aligned} \tag{3.42}$$

3.3.5 Diels-Alder adduct, AH

$$\frac{1}{V}\frac{d(V \cdot AH)}{dt} = k_1 \cdot M^2 - k_{-1} \cdot AH - ((k_2 + k_C) \cdot M + k_{fa} \cdot (\lambda_0 + v_0)) \cdot AH \tag{3.43}$$

3.3.6 Styryl radical, MR

$$\frac{1}{V}\frac{d(V \cdot MR)}{dt} = k_2 \cdot AH \cdot M - k_B \cdot MR \cdot M \quad (3.44)$$

3.3.7 1-Phenyl tetraryl radical, AR

$$\frac{1}{V}\frac{d(V \cdot AR)}{dt} = k_2 \cdot AH \cdot M - k_A \cdot AR \cdot M + k_{fa} \cdot (\lambda_0 + \nu_0) \cdot AH \quad (3.45)$$

3.3.8 'live' and 'dead' polymer chain moments

$$\frac{1}{V}\frac{d(V \cdot \lambda_k)}{dt} = r\lambda_k \quad (3.46)$$

$$\frac{1}{V}\frac{d(V \cdot \mu_k)}{dt} = r\mu_k \quad (3.47)$$

3.3.9 'live' and 'dead' graft polymer chain moments

$$\frac{1}{V}\frac{d(V \cdot \nu_k)}{dt} = r\nu_k \quad (3.48)$$

$$\frac{1}{V}\frac{d(V \cdot \xi_k)}{dt} = r\xi_k \quad (3.49)$$

3.3.10 Reactor volume, V

$$\frac{1}{V}\frac{d(V)}{dt} = r_M \cdot \left(\frac{1}{dm} - \frac{1}{dp}\right) \cdot MW_m \quad (3.50)$$

For the facilitation of the numerical solution of the model, the Quasi-Steady-State Approximation (QSSA) was applied to both types of primary radicals, thus reducing the system of ordinary differential equations (ODE) by 2, to a total of 20 (i.e., 19 ODEs for the different species + 1 ODE for the volume contraction). Note that the three leading moments of the chain-length distributions of each of the different macromolecular species (i.e., R_n, D_n, GR_n and GD_n) was followed. Finally, following the developents of Woloszyn [82], the initial concentration of AH was calculated on the basis of a QSSA at time zero.

3.4 Polymer Properties

The evolution of the monomer conversion, grafting efficiency and the average molecular weights of the produced polymer, along the polymerization, is calculated according to the following expressions:

3.4.1 Monomer conversion, X

$$X = \frac{V_0 M_0 - VM}{V_0 M_0} \tag{3.51}$$

3.4.2 Graft efficiency, GE

$$GE = \frac{\xi_1}{\xi_1 + \mu_1} \tag{3.52}$$

3.4.3 Number and weight - average molecular weight of free polymer

$$\overline{M_n} = \frac{\mu_1 + \lambda_1}{\mu_0 + \lambda_0} MW_m \approx \frac{\mu_1}{\mu_0} MW_m \tag{3.53}$$

$$\overline{M_w} = \frac{\mu_2 + \lambda_2}{\mu_1 + \lambda_1} MW_m \approx \frac{\mu_2}{\mu_1} MW_m \tag{3.54}$$

3.4.4 Number and weight - average molecular weight of graft polymer

$$\overline{M_n} = \frac{\xi_1 + \nu_1}{\xi_0 + \nu_0} MW_m \approx \frac{\xi_1}{\xi_0} MW_m \tag{3.55}$$

$$\overline{M_w} = \frac{\xi_2 + \nu_2}{\xi_1 + \nu_1} MW_m \approx \frac{\xi_2}{\xi_1} MW_m \tag{3.56}$$

3.5 Diffusion controlled reactions

Due to the increasing of the viscosity of the reaction system at the high monomer conversions, the mobility of the macromolecules and, eventually (at very high monomer conversion) of smaller molecules, is significantly reduced, thus affecting the respective chemical reactions [106], [107]. There are four stages to exhibit the diffusion-control phenomenon. Initially, it is the segmental diffusion-control, when the free volume of the reaction system is high. Secondly, the termination-diffusion-control occurres, as the gel effect. Thirdly, at high conversion

levels, the prorogation-diffusion-control takes place, also known as the glass effect. Finally, when the viscosity is too high to hinder the motion of the imitator, the cage effect occurs. These diffusion-controlled phenomena can not only affect the rate of polymerization, but also the molecular weight. In the present work, these phenomena where taken into account in terms of a diffusion-control model [107]. The equations of this model are presented in Appendix III.

It should be noted at this point that, the developed comprehensive polymerization kinetic accounts for the different chemical reactions that take place in the bulk monomer phase and on the surface of the GTR particles, leading to the synthesis of two distinct polymer chain populations (i.e., the free polymer and the grafted polymer chains) with distinct characteristics and properties. During the development of this model, the assumptions of thermal homogeneity and negligible mass-transfer limitations have been considered in order to simplify this initial kinetic modeling approach of this complex system. The diffusion phenomena, associated with the approach and penetration of the radicals within the GTR particles has been taken into account via the consideration of different kinetic rate constants for the reactions of propagation and termination that occur on the surface or within the GTR particles, with respect to the same reactions that occur in the bulk St/PS phase.

Although these assumptions might not hold strictly under different conditions than the ones implemented in the present work and, thus, limit the generality of the proposed specific model and parameters but, in any case, do not affect the validity of the developed general modeling framework that can be easily modified to account for varying concentration and/or temperature conditions, on the basis or relevant experimental evidence. Even under this simplifying prism and to the best of the authors' knowledge, it is the first time that such a comprehensive kinetic modeling study is presented for the free-radical graft polymerization of styrene on ground rubber particles.

Chapter 4 Results and Discussion

4.1 Polymerization of styrene inside cross-linked GTR particles

4.1.1 Characterization of GTR-g-PS particles

4.1.1.1 Scanning Electron Microscopy (SEM) and Energy Dispersive Spectrometry (EDS)

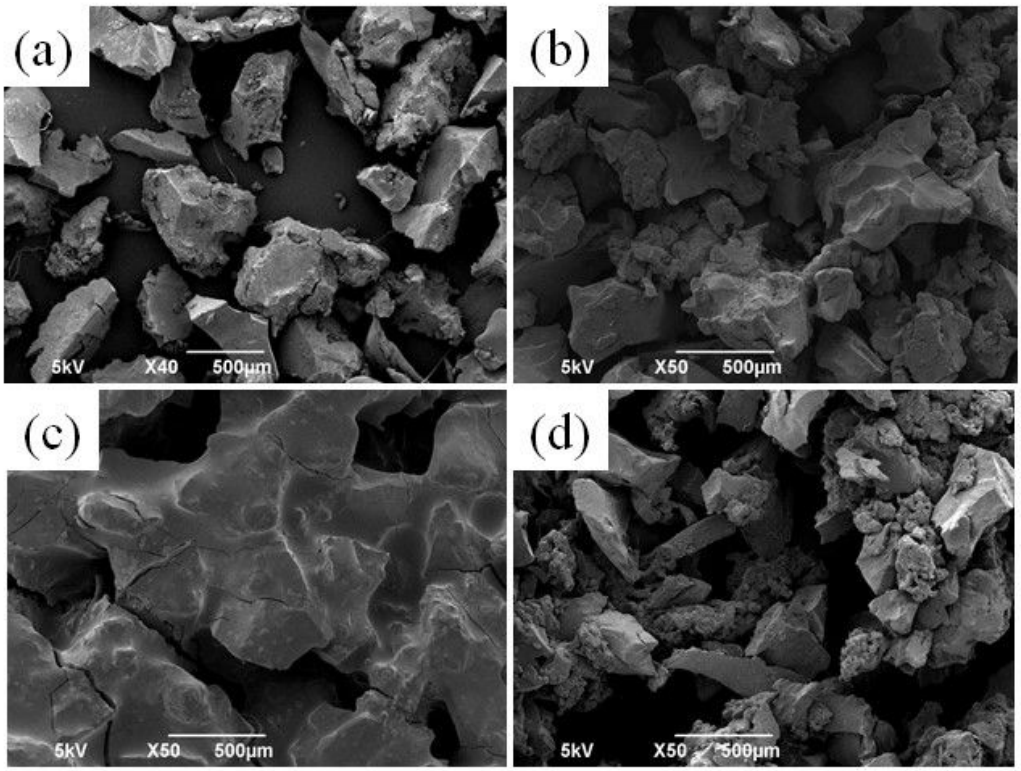

Figure 4.1 - SEM photographs of the original GTR (a), purified GTR (b), GTR-g-PS+ Free-PS (c) and GTR-g-PS (d) particles.

Table 4.1 - Surface element contents of the original GTR particles and GTR-g-PS particles, determined by EDS analysis.

	Atomic composition (%)					
	C	O	Si	S	Ca	Zn
Purified GTR	70.80	14.25	9.67	2.66	0.36	2.27
Purified GTR-g-PS	90.58	8.62	0.27	0.17	-	-

Figure 4.1 shows the SEM photographs of particles of the original GTR (a), purified GTR (b), GTR-g-PS+ Free-PS (c) and GTR-g-PS (d). The purified GTR particles are obtained from the original GTR particles washed by chloroform. The shapes of the original GTR and purified GTR particles are very similar, implying that simple washing in chloroform does not alter the shape of the original GTR particles. In Figure 4.4 c, the surfaces of the GTR particles after in-situ polymerization (GTR-g-PS + free PS) are coated with PS. After the removal of the free PS by chloroform, the pure GTR-g-PS particles rougher and more porous surfaces (Figure 4.5 d). The successful grafting of the PS onto the GTR particles is verified by EDS analysis. Table 4.1 shows the surface atomic composition of the purified GTR, and the purified GTR-g-PS particles. The purified GTR particles contain not only rubber, but also carbon black. The increase in percentage of carbon and the decrease in the percentage of Si content indicate that PS is grafted successfully onto the GTR.

4.1.1.2 Fourier Transform Infrared Spectroscopy (FTIR)

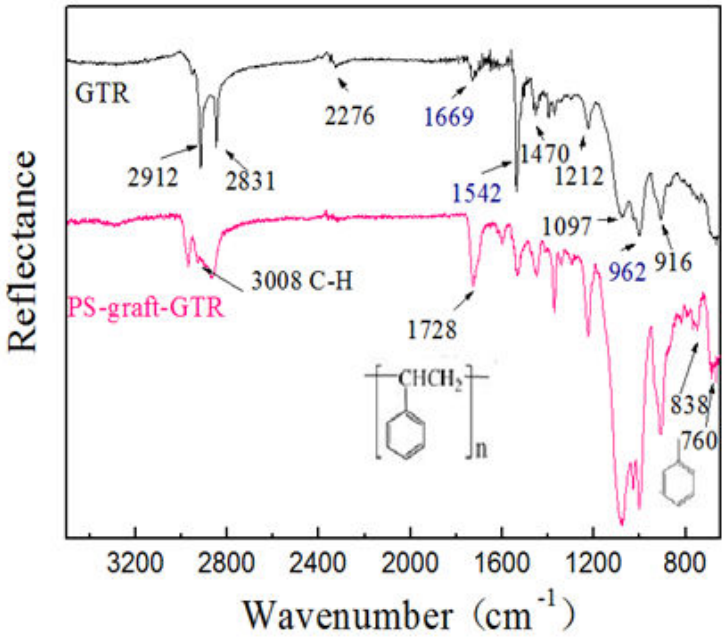

Figure 4.2 - FTIR of GTR particles and GTR-g-PS particles.

Figure 4.2 shows the FT-IR spectra of the in-situ polymerized product (GTR-g-PS + free PS) and pure GTR-g-PS (after removal of the free PS from the in-situ polymerized product). The IR spectrum of the pure GTR-g-PS shows peaks

characteristic of polystyrene. The one at 3028 cm^{-1} is the C–H stretching vibration of benzene ring, those from 1950 to 700 cm^{-1} are the C–H out-plane deformation vibration of benzene ring, and those at 758 and 684 cm^{-1} are the C–H vibration of monosubstituted benzene. This confirms that polystyrene is grafted onto the GTR.

4.1.2 Conversion and GE results

Table 4.2- Experimental design of the polymerization of styrene inside cross-linked GTR particles.

NO	GTR/Styrene	Initiator	I/M(by mole)	Temperature (℃)	Time (h)
1	1/1	BPO	0.6%	80	9
2	1/1	BPO	0.6%	110	9
3	1/1	DCP	0.6%	80	9
4	1/1	DCP	0.6%	110	9
5	1/1	BPO	1.8%	70	9
6	1/1	BPO	1.8%	80	9
7	1/1	BPO+DCP	BPO (2%) DCP (1%)	70℃ (3h), 80℃ (3h), 90℃ (2h),100℃ (2h)	
8	1/1.5	BPO+DCP	BPO (2%) DCP (1%)	70℃ (3h), 80℃ (3h), 90℃ (2h), 100℃ (2h)	

Table 4.2 shows the experimental design of the polymerization of styrene inside GTR. The conditions of the polymerization were optimized according to experimental results. First, two initiators (BPO and DCP) were selected to study the polymerization process. The polymerization was performed with 30 g of styrene and 30 g of GTR particles at a reaction temperature of 80℃and 110℃ and the reaction time of 9h.

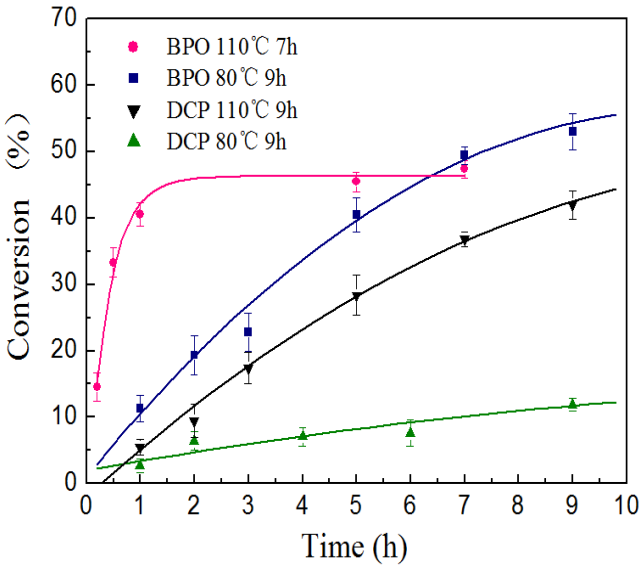

(a)Conversion as a function of time

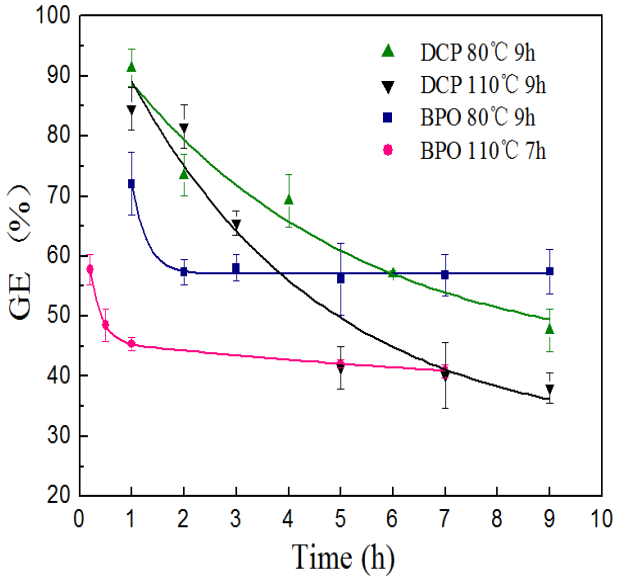

(b) GE as a function of time

Figure 4.3 - Effects of the concentration of BPO or DCP and polymerization temperature on the total styrene conversion (a) and GE (b).

Figure 4.3 shows the effects of the concentration of BPO or DCP and polymerization temperature on the total styrene conversion (a) and GE (b). In the case of BPO, initially the conversions at 80℃ are significantly lower than those at 110℃. However, in the late stage of the polymerization, those at 80℃ exceed those at 110℃. On the other hand, the GE at 80℃ is always higher than those at 110℃. As for DCP,

the conversions at 80℃ are always lower than those at 110℃ within the polymerization time range of 9h, while the GE is exactly the opposite.

We are more interested in the percentage of styrene that is grafted onto GTR, denoted as St-g as a function of the total styrene conversion because we want to maximize both St-g and the total styrene conversion. This is shown in Figure 4.4. It is seen that BPO always outperforms DCP, whatever the temperature. In other words, for a given total styrene conversion, BPO yields a higher St-g. Moreover, for a given total styrene conversion, St-g is higher at a lower temperature.

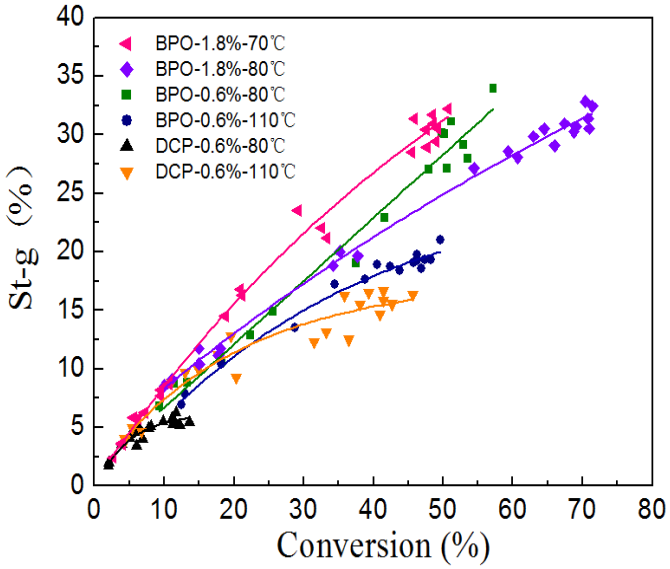

Figure 4.4 - Effects of the concentration of BPO or DCP and polymerization temperature on St-g as a function of the total styrene conversion (data from Figure 4.3).

The problem is that when we maximize St-g and the total styrene conversion, we may also maximize the percentage of free PS in the system. In order to solve this problem, we define a ratio between St-g and the percentage of free PS, denoted as St-g/St-f. We then look to maximize both St-g/St-f and the total styrene conversion.

Figure 4.5 shows the effects of the concentration of BPO or DCP and polymerization temperature on St-g/St-f as a function of the total styrene conversion (data from Figure 4.3). When St-g/St-f is 1, it means that 50% of the total styrene

conversion is in the form of styrene grafted onto GTR and the other 50% in the form of free PS. It is seen that:

(a) For a given initiator, St-g/St-f ratio decreases with increasing temperature
(b) St-g/St-f ratio decreases with increasing the total styrene conversion.
(c) When the total styrene conversion is high enough, St-g/St-f ratio decreases with increasing initiator concentration.
(d) BPO outperforms DCP, at least for sufficiently high total styrene conversion.

All these results except (d) are bad news for maximizing both St-g/St-f and the total styrene conversion, especially if we want the polymerization to reach a sufficiently high total styrene conversion within a reasonable time. The competition between graft-polymerization and homo-polymerization generated the different amounts of St-g and St-f. While the polymerization processing, the reactive radicals were shielded as a result of graft polystyrene inside of GTR. Meanwhile, the free PS is produced dramatically, due to the homo-polymerization accelerated rapidly. This effect is steric effect. The steric effect can explain that the St-g/St-f ratio decreases with increasing the total styrene conversion.

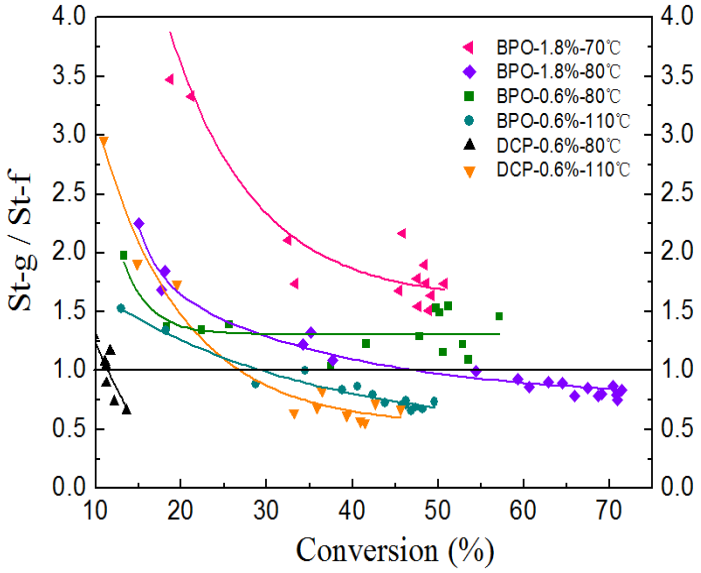

Figure 4.5 - Effects of the concentration of BPO or DCP and polymerization temperature on St-g/St-f as a function of the total styrene conversion (data from Figure 4.3).

Based on the above results, a binary initiating system composed of 2% of BPO and 1% of DCP was tested with the following temperature profile: 70℃ for 3h, 80℃ for 3h, 90℃ for 2h and 100℃ for 2h. A product with high total styrene conversion together with a reasonably higher St-g/St-f ratio is obtained.

It is interesting to further study on the monomer concentration influence the graft polymerization of styrene in the GTR particles. Figure 4.6 shows that, as the monomer concentration increases (GTR/St = 1/1 to GTR/St = 1/1.5), the St-g shows a decrease, revealing that the graft polymerization of styrene is less competitive than the homo-polymerization of styrene with increase of monomer concentration. It means that a higher amount of the free PS is produced by increasing monomer concentration. The results of our study agree well with the literature [9, 10] where low monomer concentration shows higher GE than high monomer concentration in the graft polymerization.

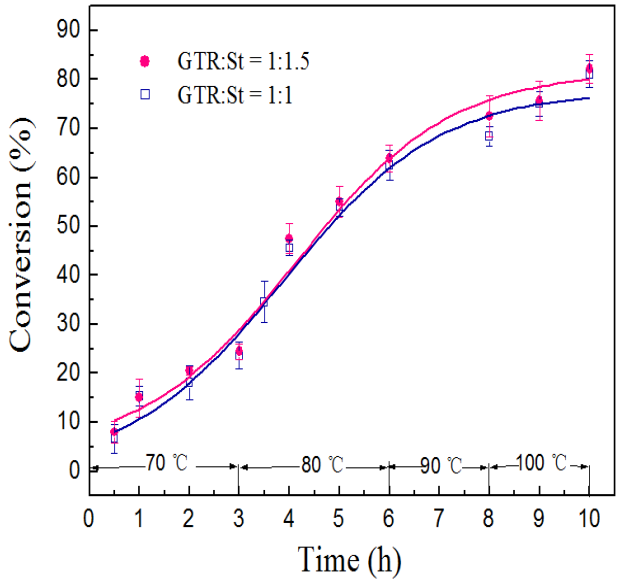

(a) Conversion as the function of time

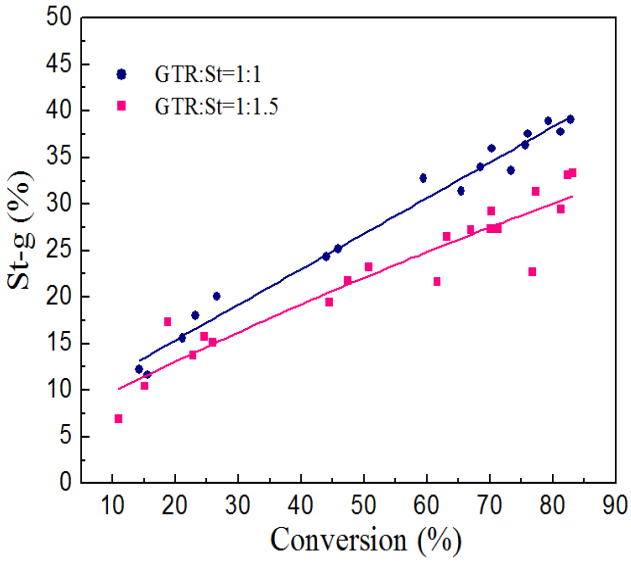

(b) St-g as the function of conversion.

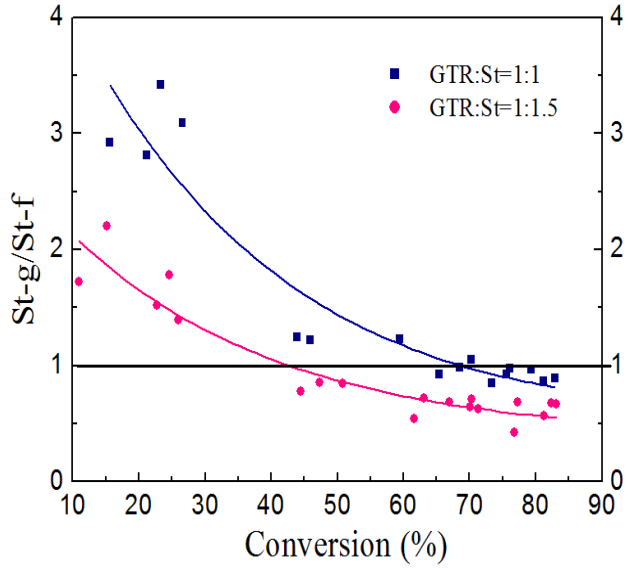

(c)St-g/St-f as the function of conversion.

Figure 4.6 - Effect of monomer concentration on the conversion (a), St-g (b) and St-g/St-f (c).

4.1.3 M_n and M_w of free PS

4.1.3.1 Effect of reaction time on M_n and M_w of free PS

Table 4.3 - M_n and M_w of free PS at different polymerization times (I_0_BPO = 0.6% mol, T = 80 ℃).

NO	M_n (g·mol^{-1})	M_w(g·mol^{-1})	M_w/M_n
PS-B-0.6-80-1h	4.04x10^4	6.71 x10^4	1.675
PS-B-0.6-80-5h	3.93x10^4	6.68 x10^4	1.702
PS-B-0.6-80-9h	3.81x10^4	6.59 x10^4	1.734

Table 4.4 - M_n and M_w of free PS at different polymerization times (I_0_BPO = 1.8% mol, T =70 ℃).

NO	M_n(g·mol^{-1})	M_w(g·mol^{-1})	M_w/M_n
PS-B-1.8-70-1h	2.89x10^4	5.29x10^4	1.87
PS-B-1.8-70-5h	2.81x10^4	5.24x10^4	1.86
PS-B-1.8-70-9h	2.74x10^4	5.03x10^4	1.83

It is seen that M_n and M_w of free PS remain virtually constant over time.

4.1.3.2 Effect of concentration of initiator on M_n and M_w of free PS

Table 4.5 - M_n and M_w of free PS at different concentrations of BPO (T = 80℃, t = 9h).

NO	M_n(g·mol^{-1})	M_w(g·mol^{-1})	M_w/M_n
PS-B-0.6-80-9h	3.81x10^4	6.59 x10^4	1.73
PS-B-1.8-80-9h	2.46x10^4	4.54 x10^4	1.84

As expected, the higher the initial concentration, the lower the molar masses of the polymer.

4.1.3.3 Effect of reaction temperature on M_n and M_w of free PS

Table 4.6 - M_n and M_w of free PS at different reaction temperature (I_0_BPO =1.8% mol, t = 9h).

NO	M_n(g·mol^{-1})	M_w(g·mol^{-1})	M_w/M_n
PS-B-1.8-70-9h	2.74x10^4	5.03x10^4	1.83
PS-B-1.8-80-9h	2.46x10^4	4.54 x10^4	1.84

Again as expected, a higher temperature results in a decrease in the molar mass of the polymer.

4.1.4 Effect of GTR-g-PS particles on the mechanical properties, compatibility and morphology of GTR/PS blends

4.1.4.1 Impact mechanical property of GTR/PS blends and GTR-g-PS/PS

To distinguish between the original GTR and the GTR in the GTR-g-PS, the GTR in the GTR-g-PS is designated as equivalent GTR. There can be two types of PS in the blends: one is the free PS generated in-situ during the polymerization of styrene inside the GTR particles and another one is commercial PS. Table 4.7 shows the compositions of various GTR-g-PS/PS blends.

Table 4.7- Compositions of GTR-g-PS/PS blends (% by weight).

Experiment code	GTR-g-PS*		PS	
	Equivalent GTR (%)	Graft PS (%)	Free PS (%)	Commercial PS (%)
1	16	6.5	7.5	70
2	22	8.4	9.6	60
3	30	11.8	13.2	45
4	38	15	17	30
5	55	21	24	0

*The composition of GTR-g-PS: equivalent GTR = 73%, graft PS = 27%

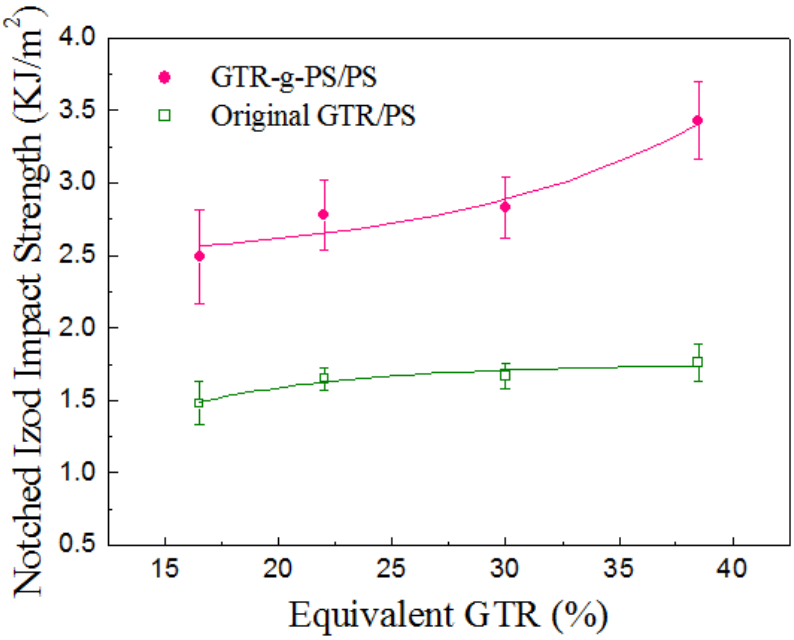

Figure 4.7 - Notched Izod impact strength of the original GTR/PS blends and GTR-g-PS/PS blends by different ratio of Effective-GTR content. The hollow squares are the GTR/PS blends, the solid dots are the PS-g-GTR/PS blends.

The original GTR/PS blends and PS-g-GTR/PS blends were prepared in a laboratory scale extruder (PTW 24). Figure 4.7 compares these two types of blends in terms of the notched impact strength based on the (equivalent) GTR in the blends. The GTR-g-PS/PS blends significantly outperform the original GTR/PS blends. For example, the notched impact strength of the GTR-g-PS/PS reaches as high as 3.3 KJ/m^2 when the equivalent content is 38%. Moreover, the notched impact strength of the GTR-g-PS/PS blends increases notably with increasing equivalent GTR content. However, the increase is much slower in the case of the original GTR/PS blends. The higher impact strength for the GTR-g-PS/PS blends compared with that of the original GTR/PS blends can be attributed to the fact that in the former cases, the GTR particles are more finely dispersed in the PS matrix, on the one hand, and the interfacial adhesion between the GTR and PS is expected to be greatly enhanced by the PS grafts onto the GTR, on the other hand. This will be further discussed below.

4.1.4.2 SEM photographs of the fractured surfaces of the original GTR/PS blends and GTR-g-PS/PS blends

Figure 4.8 shows the SEM photographs of the fractured surfaces of the original GTR/PS blends and GTR-g-PS/PS blends by impact testing at room temperature. Individual distinct GTR particles are seen on the fractured surfaces of the original GTR/PS blends, indicating a lack of interfacial adhesion between the original GTR particles and the PS matrix. In Figure 4.8 (b, d, f, h), individual GTR particles are much less visible on the fractured surfaces of the GTR-g-PS/PS blends, due to the fact that they are covered by PS grafts which are formed by the in situ polymerization of styrene inside the GTR particles. This indicates stronger interfacial adhesion between the GTR particles and the PS matrix.

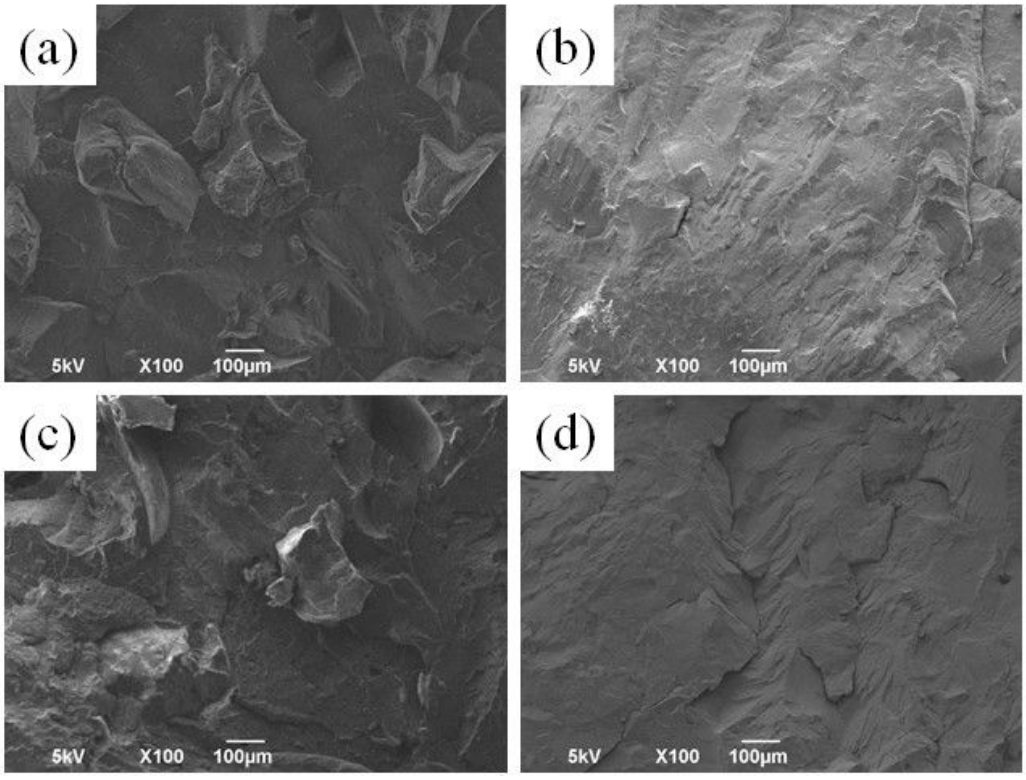

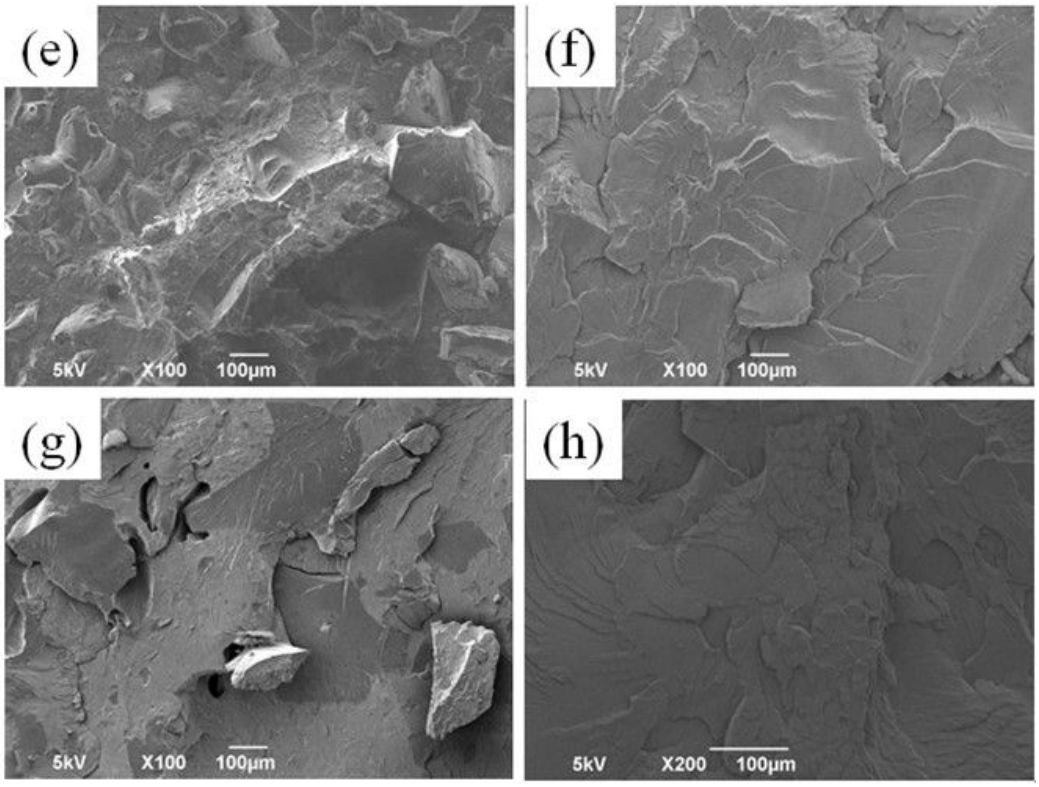

Figure 4.8 - SEM photographs of the fracture surfaces of the original GTR/PS blends and GTR-g-PS/PS blends. The equivalent GTR content is 16%, 22%, 30% and 38% from top to bottom. The original GTR/PS blends are a, c, e, and g, and the GTR-g-PS/PS blends are b, d, f, and h.

4.1.4.3 SEM photographs and PSD of the GTR particles of the original GTR/PS blends and GTR-g-PS/PS blends.

Figure 4.9 shows the SEM micrographs of the original GTR particles and the GTR-g-PS ones which are blended with the commercial PS in a twin-screw extruder. The particles are observed after removal of the free PS and/or commercial PS. Comparison of Figure 4.9 (a, c, e) with (b, d, f) shows that the size of the GTR-g-PS particles is smaller than that of the original GTR.

Figure 4.10 shows, in a more quantitative manner, the size distribution of the original GTR particles, and GTR-g-PS particles in the GTR-g-PS/PS blends whose equivalent GTR contents are 16%, 30% and 38%, corresponding to experiments 1, 3 and 4, respectively. It is seen that the size of the GTR-g-PS particles decreases slightly with increasing the equivalent GTR content due to increased viscosity or

shear stress. Table 4.8 shows the characteristic diameters of the original GTR particles and those of the GTR-g-PS ones.

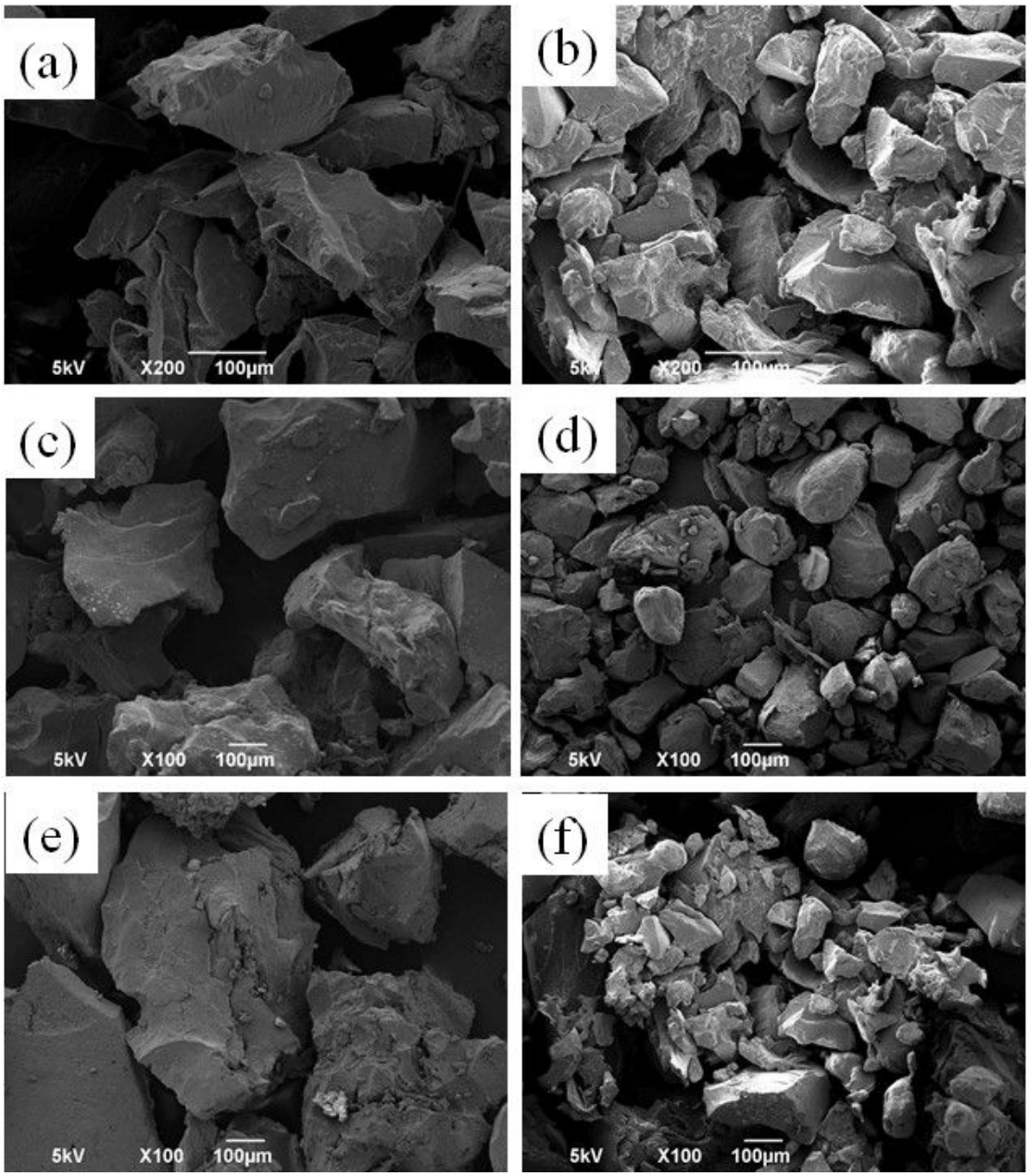

Figure 4.9 - SEM micrographs of the original GTR particles and GTR-g-PS ones. The equivalent GTR content is 16%, 30% and 38% from top to bottom. The original GTR particles are a, c, and e, and the GTR-g-PS particles are b, d, and f.

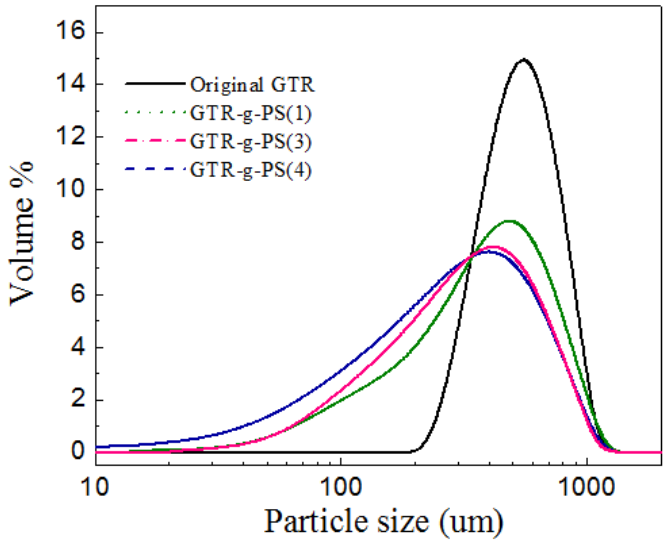

Figure 4.10 - Curves of the size distribution of the original GTR particles, GTR-g-PS particles in the GTR-g-PS/PS blends whose equivalent GTR contents are 16%, 30% and 38%, corresponding to experiments 1, 3 and 4, respectively.

Table 4.8 - Characteristic diameters of the original GTR, and GTR-g-PS particles blended with the PS with an equivalent GTR content of 16, 30 or 38% (corresponding to experiment 1, 3 or 4 respectively).

	d(0.1) µm	d(0.5) µm	d(0.9) µm	Mean µm
Original GTR	328.9	535.4	843.1	**563.3**
GTR-g-PS(1)	108.1	355.7	698.5	**356.1**
GTR-g-PS(3)	94.5	297.3	646.8	**338.2**
GTR-g-PS(4)	90.3	273.3	605.9	**309.9**

4.1.5 Effects of the number of extrusion passage on the mechanical properties, size and shape of the GTR-g-PS particles

As pointed out throughout this thesis, a big challenging facing the toughening of a brittle polymer like PS by GTR particles resides in the difficulty of finely dispersing them in the polymer matrix. For this reason, we successively extruded GTR-g-PS/PS blends in the twin screw extruder 1, 2 and 3 times and we studied the size and shape of the GTR-g-PS particles on the one hand and impact strength of the resulting GTR-g-PS/PS blends, on the other hand.

4.1.5.1 Impact strength of the GTR-g-PS/PS blends after 0, 1, 2 and 3 times of extrusion

Figure 4.11 shows the impact strength of the GTR-g-PS/PS blends with 0, 1, 2 and 3 times of extrusion. The higher the number of extrusion passage, the higher the impact strength. This is mainly due to finer dispersion of the GTR-g-PS particles with increasing the number of extrusion passages, as discussed below.

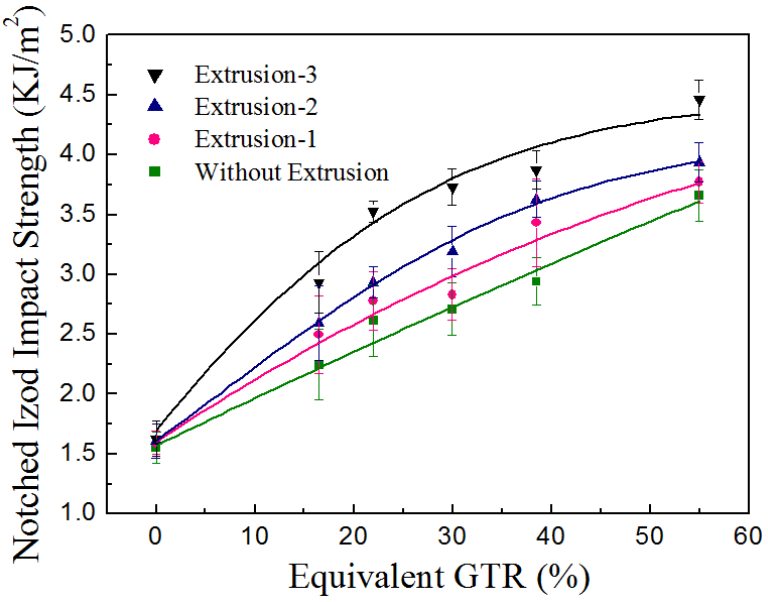

Figure 4.11 - Impact strength of the GTR-g-PS/PS blends after 1, 2 and 3 times of extrusion in a twin screw extruder of type PTW 24. The equivalent GTR content is 16, 22, 30, 38 and 55, respectively.

Figure 4.12 shows the impact strength of the GTR-g-PS/Free PS blends as the function of particle size of GTR-g-PS. The smaller particle size of GTR-g-PS, the higher the impact strength. This is mainly due to finer dispersion of the GTR-g-PS and the better interfacial adhesion between GTR-g-PS and PS matrix with the smaller particle size of GTR-g-PS.

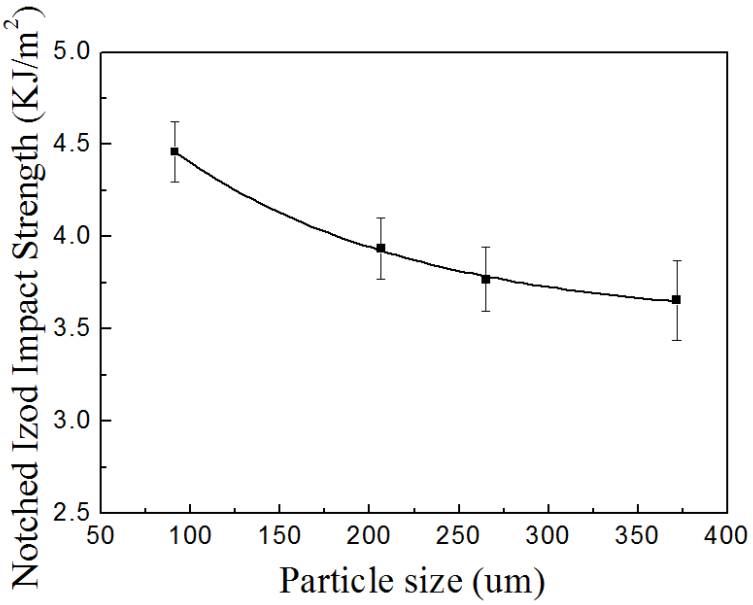

Figure 4.12 - Impact strength of the GTR-g-PS/Free PS blends as the function of particle size of GTR-g-PS.

4.1.5.2 SEM photographs of the fractured surfaces of the GTR-g-PS/PS blends after 0, 1, 2 and 3 times of extrusion

Figure 4.13 shows the fractured surfaces of the GTR-g-PS/PS blends obtained by 0, 1, 2 and 3 times of extrusion. Apparently they become smoother with increasing number of extrusion and it is not easy to identify individual GTR particles

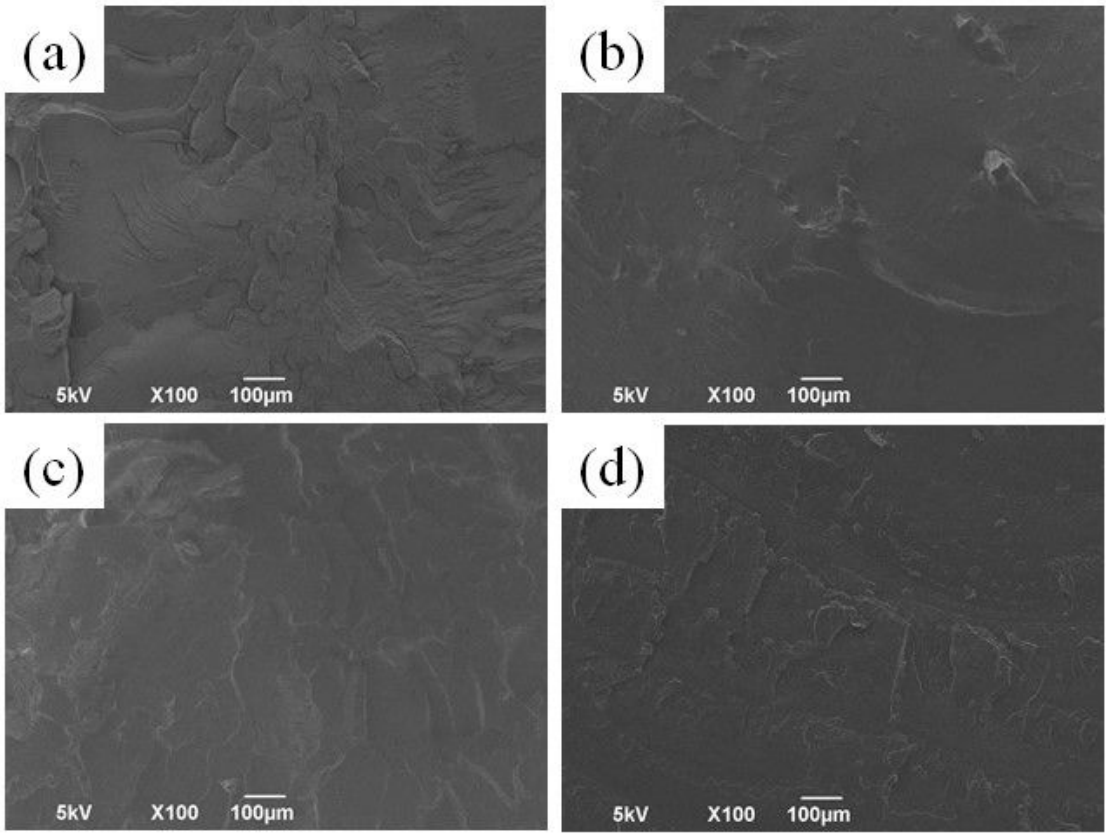

Figure 4.13 - Fractured surfaces of the GTR-g-PS/PS blends obtained by 0 (a), 1 (b), 2 (c) or 3 (d) times of extrusion, respectively.

4.1.5.3 SEM photographs and PSD of the GTR-g-PS particles obtained by 0, 1, 2 or 3 times of extrusion

Figure 4.14 shows the SEM photographs of the GTR-g-PS particles obtained by 0, 1, 2, or 3 times of extrusion of the GTR-g-PS/PS blend. It is seen that the higher the number of extrusion passage, the smaller the size of the GTR-g-PS particles.

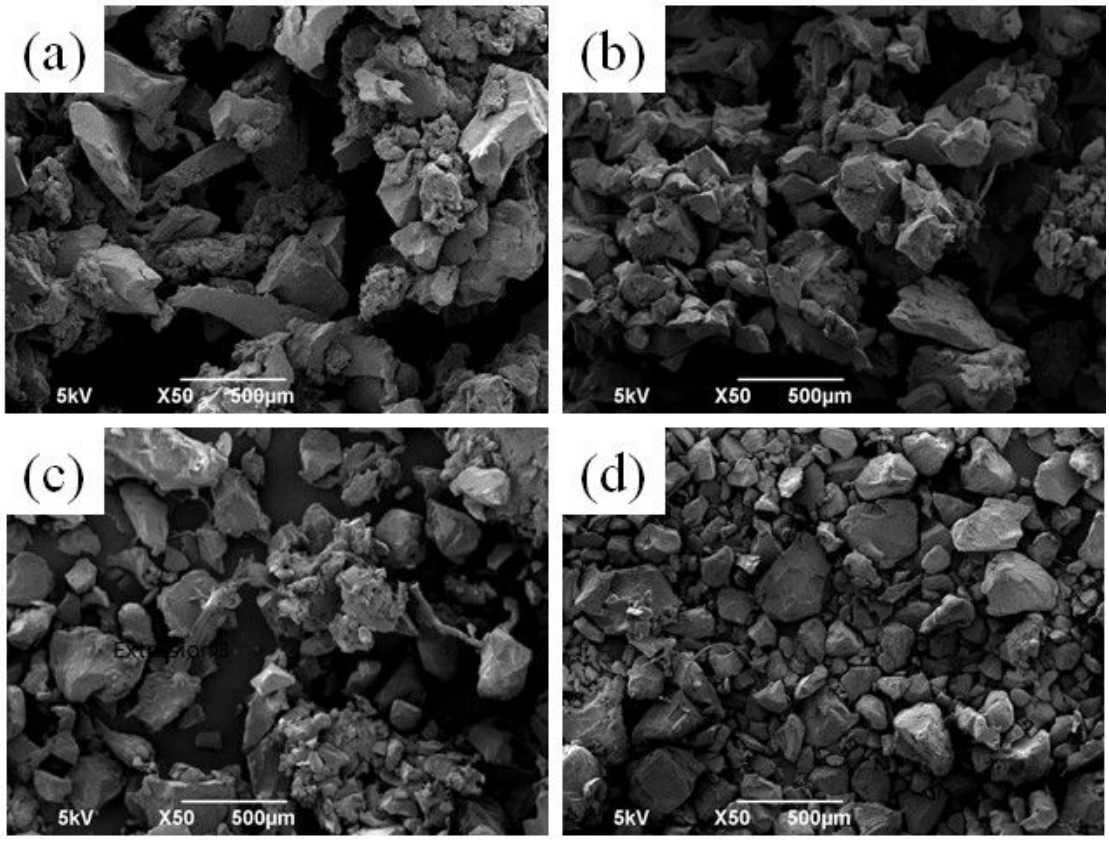

Figure 4.14 - SEM of the original GTR-g-PS and GTR-g-PS particles with 0 (a), 1 (b), 2 (c) or 3 (d) times of extrusion, respectively

This is better shown in Figure 4.15 and Table 4.9. The curve shifts to the smaller size domain as the number of the extrusion passage increases. The mean diameter is reduced to about 91 micrometers after three extrusion passages (Table 4.9).

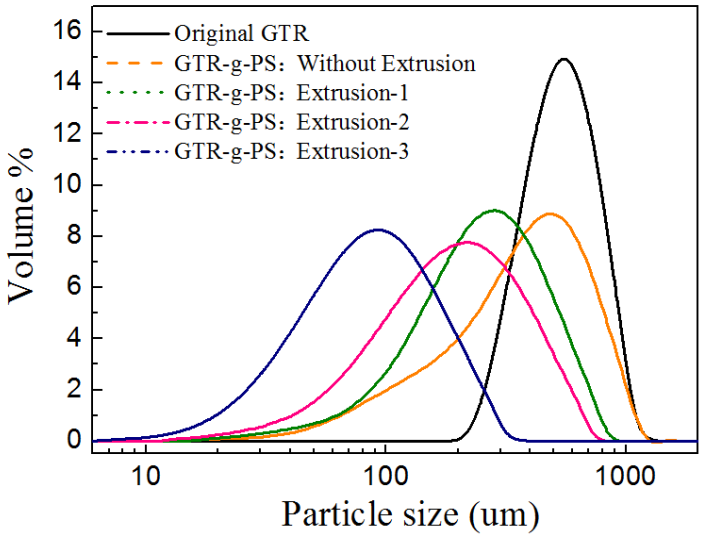

Figure 4.15 - Curves of the size distribution of the original GTR particles and GTR-g-PS ones in the GTR-g-PS/PS blends obtained by 0, 1, 2 or 3 times of extrusion.

Table 4.9 – Characteristic diameters of the original GTR, and GTR-g-PS particles after 0, 1, 2 or 3 times of extrusion.

	d(0.1) μm	d(0.5) μm	d(0.9) μm	Mean μm
Original GTR	328.9	535.4	843.1	**563.3**
GTR-g-PS without Extrusion	99.1	329.1	713.5	**371.9**
GTR-g-PS with Extrusion-1	95.6	237.5	478.3	**265.1**
GTR-g-PS with Extrusion-2	64.3	177.2	394.9	**206.4**
GTR-g-PS with Extrusion-3	31.4	78.9	170.3	**91.1**

4.1.5.4 Effect of extrusion on the M_n and M_w of free PS

Table 4.10 shows the molecular weights of the free PS after 0, 1, 2 or 3 times of extrusion. They do no change much after 3 times of extrusion, suggesting that the PS is very stable under the specified extrusion conditions.

Table 4.10 - M_n and M_w of the free PS after 0, 1, 2, or 3 times of extrusion in a twin-screw extruder.

Extrusion NO.	M_n(g·mol^{-1})	M_w(g·mol^{-1})	M_w/M_n
0	2.39 x10^4	4.47 x10^4	1.87
1	2.34 x10^4	4.36 x10^4	1.86
2	2.30 x10^4	4.24 x10^4	1.85
3	2.28 x10^4	4.23 x10^4	1.85

Conclusions

As a typical commodity plastic with low impact strength, polystyrene was successfully grafted inside cross-linked ground tire rubber powders using benzoyl peroxide and dicumyl peroxide as the compound initiators via a simple radical polymerization method. The characterization results of Scanning Electron Microscopy，Energy Dispersive Spectrometer and Fourier Transform Infrared Spectroscopy revealed that the GTR particles were grafted by PS chains. The particle size of GTR-g-PS could be decreased by extrusion. The particle size of the GTR-g-PS was smaller, when the torque of extrusion was higher. Moreover, there was little influence on the molecular weight of the free PS by extrusion. The fractured surfaces of impact samples suggested better dispersion of the GTR with grafting the PS chains in the PS matrix and higher interfacial adhesion between the two phases.

While the impact strength of the commercial PS is about 1.5 KJ/m^2, it is raised to as high as 4.5 KJ/m^2 by in-situ polymerization of styrene inside the GTR. This is a very significant improvement.

4.2 Polymerization of styrene onto GTR particles

4.2.1 SEM micrographs of GTR-g-PS particles

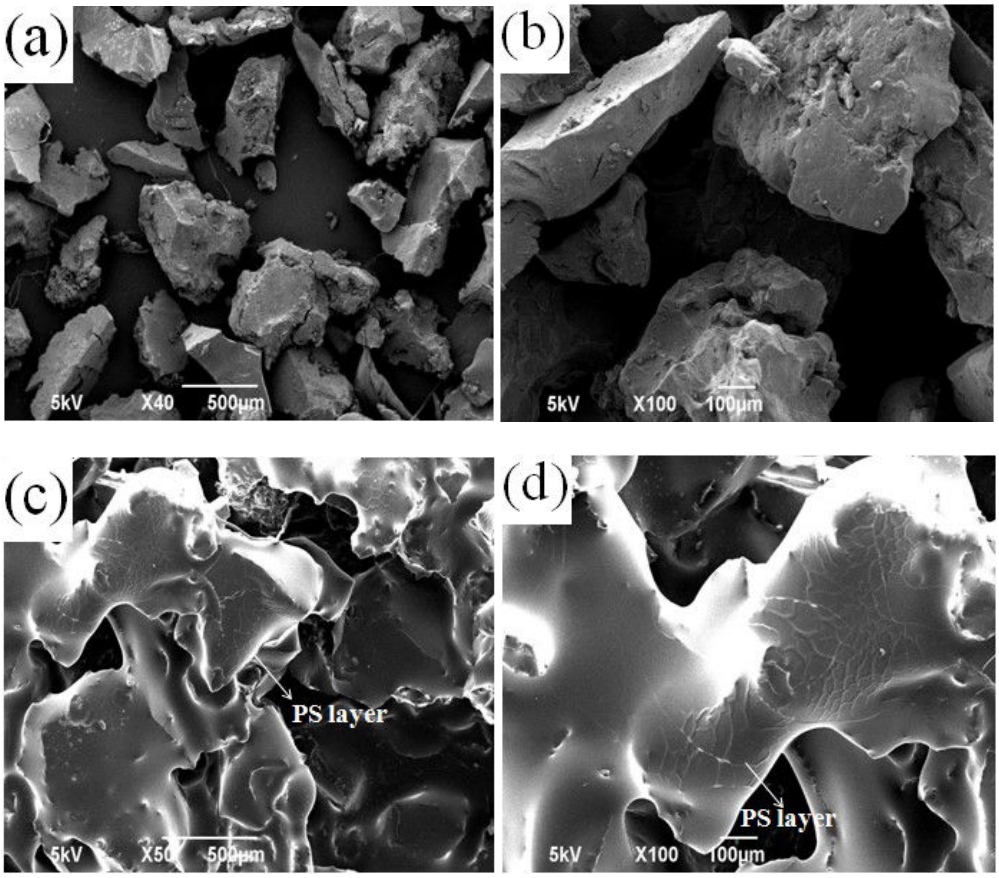

Figure 4.16 - SEM micrographs of original GTR particles and GTR-g-PS particles. The original GTR particles are a and b, and the GTR-g-PS particles are c and d.

In an attempt to confirm the presence of grafted PS onto the GTR, the samples which are removed the free PS are subjected to SEM analysis. The presence of PS grafting on GTR is evident directly from the SEM images of the composites (Figure 4.16), as it is more easily detectable by the blow up of the SEM micrograph. Figure 4.16 (a) and (b) shows an unsmooth surface of original GTR particle. In Figure 4.16 (c) and (d), the surface of GTR-g-PS particle becomes smooth. The results indicate that the encapsulation of the GTR particles by PS chains is achieved.

4.2.2 Effect of GTR content on the polymerization of styrene onto GTR particles

Table 4.11 - Effect of GTR content on monomer conversion and GE (styrene=400g, initiator = 1% mol, BPO/DCP=0.25).

GTR(g)	70	85	100
Conversion (%)	95±2	92±3	89±4
GE (%)	35±6	51±5	54±3

For the polymerization, GTR content has an important effect on the polymerization rate and graft efficiency [55]. Table 4.11 shows the influence of the GTR content on the monomer conversion and GE. The final conversion decreases with increasing GTR content. Moreover, it is observed that the graft efficiency increases with increasing GTR content. There are two kinds of polymerization, homo-polymerization of styrene and graft polymerization of styrene on GTR in the system. The important factor affecting the GE is the competition between monomer and GTR for primary radicals. Therefore, an increase in GTR content results in a respective increase in available sites for the attack of primary radicals, thus promoting the graft-polymerization over the homo-polymerization and increasing the final GE value.

4.2.3 Effect of initiator concentration on the polymerization of styrene onto GTR particles

Table 4.12 - Effect of initiator concentration on monomer conversion and GE (GTR=70g, styrene=400g, BPO/DCP=0.25).

Initiator/Styrene (% mol)	0.2	0.76	1
Conversion (%)	82±5	91±4	95±2
GE (%)	43±4	39±2	37±2

The effect of initiator concentration on the monomer conversion and GE to GTR, are shown in Table 4.12. It is seen that with the increasing initiator concentration, the conversion increases while the GE decreases. The result obtained is in agreement with the tendency, the lower GE with the higher conversion [55].

4.2.4 Effect of BPO/DCP on the polymerization of styrene onto GTR particles

Table 4.13 - Effect of the BPO/DCP on the monomer conversion and GE (GTR=70g, styrene=400g, initiator = 0.2% mol).

BPO/DCP (mol/mol)	0.25	1	4
Conversion (%)	85±2	83±2	82±3
GE (%)	41±3	42±3	44±3

In order to reduce the reaction time and increase the monomer conversion, a mix of initiators is used. BPO is known to form chemical bonds between the rubber and polystyrene [89], [56], while DCP is one kind of low activity initiator with high decomposition temperature. Therefore, the experiment is carried out with BPO and DCP as a binary initiator. The reaction time is obtained according to the principle that the half-life of initiator is generally less than or equal to polymerization reaction time at the polymerization temperature. The half-life time of BPO is 1h at 90℃, however, the BPO is decomposed rapidly at the high temperature to complete the reaction.

Table 4.13 shows the effect of the BPO/DCP on the conversion and GE. The results indicate that DCP is a slightly more effective initiator than BPO for the graft polymerization reaction of PS onto GTR at high temperatures. However, there is no significant difference in the finally obtained values that could justify a clear advantage of the use of one of the two initiators over the other.

4.2.5 Effect of reaction conditions on the glass transition temperature of GTR-g-PS particles

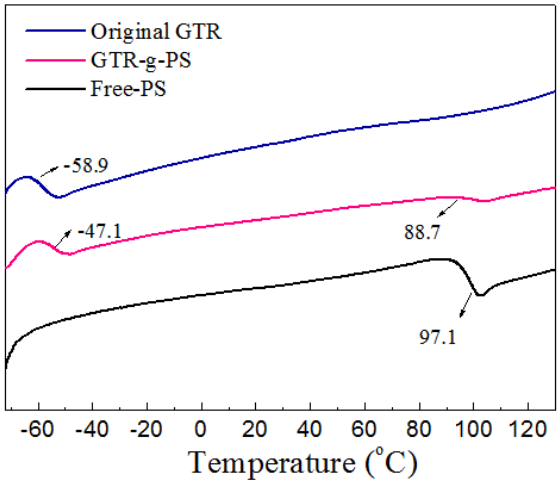

Figure 4.17 - DSC curves of original GTR particles, GTR-g-PS particles and Free-PS.

DSC analysis is generally one of the most convenient methods for analyzing glass transition temperature of polymers, which is one of the most important properties of polymers, denoting the temperature region where the polymer transitions from a hard, glassy material to a soft, rubbery material. The DSC curves (Figure 4.17) show that the Tg ascribed to rubber is increased from –58.92℃ to –47.10℃ while the Tg corresponding to PS decreases (from 97.07℃ to 88.77℃), with respect to the original materials.

The effect of the reaction factors on the glass transition temperature of GTR-g-PS particle was also studied. From Figures 4.18 - 4.20, it is seen that by increasing the GTR content, decreasing the initiator concentration and increasing the percentage of BPO, an increase in the glass transition temperature of GTR is observed. This is due to the increasing of GE.

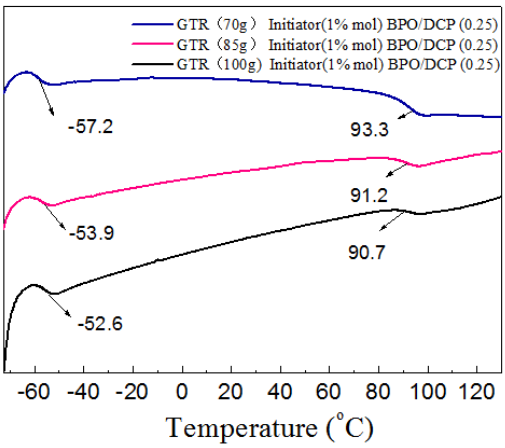

Figure 4.18 - Effect of GTR content on the glass transition temperature of GTR-g-PS particles.

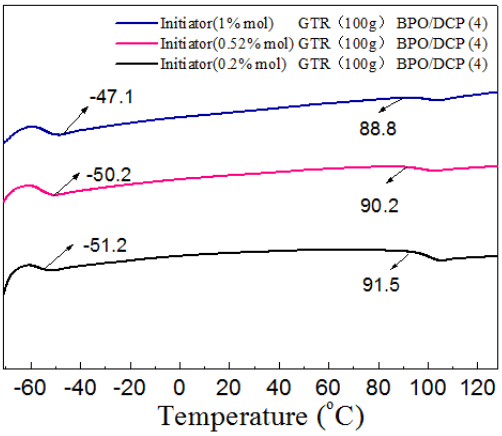

Figure 4.19 - Effect of initiator concentration on the glass transition temperature of GTR-g-PS particles.

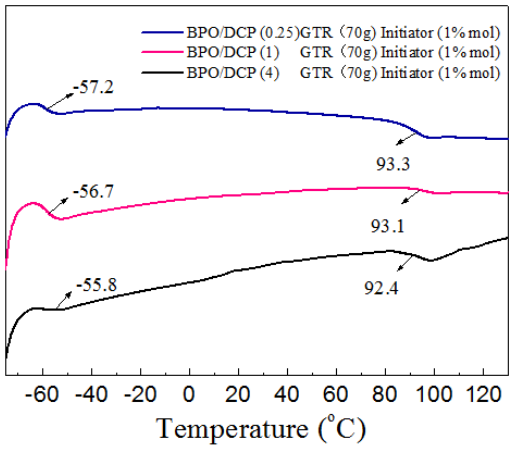

Figure 4.20 - Effect of BPO/DCP on the glass transition temperature of GTR-g-PS particles.

4.2.6 Effect of reaction conditions on thermal stability of GTR-g-PS particles

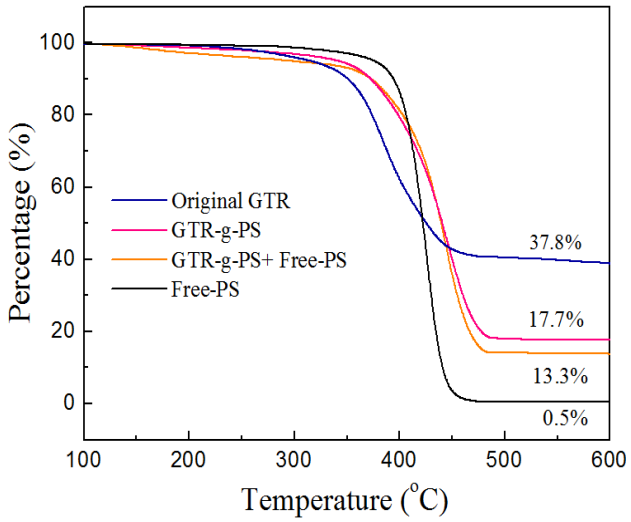

(a)

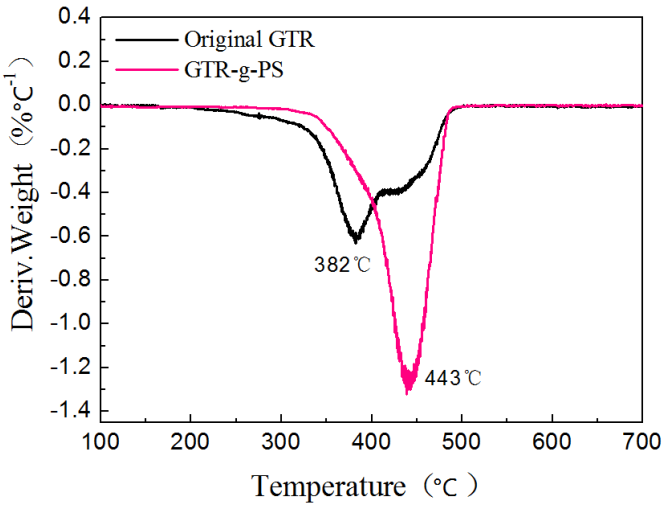

(b)

Figure 4.21 - TG curves (a) of original GTR particles, GTR-g-PS particles and free PS and DTG curves (b) of original GTR particles and GTR-g-PS particles.

The GTR particles are made up of natural rubber, styrene butadiene rubber, carbon black, and inorganic fillers. Figure 4.21 displays the TG/DTG curves of original GTR, Free-PS and GTR-g-PS. For the DTG curve, the degradation temperature of GTR-g-PS is raised to 443 ℃ from the original GTR onset of

degradation temperature 382℃. The results indicate that the thermal stability of GTR is improved by grafting PS.

The residual material is carbon black (CB), which is still excised after 500℃ under the nitrogen atmosphere. The amount of Graft-PS could be detected by calculating the percentage of CB in the composites with the TGA analysis, such as the residual weights are 37.81%, 17.66% and 13.29% for the original GTR, PS-g-GTR and PS-g-GTR + Free-PS, respectively. The residual content of PS-g-GTR particles is lower than the original GTR. The effects of various factors (monomer content, initiator types and initiator content) on the TGA results of GTR-g-PS particles are shown from Figure 4.22 to 4.24. It can be seen that the thermal stability of GTR-g-PS particles is increased by increasing the GE.

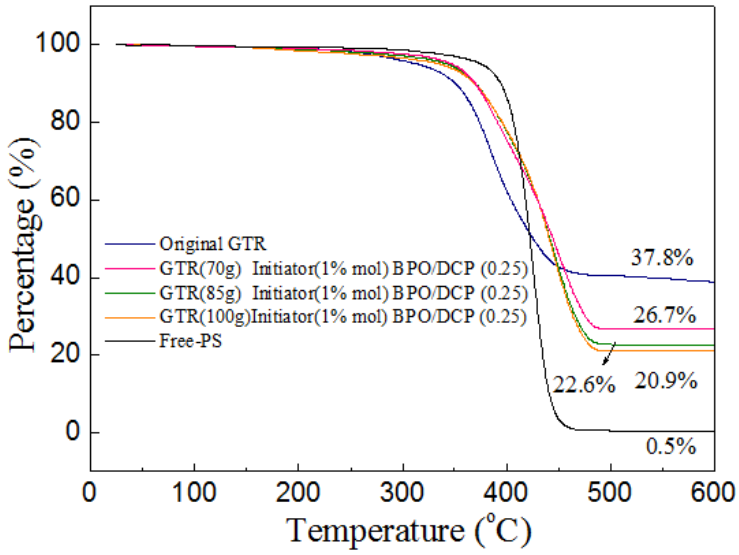

Figure 4.22 - Effect of GTR content on the TGA of GTR-g-PS particles.

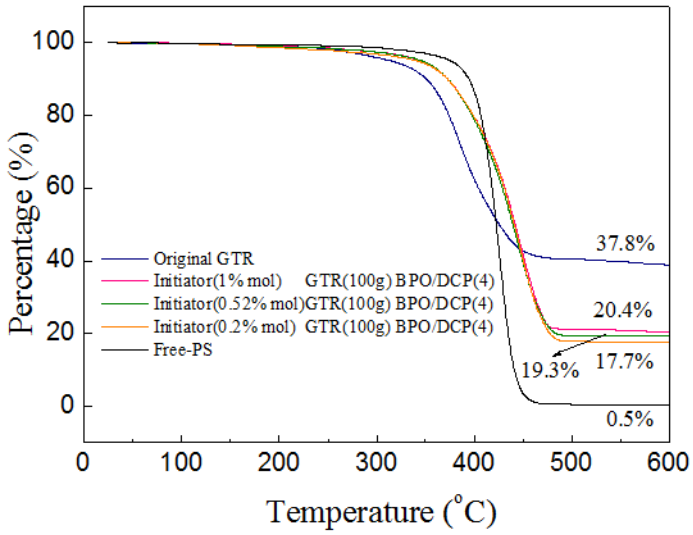

Figure 4.23 - Effect of concentration of initiator on the TGA of GTR-g-PS particles.

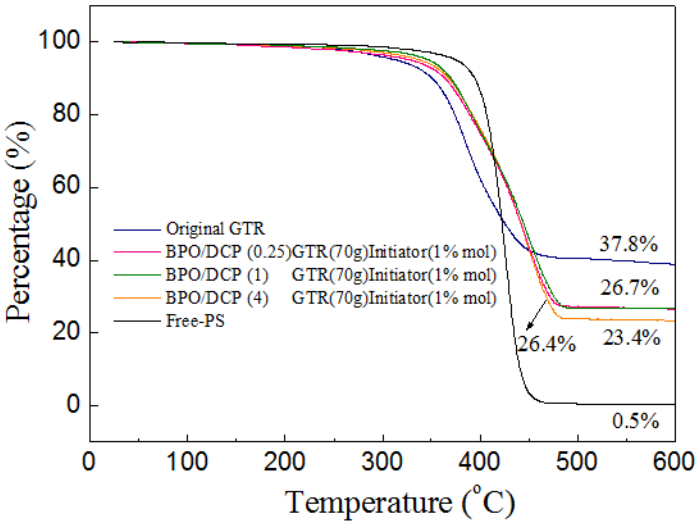

Figure 4.24 - Effect of BPO/DCP on the TGA of GTR-g-PS particles.

4.2.7 Effects of number of extrusion passage on the mechanical properties and size of the GTR-g-PS particles

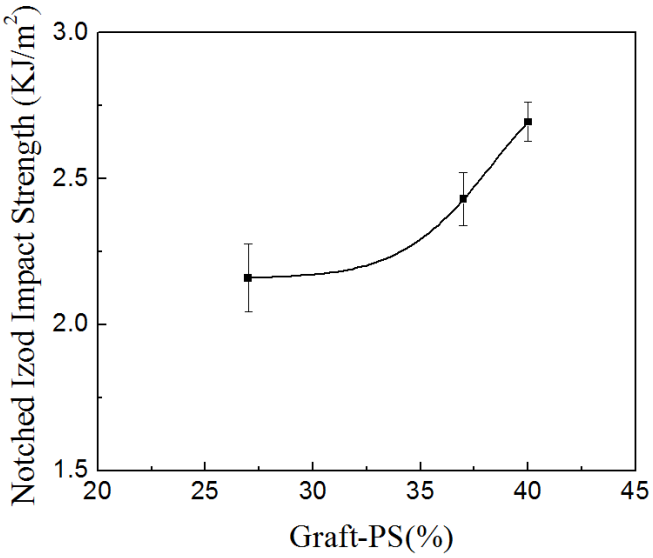

Figure 4.25 - Notched Izod impact strength of GTR-g-PS particles with different amount of Graft-PS.

Table 4.14 - Composition of GTR-g-PS and Free PS (% by weight), the experimental number are 9, 16 and 1.

NO	Equivalent-GTR (%)	Graft-PS (%)	Free-PS (%)
9	19	27	54
16	19	37	44
1	20	41	39

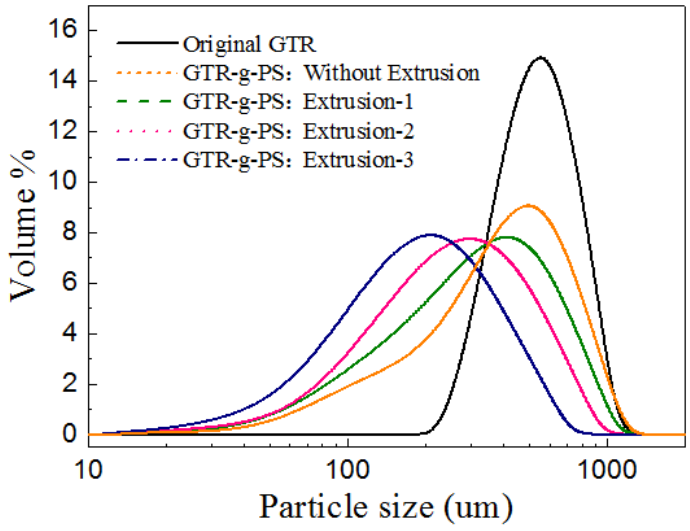

Figure 4.26 - Curves of the size distribution of original GTR particles and GTR-g-PS ones obtained by 0, 1, 2 or 3 times of extrusion.

Table 4.15 - Characteristic diameters of the original GTR particles and GTR-g-PS ones obtained by 0, 1, 2 or 3 times of extrusion.

	d(0.1) μm	d(0.5) μm	d(0.9) μm	Mean μm
Original GTR	328.9	535.4	843.1	**563.3**
GTR-g-PS without Extrusion	110.8	367.6	707.7	**392.3**
GTR-g-PS with Extrusion-1	92.2	293.2	625.9	**329.9**
GTR-g-PS with Exrtusion-2	86.5	237.1	520.5	**273.9**
GTR-g-PS with Extrusion-3	63.7	172.5	380.5	**200.3**

There are two key factors to toughen the PS using rubber, one is by improving the adhesion between the rubber and the PS matrix and the other is by reducing the particle size of rubber.

Table 4.14 presents the composition of GTR-g-PS and free PS of the products after polymerizations (NO 9, 16 and 1 in Table 4.17). Figure 4.25 shows an increase the St-g results in an increase in toughness. The highest St-g (41%) has the highest notched impact strength 2.21 KJ/m^2. The improvement in the impact strength of GTR-g-PS/PS composition is most likely attributable to a better dispersion of GTR particle in the PS matrix. Therefore, for this work, the higher grafting efficiency, the higher notched impact strength is achieved.

The size of the rubber particles is also very important in polymer matrix modification for improved mechanical behavior [28]. The mean size of GTR is decreased from 563.3μm of original GTR to 392.3μm of GTR after grafting with PS, and even decreased to 200.3μm after three times of extrusion. Generally, the size of rubber should be (0.5-2μm) to toughen the PS [24]. However, the particle size of GTR-g-PS particles (200μm) is still too high to toughen PS efficiently (Figure 4.26 and Table 4.15).

Conclusions

The effects of grafting factors on GE of GTR-g-PS particles were studied. These factors were the GTR content, initiator concentration and BPO/DPC. There was a tendency that the GE of PS onto the GTR powders was increased with increasing the GTR content, decreasing the initiator content and increasing the ratio between BPO and DCP, whereas the conversion of monomer was decreased. The glass transition temperature of GTR-g-PS particle was measured by DSC. It showed that the GTR-g-PS particle with higher GE resulted in the higher Tg. The thermal stability of GTR-g-PS was investigated by thermogravimetric analysis. The experimental results showed that the GTR-g-PS particles showed better thermal stability compared to the original GTR particles. For the notched Izod impact strength testing, it was concluded that the notched Izod impact strength of GTR-g-PS particle was increased with the higher GE. A reduction in size of the PS-graft-GTR particles was accomplished by extrusion. However, the particle size of GTR-g-PS particles was still too big to toughen PS.

4.3 ANNs model and kinetic model

4.3.1 Experimental design

In general, Design of Experiments (DoE) is a concept that uses a desired set of experiments to optimize or investigate a studied object. DoE can be used to plan experimental designs and perform sets of well selected experiments to get the most informative combination out of the given factors.

4.3.1.1 Selection of operating conditions

The preliminary experiments as well as the knowledge already acquired on the polymerization of styrene inside the cross-linked GTR particles led us to choose three factors (G/M, I/M and BPO/DCP) as the most important conditions affecting the desired properties of the produced polymer. Subsequently, a variation range is set for each of these factors, on the basis of the physical boundaries and limitations of the process. A normalized range between [−1,+1] is finally obtained, as shown in Table 4.16.

Table 4.16 - Variation range of the different factors.

Factor	- 1	0	+1
G/M(g/g)	70/400	85/400	100/400
I/M(% mol)	0.2	0.6	1.0
BPO/DCP(mol/mol)	0.25	1	4

4.3.1.2 D-optimality criterion

In order to obtain a valid model of the process, a series of experiments must be carried out. The D-Optimality criterion is the most common criterion of DoE, after the full factorial designs that usually lead to unrealistically large numbers of experiments (i.e., for the exploitation of an experimental space composed of more than 2 factors

with several levels). It is based on the principle of maximizing $|(X^TX)|$, the determinant of the information matrix (X^TX), while is equivalent to minimizing the determinant of the dispersion matrix $(X^TX)^{-1}$. This procedure ensures an optimal representation of the experimental space by a limited number of experimental runs [108]. In the present study, a total of twenty one (21) different experimental runs were identified, over the 1331 experiments that result for a normalized step change of the order of 0.2 for the three factors. The experimental conditions of these 21 experiments are given in Table 4.17.

Table 4.17 - DOE of the different factors.

Exp Number	G/M	I/M	BPO/DCP
1	1	1	-1
2	1	0.4	0.2
3	1	-1	1
4	1	-1	-1
5	0	1	1
6	0	0	-1
7	0	-1	0
8	-1	1	-1
9	-1	1	-1
10	-1	0.4	1
11	-1	-1	1
12	-1	-1	-1
13	1	1	1
14	0	0	0
15	1	-0.2	1
16	0	1	-1
17	0	0	0
18	-1	1	1
19	-1	0	-1
20	0	0	0
21	-1	-1	0

The center point of the experimental design is replicated three times in order to obtain the confidence interval of the calculated coefficients of the model and to assess the reproducibility of the manipulations (Table 4.17 NO 14, 17, 20). The D-optimal design methodology was implemented in terms of custom created computer algorithm on Matlab®.

When the result P_i of an experiment x_j can be predicted by $P_i = f^T(x_j)\,\theta$ where θ is a vector of coefficients, a set P of experiments can be modeled by $P = X\,\theta$, where X is the matrix of the row vectors $f^T(x_j)$ and x_j the vector of factors which defines the j^{th} experiment. When the results of the experiments are obtained, the vector of coefficients can be calculated.

Equation 4.1 gives the confidence region for the coefficients [109].

$$(\theta - \hat{\theta})^T (X^T - X)(\theta - \hat{\theta}) \leq \frac{p}{q-p}(e^T e) F_\alpha(p, q-p) \tag{4.1}$$

Here:

$\hat{\theta}$: vector of calculated coefficients,

θ : the vector of unknown coefficients,

e : vector of residues,

X: model matrix.

p : number of coefficients of the model,

q : e number of experiments,

Fa : Fisher-Snedecor variable with a probability α [110].

When fitting the model to the experimental data, the experimental error and the model error are transmitted to the coefficients. An ellipsoid describes the confidence interval for each coefficient (Figure 4.27). σ_m^2 is the experimental variance. σ_r^2, is the error variance on the coefficients of the model. The smaller the axes, the more precise are the coefficients and consequently, the more accurate are the predictions. The volume of this ellipsoid is inversely proportional to the square root of the determinant of the information matrix. The D-optimality criterion leads to the

maximization of this determinant, which is the same as minimizing the volume of the ellipsoid [111].

A 2D representation of the confidence region is shown in Figure 4.27 For a number of degrees of freedom different from zero, there is a confidence region, [$\hat{\theta}_{min}$; $\hat{\theta}_{max}$], for the parameter $\hat{\theta}$ based on Eq. (4.1) [112].

$$\hat{\theta}_i - \sigma_r^2\sqrt{p \cdot F_{0.05}(p, q-p) \cdot (X^T X)^{-1}_{ii}} \leq \theta_i \leq \hat{\theta}_i + \sigma_r^2\sqrt{p \cdot F_{0.05}(p, q-p) \cdot (X^T X)^{-1}_{ii}} \quad (4.2)$$

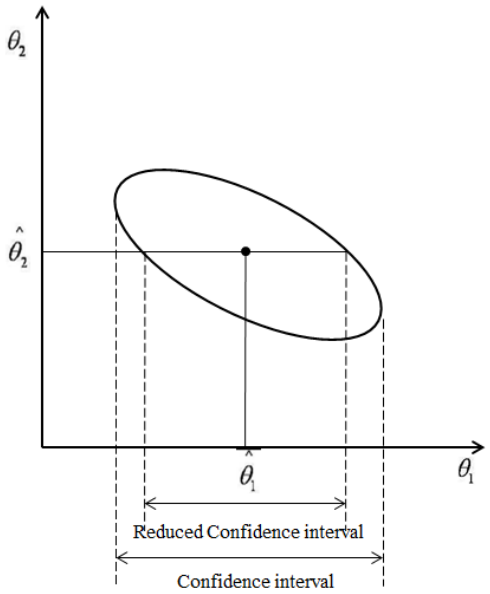

Figure 4.27 - 2D representation of the confidence region and the reduced interval.

It also gives information on the degree of correlation of the coefficients considered. A reduced confidence interval, red[$\hat{\theta}_{min}$; $\hat{\theta}_{max}$], is also calculated considering all the coefficients at their optimal value except one

$$\hat{\theta}_i - \sigma_r^2\sqrt{\frac{p \cdot F_{0.05}(p, q-p)}{(X^T X)^{-1}_{ii}}} \leq \theta_i \leq \hat{\theta}_i + \sigma_r^2\sqrt{\frac{p \cdot F_{0.05}(p, q-p)}{(X^T X)^{-1}_{ii}}} \quad (4.3)$$

This interval is used to determine whether the parameter value is significantly different from zero. If 0 belongs to the confidence interval, the corresponding coefficient is negligible [112].

4.3.1.3 Polynomial model description

On the basis of the experimental design, an initial simple model can be developed. A possibility is to consider the reactor as a black box and to develop empirical relationships between factors and conversion and GE. Polynomials allow to simulate, with a given precision, any set of experimental values. The only restriction is to choose a high enough degree to obtain a satisfactory representation of the phenomenon and small enough to avoid a too high number of parameters. In order to determine a polynomial model, the first step is to begin by a first-degree model. However such a model does not permit to treat non-linear phenomena. For this reason, a second-degree polynomial model has been chosen so as to be able to represent the non-linear phenomena of the process in a satisfactory way.

Besides the quadratic terms, a set of multiplicative terms was also included in the model expression to better simulation the binary linear effects of the factors. Indeed, a quadratic model with three factors has the following form:

$$P_i = \theta_0 + \theta_1 x_{1,i} + \theta_2 x_{2,i} + \theta_3 x_{3,i} + \theta_4 x_{1,i}^2 + \theta_5 x_{2,i}^2 + \theta_6 x_{3,i}^2 + \ldots$$
$$+ \theta_7 x_{1,i} x_{2,i} + \theta_8 x_{1,i} x_{3,i} + \theta_9 x_{2,i} x_{3,i} + \varepsilon_i \quad (4.4)$$

where i is each experiment, ε is the unknown experimental error, x_1, x_2 and x_3 represent GTR content, initiator concentration and BPO/DCP, respectively. θ is the model coefficient.

This leads to a system of equations represented in the following matrix form

$$\mathbf{P} = \mathbf{X}\boldsymbol{\theta} + \varepsilon \quad (4.5)$$

The model coefficients were calculated using a multilinear regression. A 95% confidence interval is defined to estimate the uncertainty on the calculated coefficients:[113]

$$\hat{\theta} = (X^T X)^{-1} \cdot X^T \cdot P \tag{4.6}$$

4.3.1.4 Reduction of the model

Model reduction could simplify a model by eliminating insignificant terms. Reducing the number of terms can make the model easier to work with. The degree of freedom is equal to the number of experiments selected for estimation model minus the number of coefficients. Moreover, the degree of freedom should be higher than zero for the validation of the model. It could minimize the coefficients which is not very important of the model. A model can be reduced manually, or it can be reduced automatically using an algorithmic procedure, such as stepwise regression. In this work, the confidence interval determined for each coefficient was used to reduce the model. Figure 4.28 shows the methodology of reduction of model. When a cycle is completed, the number of coefficients in the model dropped a unity. After eliminating unimportant factor, a new polynomial model cycle will stop until zero belongs to no confidence intervals, which will lead to the final model.

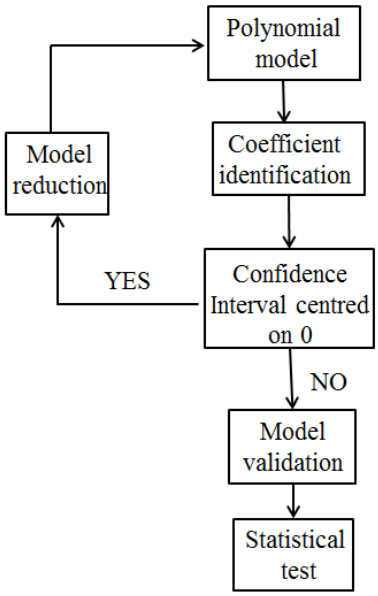

Figure 4.28 - Steps of the polynomial modelling.

4.3.1.5 Modelling results

The experimental design strategy was initially implemented to identify the experiments that would serve for the identification of the model parameters (i.e., 12 experiments in total, NO1-NO12). Subsequently, the same procedure was followed in order to increase this number of experiments by 6 additional experiments (i.e., NO13 NO15 NO16 NO18 NO 19 NO21) that would serve for the model validation, whilst 3 repetition experiments at the center of the domain (i.e., NO 14 NO17 NO20) were also included in the overall design.

Table 4.18 - Fisher-Snedecor test for conversion of styrene

Ratio	1/F0.025	$F=\sigma_1^2/\sigma_2^2$	F0.025	Validation
Identification/Validation	0.4590	0.5361	2.3082	Yes
Identification/Replication	0.4278	0.6960	2.7324	Yes
Validation/ Replication	0.3901	1.2983	2.8282	Yes

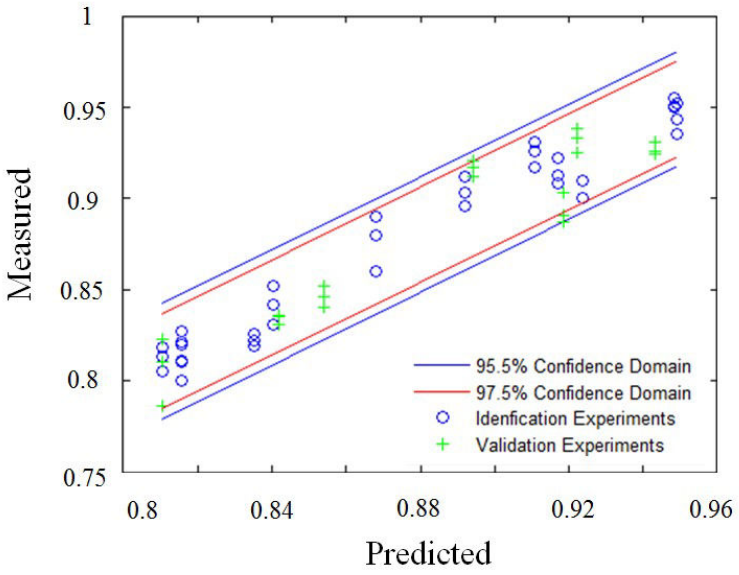

Figure 4.29 - Student test for conversion of styrene.

Table 4.19 - Fisher-Snedecor test for GE of styrene.

Ratio	1/F0.025	$F=\sigma_1^2/\sigma_2^2$	F0.025	Validation
Identification/Validation	0.4719	0.9159	2.2010	Yes
Identification/Replication	0.4308	0.5412	2.7250	Yes
Validation/ Replication	0.4052	0.5909	2.7888	Yes

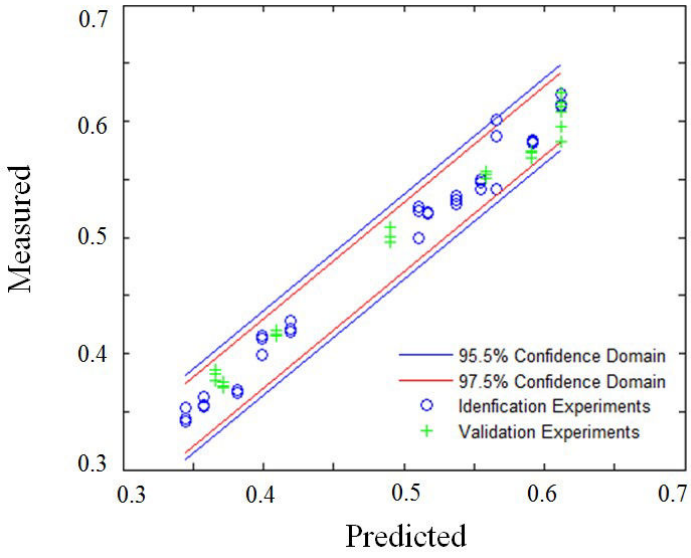

Figure 4.30 - Student test for GE of styrene.

According to the Fisher-Snedecor statistical test [114] (Table 4.18 and 4.19), both model of monomer conversion and GE are validated, while from Student test (Figure 4.29 and 4.30), most of the data points for the validation and replication are found to be within the 95.5% and 97.5 % confidence intervals. The final values of the model coefficients for the conversion quadratic model and GE quadratic model are given in Tables 4.20 and 4.21, respectively.

Table 4.20 - Values of coefficients of conversion quadratic model.

Coefficients	Values of θ	Significant
θ_0	0.8696	Yes
θ_1	-0.0123	Yes
θ_2	0.0540	Yes
θ_3	-0.0025	Yes
θ_4	0	No
θ_5	-0.0039	Yes
θ_6	0	No
θ_7	0	No
θ_8	0	No
θ_9	0	No

Table 4.21 - Values of coefficients of GE quadratic model.

Coefficients	Values of θ	Significant
θ_0	0.5277	Yes
θ_1	0.0964	Yes
θ_2	-0.271	Yes
θ_3	0.0103	Yes
θ_4	-0.0491	Yes
θ_5	0	No
θ_6	0	No
θ_7	0	No
θ_8	0	No
θ_9	0	No

Due to the great number of model reduction steps, it was decided that the final form of the model was very simple to represent the non-linear nature of the system. To overcome this problem, a new form of the model expression should be tested all over again or a different modeling approach should be adopted. The second option was adopted and an Artificial Neural Network modeling approach was selected, in order to better capture the highly non-linear, complex character of the process. The characteristics and results of this new model are presented in next section. In what follows, a series of experimental measurements is presented that show the effects of the different process conditions on the measured properties of the produced polymer.

4.3.2 Results of ANNs model

In the present work, an Artificial Neural Network (ANN) model is implemented to investigate the influence of three principal factors of the process, related to the initial amounts of GTR, styrene and initiators, on two types of response (i.e., properties or indexes) of the process, namely the overall styrene conversion and the grafting percentage of styrene onto ground tire rubber. For this, a three-layered feed-forward back-propagation ANN configuration is chosen comprised of an input layer (i.e., containing the independent variables or factors of the system), an output layer (dependent variable) and a hidden layer.

The "training" of the developed networks (i.e., the process of identification of the values of the different weights and biases, c.f. Section 1.5) is carried out on the basis of a total of 75 experimental data sets from 21 experiments that have been produced under different combinations of the input parameters. These data are randomly divided into three distinct subcategories, namely the *training*, *testing* and *validation* data sets that correspond to 70%, 15% and 15% of the total data, respectively. The testing and validation data subsets serve for the monitoring of the training process, in order to avoid "over fitting" problems, and to the comparison of the produced model to a set of unused data, respectively.

In order to identify the optimal architecture of the implemented ANN models (i.e., two models are developed, one for the simulation of the monomer conversion and a second one for the simulation of the grafting efficiency (GE) of the process), the accuracy of different model structures is assessed on the basis of different statistical indexes. The two most commonly used criteria are the determination coefficient of a linear regression of a plot of the simulated versus the experimental output (also referred to as targets) as well as the mean squared error (MSE) of the simulated output in terms of the targets:

$$MSE = \frac{1}{N}\sum_{i=1}^{N}\left(y_{i,pred} - y_{i,\exp}\right)^2 \tag{4.6}$$

In Eq 4.6, N is the number of data points and $y_{i,pred}$ and $y_{i,exp}$ are the predicted and experimental data, respectively.

These tests can be performed over the complete data set as well as over the different data subsets. An indicative number of cases of such an analysis of the structure of the two developed models, in terms of the value of the determination coefficient, is given in Tables 4.22 and 4.23. As can be seen, the overall accuracy of the models is quite high, with the values of R^2 ranging from 85% to over 99%. The finally selected architectures are marked in bold. The respective plots are given in Figures 4.31 and 4.33.

Table 4.22 - Results of different ANN model structures of training, validation, testing and all R^2 for GE.

ANN model structure	R^2			
	Training	validation	Testing	All
10-0-0	0.932	0.912	0.845	0.899
10-8-0	0.981	0.962	0.958	0.978
5-8-4	0.998	0.991	0.984	0.992
10-4-6	0.997	0.993	0.991	0.992
4-9-10	**0.997**	**0.995**	**0.991**	**0.993**
5-9-10-8	0.994	0.984	0.971	0.981

Table 4.23 - Results of different ANN model structures of training, validation, testing and all R^2 for Conversion.

ANN model structure	R^2			
	Training	validation	Testing	All
10-0-0	0.914	0.884	0.862	0.871
10-8-0	0.974	0.945	0.884	0.934
10-8-2	0.979	0.978	0.978	0.978
5-7-4	0.978	0.977	0.977	0.977

8-7-5	**0.980**	**0.977**	**0.977**	**0.979**
4-9-2-3	0.969	0.967	0.951	0.966

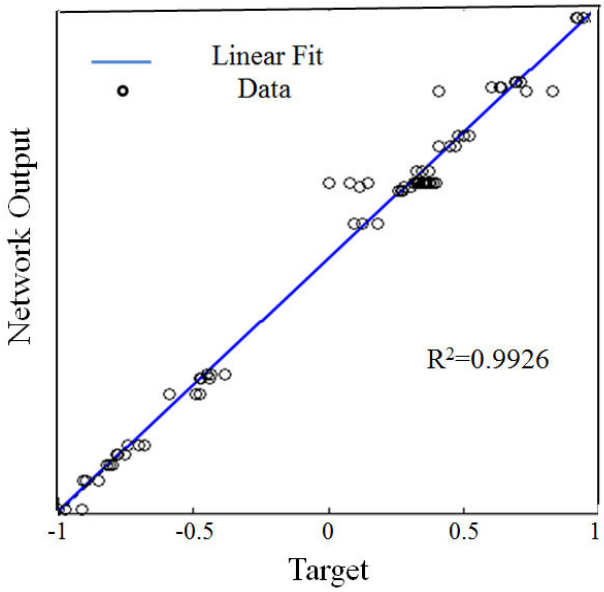

Figure 4.31 - Network outputs (GE) versus targets with the structure (4 9 10).

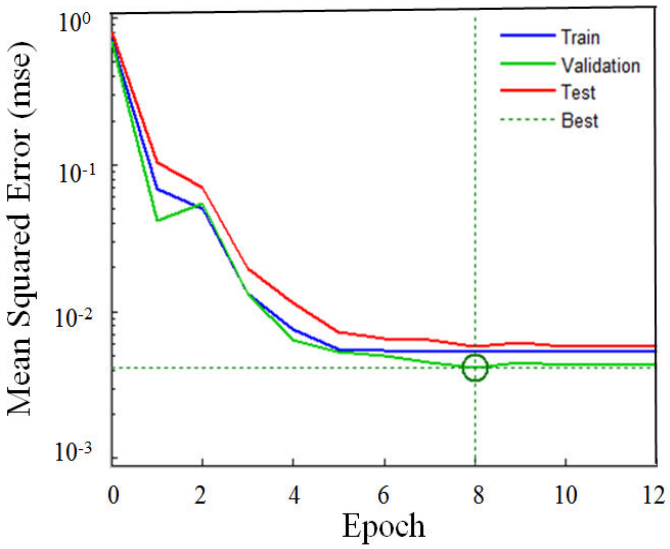

Figure 4.32 - Mean squared error history versus epoch during training, validation and testing of the network of GE with the structure (4 9 10).

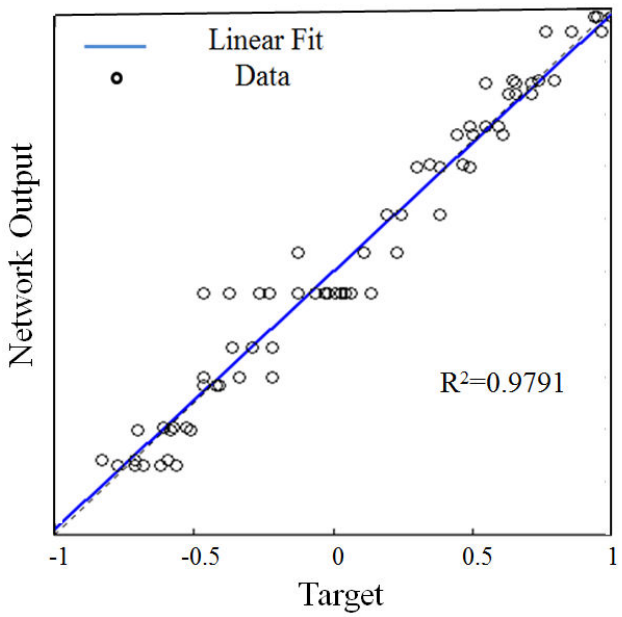

Figure 4.33 - Network outputs (conversion) versus targets with the structure (8 7 5).

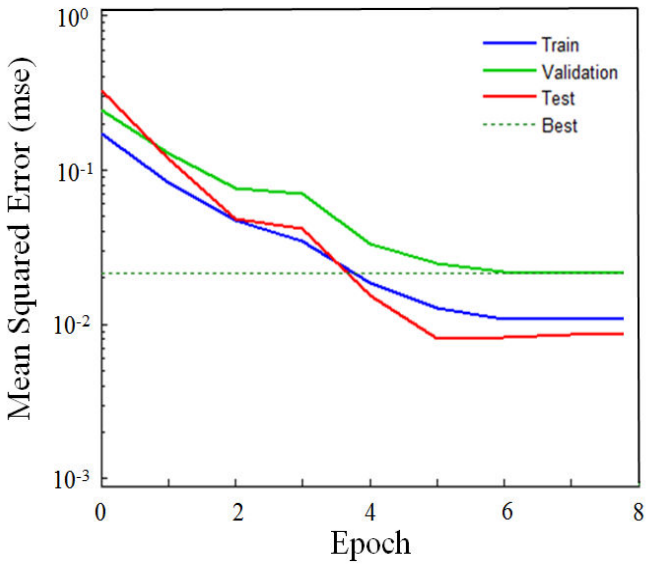

Figure 4.34 - Mean squared error history versus epoch during training, validation and testing of the network of conversion with the structure (8 7 5).

Figures 4.32 and 4.34 show the convergence characteristics of the ANN models of GE and conversion during training, validation and testing phases, respectively. It is clearly seen that the MSE is high in the early stages of the training process, but decrease in later iterations to reach a minimum value for the “trained” model.

Table 4.24 – Optimal results of different structure of ANNs models of monomer conversion and GE.

NO	ANNs		Conditions			Optimal Results	
	Structure for conversion	Structure for GE	GTR/M (g/g)	I/M (% mol)	BPO/DCP (mol/mol)	Conversion (%)	GE (%)
1	10-0-0	10-0-0	91.7 / 400	0.847	3.91	88.8	63.0
2	10-8-0	10-8-0	99.3 / 400	0.598	2.29	86.1	61.4
3	10-8-2	5-8-4	99.8 / 400	0.441	2.13	86.5	61.0
4	5-7-4	10-4-6	99.9 / 400	0.548	2.96	87.2	58.7
5	**8-7-5**	**4-9-10**	**91.8 / 400**	**0.761**	**1.97**	**89.9**	**65.3**

The aim of this work is to obtain both of high monomer conversion and high graft efficiency of styrene with ground tire rubber. Traditionally, optimizing this process has been done by minimizing an objective cost function made up of the weighted sum of all individual criteria. However, this approach often fails because of the difficulty to attribute a relative weight to individual criteria and because of the large number of local minima inherent in these complex systems [112]. Recent progress in multicriteria optimization has led to methods for obtaining a solution to these complex problems using the knowledge of a human expert in a natural way.

In this work, we used the evolutionary algorithm (EA) to optimize the reaction conditions to obtain both the high monomer conversion and the high graft efficiency of styrene with GTR. It was based on the ANNs models of monomer conversion and GE. Evolutionary algorithm is a direct search algorithm that is based on the natural evolution concept coming from Darwin s theory of evolution [115]. Table 4.24 showed the optimal results of monomer conversion and graft efficiency of styrene with GTR with the different structure of ANN models of monomer conversion and GE. No 5 was chosen for validation of the optimal result due to the highest monomer conversion and GE. An experimental validation test was conducted to verify the improvement in the chosen responses using the predicted optimal reaction conditions of No 5.

The experimental values of monomer conversion and GE were found to be 88.2±2% and 64.1±4%, which gave predicted results as 89.9% and 65.3%, respectively (Table 4.25). It was seen that this experimental values was closed to the predicted results obtained for No 5.

Table 4.25 –Simulation and experimental values of optimal results of No 5.

NO 5	Conversion(%)		GE(%)	
	Experiment	Simulation	Experiment	Simulation
	88.2±2	89.9	64.1±4	65.3

4.3.3 Results of kinetic model

4.3.3.1 Model development

For the estimation of the model parameters, the ranking of parameters should be established at first. Recent work by Woloszyn et al. [82], [83] showed the approach to parameter selection and estimation of polymerization of styrene. They considered that the rate of chemical initiation, transfer reaction and the onset time for gel effect were the key factor to influence the conversion of styrene and molecular weight of polystyrene. In this work, these conditions are also taken into account. Firstly, 12 are used for the estimation of the model parameters. Then, the remaining 9 experiments are used for the comparison and validation of the developed model. The importance for the various model parameters is identified on the basis of the literature data. Table 4.26 gives the lower and higher bounds of the pre-exponential factors and activation energies for each parameter (i.e., considering an Arrhenius function for the kinetic rate constants). In Table 4.27 the values of the parameters used in the calculation of the diffusion-controlled rate constants are reported [65]. In order to differentiate the propagation and termination rate constants between reactions where free chains participate and reactions that take place exclusively between grafted chains, k_{pG} and k_{tG} rate constants are added into the model. The k_{pG} and k_{tG} constants (for the grafted chains) are expected to be lower due to decreased mobility. The values of the rates k_{pG}/k_p and k_{tG}/k_t were set via the model fitting procedure to 0.6 and 0.4, respectively.

Table 4.26 - Literature values of the pre-exponential factors and activation energies for the kinetic rate constants.

Par.	Pre-exponential factor	Lower bound	Higher bound	E	Lower bound	Higher bound	Ref
$k_{d\mathrm{BPO}}$	3.06×10^{13}	2.88×10^{12}	1.7×10^{15}	29.68	27.21	30.39	[96],[82]
$k_{d\mathrm{DCP}}$	9.16×10^{15}	3.06×10^{12}	1.0×10^{16}	36.65	30.01	36.65	[82],[97]
$k_{i1\mathrm{BPO}}$	1.02×10^{7}	1.02×10^{7}	7.138×10^{9}	7.068	6.572	11.159	[80], [96]
k_{i1DCP}	1.02×10^{7}	1.02×10^{7}	7.138×10^{9}	7.068	6.572	11.159	[80], [96]
k_1	7.3×10^{6}	3.21×10^{4}	7.3×10^{6}	26.440	22.251	26.440	[82],[65]
k_{-1}	1.14×10^{2}	1.14×10^{2}	1.73×10^{6}	13.533	13.533	22.251	[82], [65]
k_2	1.63×10^{6}	1.63×10^{6}	1.44×10^{7}	23.883	22.3	23.883	[82], [65]
k_A	1.02×10^{7}	1.02×10^{7}	7.138×10^{9}	7.068	6.572	11.159	[80], [96], [65]
k_B	1.02×10^{7}	1.02×10^{7}	7.138×10^{9}	7.068	6.572	11.159	[80], [96], [65]
k_C	3.93×10^{4}	-	3.93×10^{4}	21.346	-	21.346	[65]
k_{i2}	1.02×10^{7}	1.02×10^{7}	7.138×10^{9}	7.068	6.572	11.159	[80], [96], [74]
k_p	1.02×10^{7}	1.02×10^{7}	7.138×10^{9}	7.068	6.572	11.159	[80], [96]
k_{fm}	2.31×10^{6}	2.31×10^{6}	7.67×10^{7}	12.672	12.672	14.43	[65], [98]
k_{fa}	5.79×10^{6}	1.04×10^{6}	1.22×10^{7}	30.8	23.3	30.8	[82], [65]
k_S	3.30×10^{5}	-	3.30×10^{5}	30.1		30.1	[82]
k_{tc}	1.34×10^{9}	2.67×10^{8}	1.02×10^{11}	2.084	1.49	4.46	[76], [98]
k_{td}	1.53×10^{8}	-	1.53×10^{8}	1.496		1.496	[82]
k_{tpr}	1.06×10^{9}	-	1.06×10^{9}	1.496		1.496	[82]
k_{tprg}	-	-	-	-	-	-	

Units (kcal, L, mol, s.)

Table 4.27 - Parameters of the styrene/PS/GTR system.

Parameters	Units
$d_{\mathrm{m}} = 0.9236 - 0.887\times10^{-3}\ (\mathrm{T} - 273.15)$	$\mathrm{g \cdot cm^{-3}}$
$d_{\mathrm{P}} = 1.085 - 6.05\times10^{-4}\ (\mathrm{T} - 273.15)$	$\mathrm{g \cdot cm^{-3}}$
$d_{\mathrm{I\,BPO}} = 1.16\ ;\ d_{\mathrm{I\,DCP}} = 1.56\ ;\ d_{\mathrm{I\,GRR}} = 0.42$	$\mathrm{g \cdot cm^{-3}}$
$k_B = 1.3806488\times10^{-23}$	$\mathrm{m^2 \cdot kg \cdot s^{-2} \cdot K^{-1}}$
$T_{gm} = 185.0;\ T_{gp} = 378.0$	K

The ranking of the parameters is carried out on the basis of the degree of influence on conversion and molecular weight of the polymer. The initiation reaction is of critical importance for the polymerization, with the decomposition parameters of initiator displaying an important influence on conversion and molecular weight of

polymer. Therefore, the k_d of the initiators should be considered at first. Then, the chain transfer reaction, termination and the thermal initiation are considered in turn from the list of Table 4.28.

Table 4.28 - Ranked list of parameters of graft polymerization and the final estimated value of pre-exponential factors and activation energies for kinetic parameter.

Rank	Parameter	Final estimated value	Final E
1	$\boldsymbol{k_{d\mathrm{DCP}}}$	$\mathbf{3.05\times10^{15}}$	**35.65**
2	$\boldsymbol{k_{d\mathrm{BPO}}}$	$\mathbf{4.59\times10^{13}}$	**29.68**
3	$\boldsymbol{k_{tc}}$	$\mathbf{2.34\times10^{9}}$	**2.084**
4	$\boldsymbol{k_{tcG}}$	$\mathbf{9.36\times10^{8}}$	**2.084**
5	$\boldsymbol{k_{fm}}$	$\mathbf{5.77\times10^{6}}$	**12.672**
6	k_{fg}	34.047	1.67
7	k_{td}	1.53×10^{8}	1.49
8	k_{tdG}	6.12×10^{7}	1.49
9	k_{fa}	5.79×10^{6}	30.8
10	k_p	3.264×10^{7}	7.068
11	k_{pG}	1.958×10^{7}	7.068
12	$k_{i1\mathrm{BPO}}$	3.264×10^{7}	7.068
13	k_{i1DCP}	3.264×10^{7}	7.068
14	k_1	7.3×10^{6}	26.44
15	k_{-1}	1.14×10^{2}	13.53
16	k_2	1.63×10^{6}	1.670
17	k_A	3.264×10^{7}	7.068
18	k_B	3.264×10^{7}	7.068
19	k_C	3.93×10^{4}	2.135
20	k_{iG}	2.16×10^{8}	7.068
21	k_{i2}	3.264×10^{7}	7.068
22	k_S	3.30×10^{5}	30.1
23	k_{tpr}	1.06×10^{9}	1.49
24	k_{tprg}	-	-

Units (kcal, L, mol, s.)

The description of diffusion controlled reactions is based on the free volume theory. Therefore the most influence parameter of the free volume of the system should be concerned firstly of ranking of the parameters of diffusion controlled reactions. From the expression of the diffusion controlled reactions, the total free volume of the system (V_f) influence other rate constants (k_p, k_t) at the different stages

of the polymerization. The ranked list of parameters used in the diffusion-control model is presented in Table 4.29.

Table 4.29 - Ranked list of parameters used in diffusion-control equations.

Rank	Symbol	Final values	Units	Lower bound	Higher bound	Ref.
1	**α_m**	**1.0×10^{-3}**	**K^{-1}**	**5.0×10^{-4}**	**1.5×10^{-3}**	[82] [106]
2	**α_p**	**4.8×10^{-4}**	**K^{-1}**	**2.4×10^{-4}**	**7.2×10^{-4}**	[82] [106]
3	***A***	**0.348**	**unitless**	**0.17**	**0.52**	[82] [106]
4	***n***	**2.5**	**cal/mol**	**1.1**	**2.5**	[82] [106]
5	**E_{crm}**	**1.74×10^{3}**	**cal· mol^{-1}**	**1.0×10^{3}**	**2.3×10^{3}**	[82]
6	A_{crm}	0.331	unitless	0.251	0.331	[82]
7	*B*	0.5	unitless	0.5	1	[82] [106]
8	C_{rRatio}	0.8	unitless	0	1	[82]
9	*C*	0.45	unitless	0.5	1	[82]
10	jc	175	num	88	260	[82] [65]
11	δ	3.8×10^{-10}	m·num-$^{0.5}$	3.8×10^{-10}	1.1×10^{-9}	[82] [78]
12	σ	3.7×10^{-10}	m	3.7×10^{-10}	1.1×10^{-9}	[82] [78]
13	δ_c	5.0×10^{-4}	L· g^{-1}	5.0×10^{-4}	1.5×10^{-3}	[82]
14	A_{cr}	9.44	$(g\cdot mol^{-1})^{0.5}$	-	9.44	[106]
15	E_{cr}	1.929×10^{3}	1· K^{-1}	-	1.929×10^{3}	[82] [106]

There are several ways to increase the match between model predictions and experimental data, such as the use of automated estimation or optimization routines. For example, Rached et al.(2013) [116] determined the parameters of the developed model via the implementation of an evolutionary algorithm in order to minimize the error of the model. Another commonly employed approach is based on a "manual" tuning of the parameters until the model predictions match the experimental data. In this work, several influential parameters values are tuned by hand [117]. According to the ranking of parameters, the appropriate model parameters are adjusted by comparing the simulation results with the experimental data. The comparison between experimental measurements and theoretical predictions of monomer conversion for estimation is shown in Figure 4.35, while the GE are given in Figure 4.36.

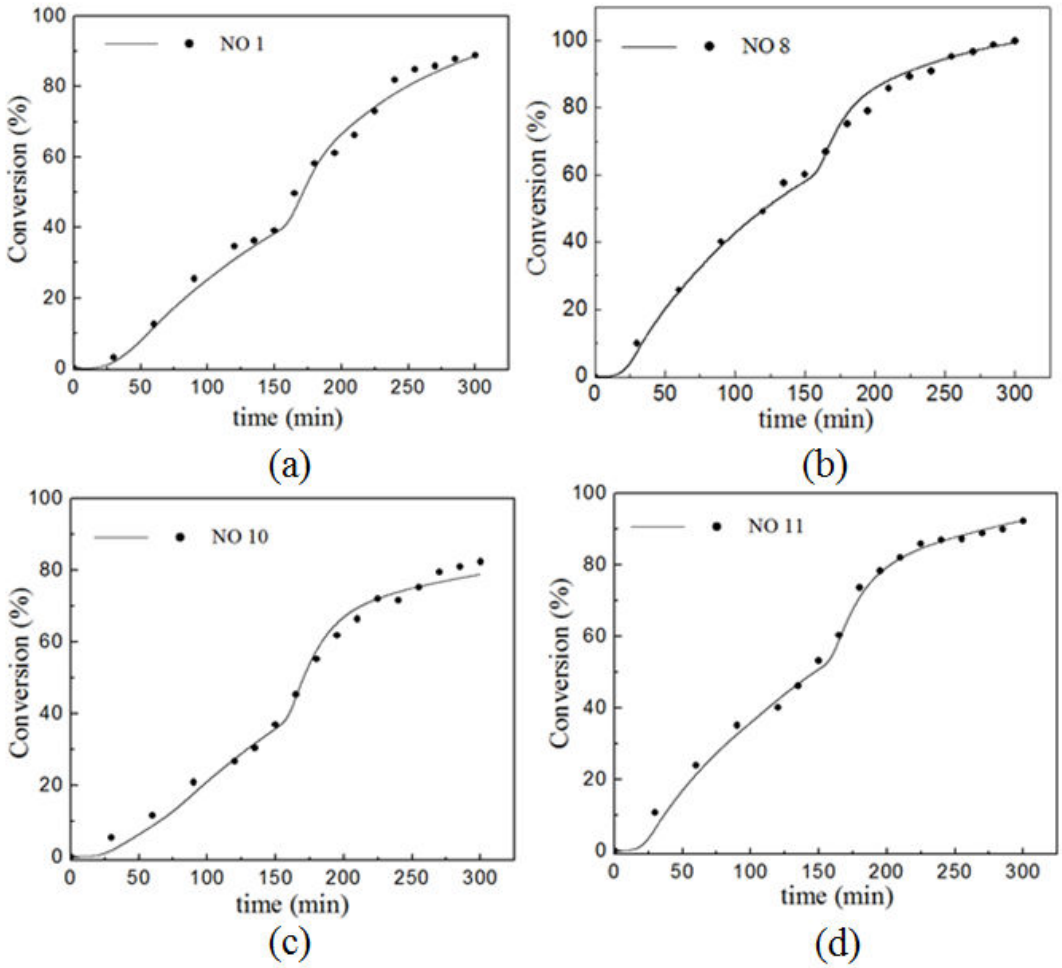

Figure 4.35 - Comparison between experimental measurements (points) and theoretical predictions (lines) of the evolution of monomer conversion under different experimental conditions.

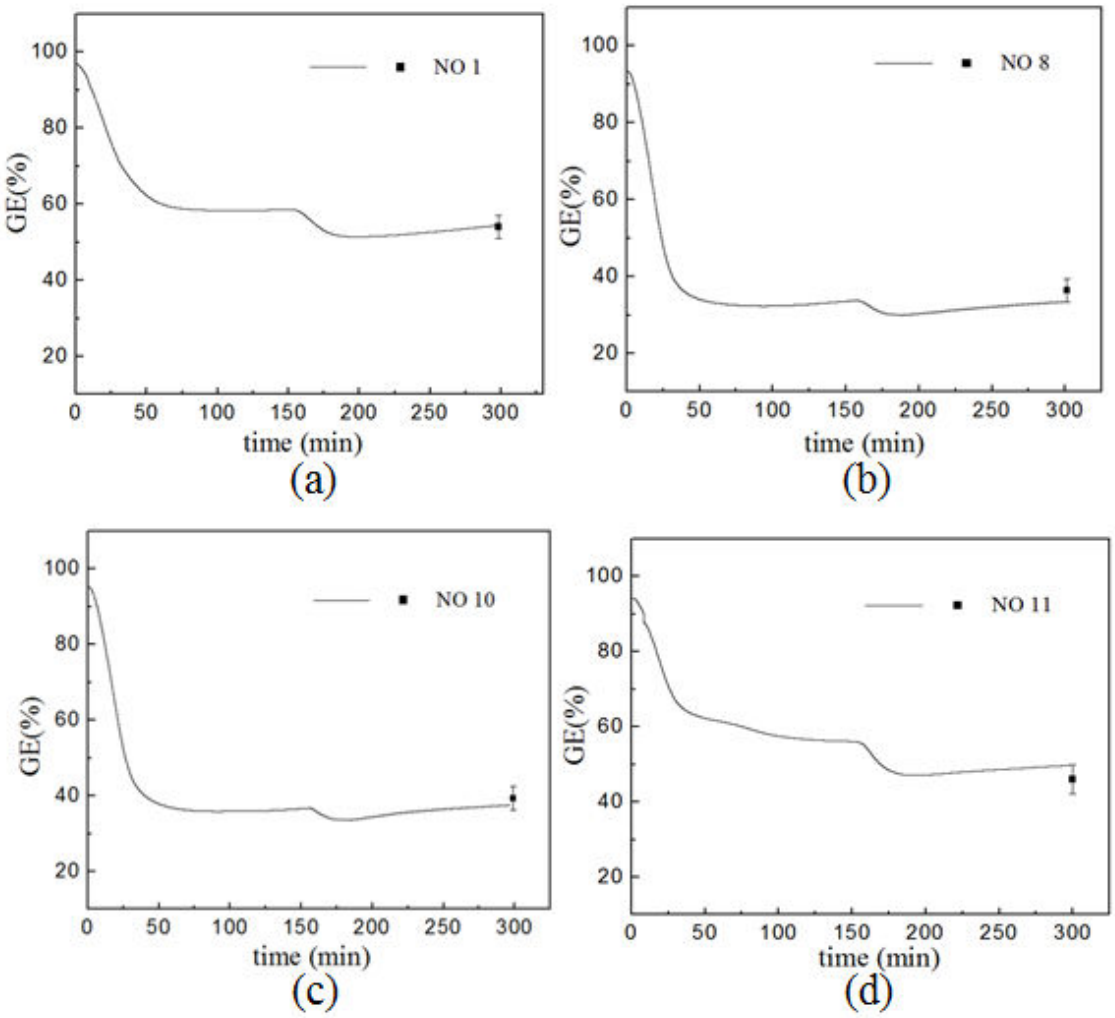

Figure 4.36 - Comparison between experimental measurements of the final value (points) and theoretical predictions (lines) of the evolution of GE, under different experimental conditions.

Adequate control of temperature and good heat transfer can increase the accuracy of kinetic model. The temperature of the polymerization was 90℃for 2.5 hours and was then increased to 120℃ for 2.5 hours. The reaction temperature was controlled by the oil bath cooling system. The good control of reaction temperature is shown in Figure 4.37.

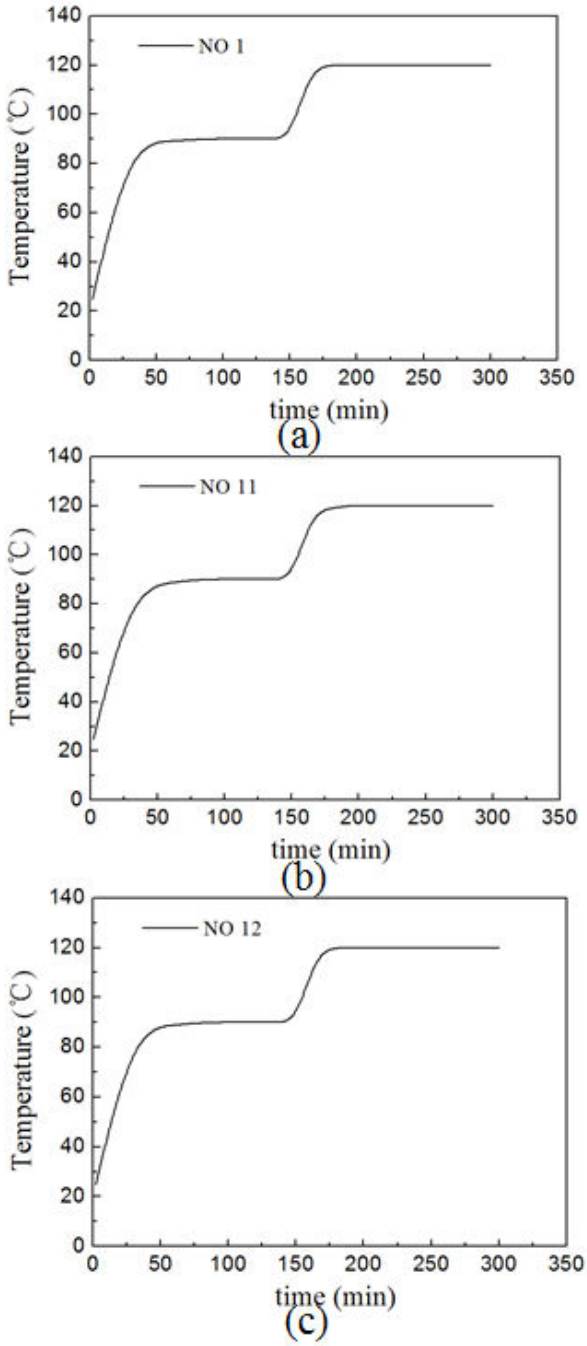

Figure 4.37 - Temperature of the polymerization of styrene onto GTR particles.

4.3.3.2 Model Validation

In order to validate the developed model, the model predictions were compared with a series of new experimental data (i.e., experiments 13-21 of Table 4.17), different the ones used for the estimation of the model parameters (i.e, experiments 1-12 of Table 4.17). The comparisons showed a very good agreement between the model predictions and experimental measurements, thus providing proof

of the accuracy and validity of the developed kinetic model. Some indicative results of this comparison are shown in Figures 4.38 and 4.39.

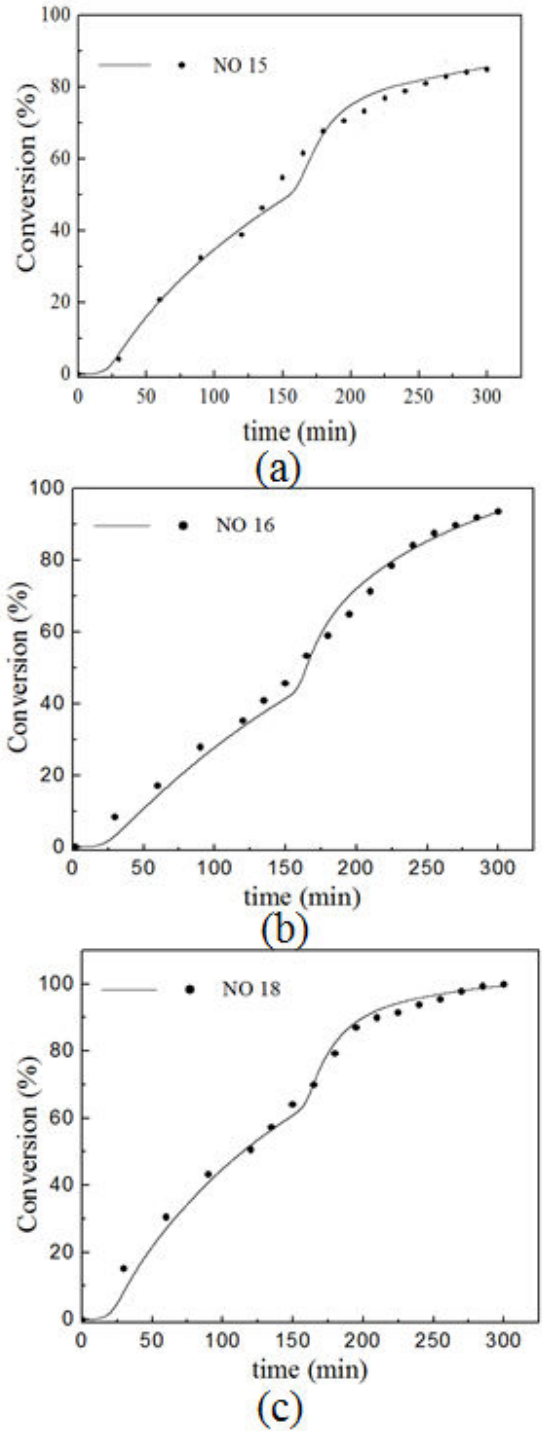

Figure 4.38 - Comparison between experimental measurements (points) and theoretical predictions (lines) of the evolution of monomer conversion, under different experimental conditions.

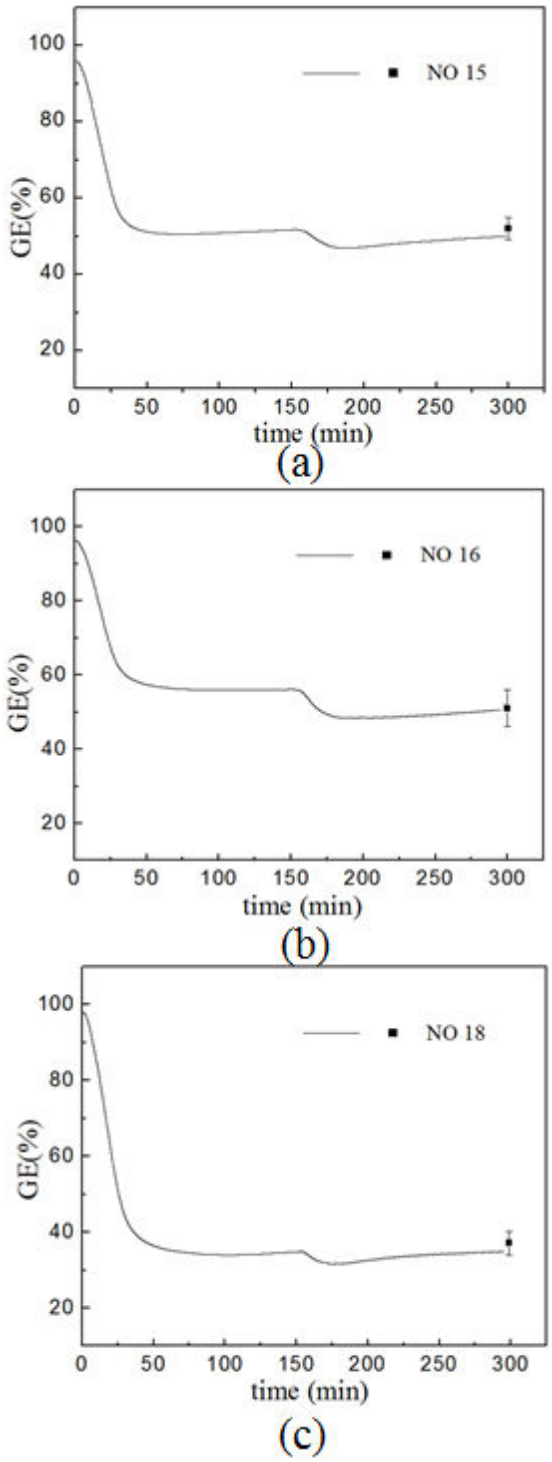

Figure 4.39 - Comparison between experimental measurements at the end of the polymerization (points) and theoretical predictions (lines) of the evolution of GE, under different experimental conditions.

4.3.3.3 Effect of GTR concentration on conversion and GE

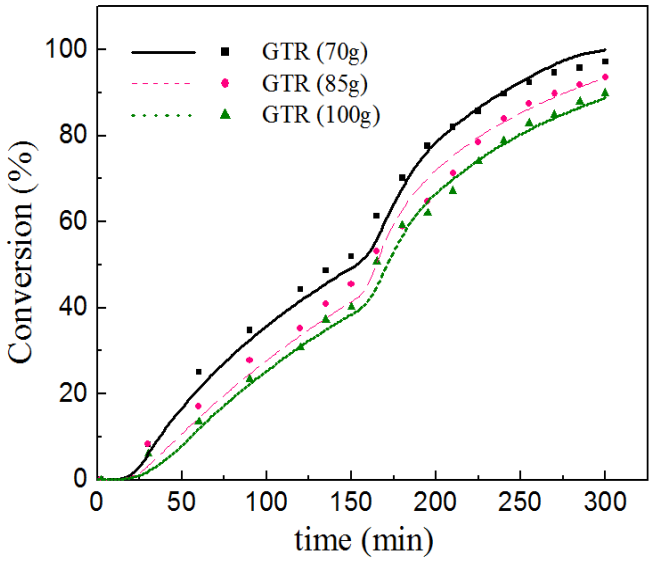

Figure 4.40 - Influence of the GTR content on the conversion. Comparison between experimental measurements (points) and theoretical predictions (lines).

Table 4.30 - Influence of the GTR content on the GE.

GE	Experimental value(%)	Simulation value(%)
GTR(70g)	35±6	31
GTR(85g)	51±5	53
GTR(100g)	54±3	56

GTR content is from 70 to 85 and 100g with the fixed concentration of initiator at 1 % by monomer by molar and styrene mass at 400g. As expected, it becomes apparent that the model displays a good agreement with the experimental measurements for the cases studied (Figure 4.40 and Table 4.30). The partial conversion of the styrene in the presence GTR is probably due to the competition between the monomer and the GTR versus the free primary radicals. Moreover, the more GTR swelled in styrene, the reactive position on the GTR powder is increased more，as a result, the graft efficiency increases. The tendency is in accordance with the results reported by Coiai et al. (2006). They demonstrated that the GE seemed to largely depend on the initial styrene/rubber ratio (from 90/10 to 70/30 wt/wt) [55]. In fact an increase of GE values was detected for higher GTR/styrene ratios, while the

styrene was more readily transformed into free polymer than in a grafted product in case of lower GTR/styrene ratio values. However, they did not explain this result. Zhang et al. (2012) showed that the GE increased at first and decreased later with increasing styrene content (from 84 to 93 wt%) [21]. Due to the homo-polymerization accelerated with a further increased in monomer content, and reactive radicals were shielded as a result of graft copolymer swelling, the graft efficiency decreased.

4.3.3.4 Effect of Initiator concentration on conversion and GE

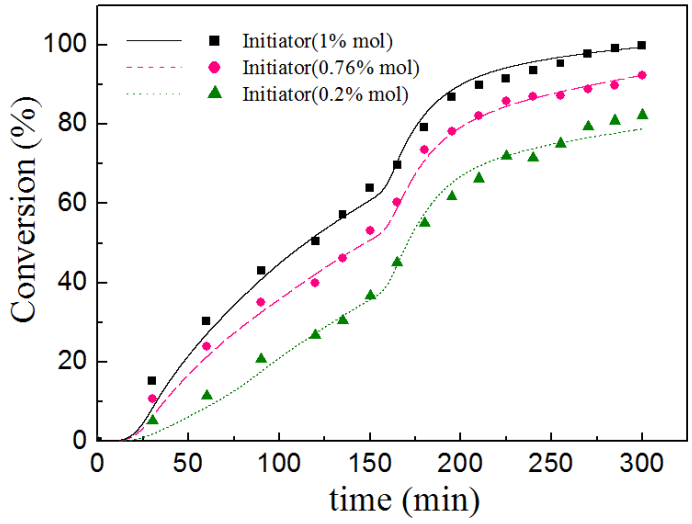

Figure 4.41 - Influence of the initiator concentration on the conversion. Comparison between experimental measurements (points) and theoretical predictions (lines).

Table 4.31 - Influence of the initiator concentration on the GE.

GE	Experimental value(%)	Simulation value(%)
Initiator (1.0%)	37±2	38
Initiator (0.76%)	39±2	41
Initiator (0.2%)	43±4	49

Figure 4.41 compares the experimental and simulated conversions. Table 4.31 shows the experimental and simulated GE. The effect of initial concentration of initiator is checked. The polymerization rate decreases with the decreasing of

concentration of initiator. In general, a good agreement is observed between model and experiments.

In previous literature it was shown that the GE can increase with increasing the initiator content, due to the increase in the free radicals of the system, capable of initiating the graft copolymerization. Pittolo et al. (1986) [59] measured the conversion of monomer to reach 98-100%, when AIBN was used, and 70-80%, when BPO was used, after 24h of polymerization. They concluded that there was little difference in composites derived from the different initiator usage. Coiai et al. (2006) demonstrated the difference in the GE of grafted PS onto GTR by using BPO and AIBN as initiators. BPO was efficient in ensuring considerable yields of grafted PS (GE=23–45%) unlike AIBN (GE<1%). However, they did not explain the reason that the GE remained always below 50% [55]. Zhang et al. (2012) studied the effect of initiator mass (BPO) on the graft polymerization. They concluded that the graft efficiency increased with the increase of the mass of initiator and attained a maximum value at 0.12 g (0.5% of monomer) [20].

4.3.3.5 Simulation of M_n and M_w of free PS and graft PS

Table 4.32 - Simulation and experimental values of M_n and M_w with the different ratio of initiator 0.2%, 0.76% and 1% mol.

Initiator (% mol)	M_n(g·mol^{-1})		M_w(g·mol^{-1})	
	Experimental values	Simulation values	Experimental values	Simulation values
0.2	6.7×10^4	6.3×10^4	1.3×10^5	1.2×10^5
0.76	5.8×10^4	4.5×10^4	1.1×10^5	9.2×10^4
1	3.9×10^4	3.7×10^4	8.3×10^4	7.6×10^4

Table 4.33 - Simulation and experimental values of M_n and M_w with the different GTR content 70, 85 and 100g.

GTR (g)	M_n(g·mol^{-1})		M_w(g·mol^{-1})	
	Experimental values	Simulation values	Experimental values	Simulation values
70	4.7×10^4	4.5×10^4	9.42×10^5	9.1×10^5

85	4.6×10^4	4.3×10^4	8.26×10^5	8.5×10^4
100	4.1×10^4	3.8×10^4	8.07×10^4	7.5×10^4

Due to the difficulty to obtain experimentally the molecular weight of graft polystyrene, this work only mentions the molecular weight of free PS by gel permeation chromatograph (GPC). Table 4.32 shows a comparison between simulation results and experimental data of the number- and weight-average molecular weights on different ratio of initiator 0.2%, 0.76% and 1% of monomer by mol. It is apparent that the predicted-molecular-weight averages are in close agreement with the corresponding measurements. As expected for a typical free-radical polymerization system, both the number- and weight-average molecular weights decrease with increasing concentration of initiator.

Table 4.33 contains the simulation and experimental data of the number- and weight-average molecular weights with respect to GTR content. Note that the observed increase in the M_n and M_w values with GTR content is attributed to the GTR effect. Decrease of GTR content, it means the concentration of monomer is increased relatively. The number-average degree of polymerization is proportional to the concentration of monomer according to the principle of kinetics of polymerization of styrene. Therefore, both of the number- and weight-average molecular weights are decreased with increasing of concentration of monomer.

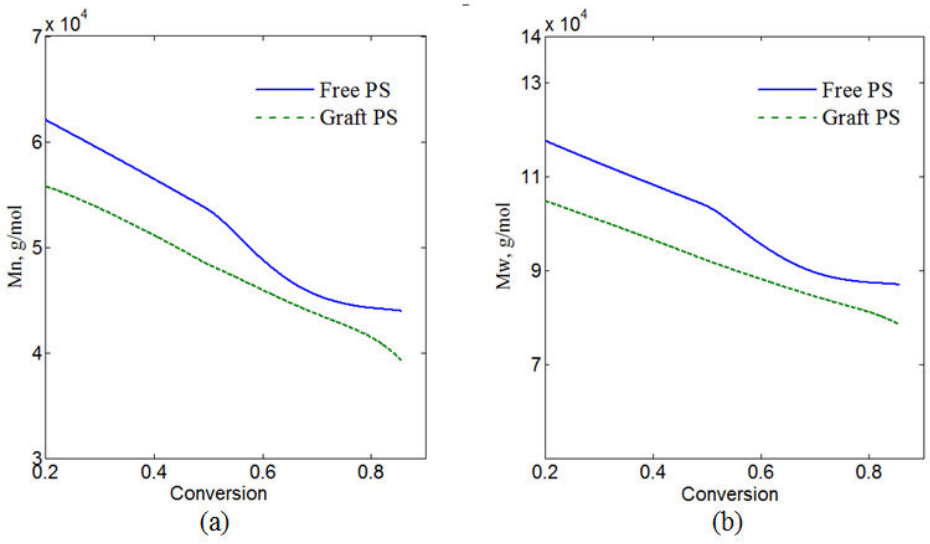

Figure 4.42 - M_n (a) and M_w (b) of the Free PS (solid line) and Graft PS (dotted line).

Using the developed model, it is also possible to calculate the M_n and M_w of grafted PS during the polymerization. Figure 4.42 shows the evolution of the M_n and M_w of free PS and grafted PS along a polymerization (NO15). This experiment was carried out at 90℃ for 2.5h and then increased to120℃, while the conversion was 0.5. It is observed that the average molecular weight of the grafted polymer is significantly lower than the respective molecular weight of the free polymer, as expected by the difference in the attributed values of the kinetic rate constants of propagation and termination, as explained earlier in the Chapter 3.

Conclusions

The artificial neural network model demonstrates the ability of a feedforward back-propagation neural network to predict the performance of graft polymerization of styrene. The model performed well in predicting not only the data used in the training process, but also those of test data that were unfamiliar to the neural network of conversion and GE of the graft polymerization of styrene to GTR particles. The kinetic model of graft polymerization of styrene inside/onto cross-linked GTR particles described not only the conversion of monomer but also the graft efficiency. This model also included the diffusion-controlled phenomena in this free radical graft polymerization. The simulation results showed that this model is capable of accurately predicting the conversion, GE and molecular weight of free PS. To our knowledge, this is the first kinetic model of graft polymerization of styrene with GTR particle including the diffusion-controlled reactions.

Chapter 5 Conclusions

The thesis is composed by two parts:

- Part I. The graft polymerizations of styrene inside cross-linked GTR particle was experimentally investigated using the BPO and DCP as the compound initiators. Firstly, the graft polymerizations of styrene inside GTR particle were investigated to obtain the high conversion and the graft efficiency. Secondly, increase the amount of monomer to study on the graft polymerizations of styrene onto GTR particle. Thirdly, the improvement of impact property of GTR-g-PS particle was studied by the twin-screw extruder.

- Part II. A mechanistic modelling approach is followed for the theoretical study of the complex grafting free-radical polymerization kinetics. Initially, an Artificial Neural Networks model is developed to study the influence of the main reaction conditions (i.e., temperature and amounts of monomer, GTR and initiators) on the monomer conversion and grafting efficiency indexes. At a second stage, a comprehensive kinetic model is developed, on the basis of the moment method, which displays extended predictive capabilities.

In part I, the cross-linked ground tire rubber was grafted by PS chains via radical polymerization using the BPO and DCP as the compound initiators. It was proven that the GTR powders were grafted by PS chains by SEM, EDS and FTIR. The effects of various factors on the graft efficiency on the radical polymerization had been discussed. There was a tendency that the GE of PS onto the GTR powders was increased with increasing the GTR content, decreasing the initiator content and increasing the ratio between BPO and DCP, whereas the conversion of monomer was decreased. It was found that the Tg of GTR-g-PS is higher than that of original GTR and it increased with increasing the GE. The thermal stability of GTR-g-PS was apparently higher than that of original GTR. Moreover, it was indicated that the presence of GTR-g-PS particle improved the notched impact strength of GTR-g-PS /PS blends. The good adhesion between the GTR-g-PS and PS after the extrusion was

very important to toughen PS. The size of GTR-g-PS particle was smaller than that of original GTR powders after the extrusion. However, the size of GTR-g-PS particle was still too big to toughen PS. Therefore, this work not only illustrated the vital effect of graft efficiency of PS graft inside cross-linked GTR to toughen the PS, but also provides the possibilities of improvement and decreasing GTR-g-PS particle size by the twin-screw extruder. To improve the impact mechanical property of GTR-g-PS/PS, decrease the particle size of GTR in the PS matrix should be further studied.

In part II, the main differences between ANN model and grafting free-radical polymerization kinetic model were related to the simulation mechanism. ANN model was not needed to understand the process of polymerization with developing a relationship between experimental inputs and experimental outputs. The kinetic model was developed based on the determining elementary reactions. The more knowledge of graft polymerization, the better kinetic modeling could be established. The obtained results showed that both of ANN model and kinetic developed model are in good agreement with experimental data.

Reference

[1] B. Adhikari, D. De, and S. Maiti, “Reclamation and recycling of waste rubber,” *Prog. Polym. Sci.*, vol. 25, no. 7, pp. 909–948, Sep. 2000.

[2] M. Awang, H. Ismail, and M. A. Hazizan, “Processing and properties of polypropylene-latex modified waste tyre dust blends (PP/WTDML),” *Polym. Test.*, vol. 27, no. 1, pp. 93–99, Feb. 2008.

[3] J. Karger-Kocsis, L. Mészáros, and T. Bárány, “Ground tyre rubber (GTR) in thermoplastics, thermosets, and rubbers,” *J. Mater. Sci.*, vol. 48, no. 1, pp. 1–38, Jun. 2012.

[4] V. Sridhar, Z. Z. Xiu, D. Xu, S. H. Lee, J. K. Kim, D. J. Kang, and D.-S. Bang, “Fly ash reinforced thermoplastic vulcanizates obtained from waste tire powder,” *Waste Manag.*, vol. 29, no. 3, pp. 1058–1066, Mar. 2009.

[5] A. K. Naskar, A. K. Bhowmick, and S. K. De, “Melt-processable rubber: Chlorinated waste tire rubber-filled polyvinyl chloride,” *J. Appl. Polym. Sci.*, vol. 84, no. 3, pp. 622–631, Apr. 2002.

[6] Y. Fang, M. Zhan, and Y. Wang, “The status of recycling of waste rubber,” *Mater. Des.*, vol. 22, no. 2, pp. 123–128, Apr. 2001.

[7] A. R. Khaloo, M. Dehestani, and P. Rahmatabadi, “Mechanical properties of concrete containing a high volume of tire–rubber particles,” *Waste Manag.*, vol. 28, no. 12, pp. 2472–2482, Dec. 2008.

[8] F. J. Navarro, P. Partal, F. Martínez-Boza, and C. Gallegos, “Thermo-rheological behaviour and storage stability of ground tire rubber-modified bitumens,” *Fuel*, vol. 83, no. 14–15, pp. 2041–2049, Oct. 2004.

[9] ETRMA, “End of life tyres.” A valuable resource with growing potential, 2011.

[10] IRENA, “Tire recycling industry: A Global view.” 2004.

[11] G. F. Freeguard, “Rubber modified polystyrene: structural variation induced during pre-polymerization,” *Polymer*, vol. 13, no. 8, pp. 366–370, Aug. 1972.

[12] E. M. Abdel-Bary, A. M. Dessouki, E. M. El-Nesr, and M. M. Hassan, “Radiation-Induced Graft Copolymerization Of Some Vinyl Monomers Onto Waste Rubber Powder,” *Polym.-Plast. Technol. Eng.*, vol. 36, no. 2, pp. 241–256, Mar. 1997.

[13] P. Fan and C. Lu, “Surface graft copolymerization of poly(methyl methacrylate) onto waste tire rubber powder through ozonization,” *J. Appl. Polym. Sci.*, vol. 122, no. 4, pp. 2262–2270, Nov. 2011.

[14] P. K. Pramanik and W. E. Bakers, “LLDPE Composites Filled with Corona Discharge Treated Ground Rubber Tire Crumb,” *J. Elastomers Plast.*, vol. 27, no. 3, pp. 253–267, Jul. 1995.

[15] A. M. Shanmugharaj, J. K. Kim, and S. H. Ryu, “UV surface modification of waste tire powder: Characterization and its influence on the properties of polypropylene/waste powder composites,” *Polym. Test.*, vol. 24, no. 6, pp. 739–745, Sep. 2005.

[16] T. Yasin, S. Khan, Y.-C. Nho, and R. Ahmad, “Effect of polyfunctional monomers on properties of radiation crosslinked EPDM/waste tire dust blend,” *Radiat. Phys. Chem.*, vol. 81, no. 4, pp. 421–425, Apr. 2012.

[17] D. Li, H. Xia, J. Peng, M. Zhai, G. Wei, J. Li, and J. Qiao, “Radiation preparation of nano-powdered styrene-butadiene rubber (SBR) and its

toughening effect for polystyrene and high-impact polystyrene," *Radiat. Phys. Chem.*, vol. 76, no. 11–12, pp. 1732–1735, Nov. 2007.
[18] W. Feng, A. I. Isayev, and E. von Meerwall, "Molecular mobility in ultrasonically treated butyl gum and devulcanized butyl rubber," *Polymer*, vol. 45, no. 25, pp. 8459–8467, Nov. 2004.
[19] C. H. Scuracchio, D. A. Waki, and M. L. C. P. da Silva, "Thermal analysis of ground tire rubber devulcanized by microwaves," *J. Therm. Anal. Calorim.*, vol. 87, no. 3, pp. 893–897, Mar. 2007.
[20] K. A. Tyler and G. L. Cerny, *Method of reducing pollution in microwave devulcanization process*. Google Patents, 1984.
[21] J. L. Zhang, H. X. Chen, C. M. Ke, Y. Zhou, H. Z. Lu, and D. L. Wang, "Graft polymerization of styrene onto waste rubber powder and surface characterization of graft copolymer," *Polym. Bull.*, vol. 68, no. 3, pp. 789–801, Feb. 2012.
[22] I. Luzinov, C. Pagnoulle, and R. Jérôme, "Dependence of phase morphology and mechanical properties of PS/SBR/PE ternary blends on composition: transition from core–shell to triple-phase continuity structures," *Polymer*, vol. 41, no. 9, pp. 3381–3389, Apr. 2000.
[23] B. Maridass and B. r. Gupta, "Process optimization of devulcanization of waste rubber powder from syringe stoppers by twin screw extruder using response surface methodology," *Polym. Compos.*, vol. 29, no. 12, pp. 1350–1357, Dec. 2008.
[24] E. Sipahi-Saglam, G. Akovali, C. Kaynak, N. Akkas, and M. Yetmez, "Studies on epoxy modified with recycled rubber," *Polym. Eng. Sci.*, vol. 41, no. 3, pp. 514–521, Mar. 2001.
[25] C. B. Bucknall, "Compatibility and Copolymerisation," in *Toughened Plastics*, Springer Netherlands, 1977, pp. 9–38.
[26] C. R. Kumar, I. Fuhrmann, and J. Karger-Kocsis, "LDPE-based thermoplastic elastomers containing ground tire rubber with and without dynamic curing," *Polym. Degrad. Stab.*, vol. 76, no. 1, pp. 137–144, 2002.
[27] C. B. Bucknall, "Manufacture of Toughened Plastics," in *Toughened Plastics*, Springer Netherlands, 1977, pp. 66–106.
[28] D. A. I. Isayev, S. P. Yushanov, S.-H. Kim, and V. Y. Levin, "Ultrasonic devulcanization of waste rubbers: Experimentation and modeling," *Rheol. Acta*, vol. 35, no. 6, pp. 616–630, Nov. 1996.
[29] C. H. Scuracchio, R. E. S. Bretas, and A. I. Isayev, "Blends of PS with SBR Devulcanized by Ultrasound: Rheology and Morphology," *J. Elastomers Plast.*, vol. 36, no. 1, pp. 45–75, Jan. 2004.
[30] G. G. Wicks, R. L. Schulz, D. E. Clark, and D. C. Folz, "Microwave Treatment of Vulcanized Rubber," Westinghouse Electric Company, 6,420,457, Jul. 2002.
[31] R. Sonnier, E. Leroy, L. Clerc, A. Bergeret, and J. M. Lopez-Cuesta, "Polyethylene/ground tyre rubber blends: Influence of particle morphology and oxidation on mechanical properties," *Polym. Test.*, vol. 26, no. 2, pp. 274–281, Apr. 2007.
[32] R. Scaffaro, N. T. Dintcheva, M. A. Nocilla, and F. P. La Mantia, "Formulation, characterization and optimization of the processing condition of blends of recycled polyethylene and ground tyre rubber: Mechanical and rheological analysis," *Polym. Degrad. Stab.*, vol. 90, no. 2, pp. 281–287, Nov. 2005.
[33] A. Shojaei, H. Yousefian, and S. Saharkhiz, "Performance characterization of composite materials based on recycled high-density polyethylene and ground tire rubber reinforced with short glass fibers for structural applications," *J. Appl.*

Polym. Sci., vol. 104, no. 1, pp. 1–8, Apr. 2007.
[34] I. Fuhrmann and J. Karger-Kocsis, "Promising approach to functionalisation of ground tyre rubber -photochemically induced grafting: Short Communication," *Plast. Rubber Compos.*, vol. 28, no. 10, pp. 500–504, Oct. 1999.
[35] O. P. Kuznetsova, L. A. Zhorina, and E. V. Prut, "Blends based on ground tire rubber," *Polym. Sci. Ser. Chem. Phys.*, vol. 46, no. 2, pp. 151–159, 2004.
[36] M. D. Stelescu, "Polymer Composites Based on Plasticized PVC and Vulcanized Nitrile Rubber Waste Powder for Irrigation Pipes," *Int. Sch. Res. Not.*, vol. 2013, p. e726121, Aug. 2013.
[37] G. E. McKee, A. Kistenmacher, H. Goerrissen, and M. Breulmann, "Synthesis, Properties and Applications of Acrylonitrile–Styrene–Acrylate Polymers," in *Modern Styrenic Polymers: Polystyrenes and Styrenic Copolymers*, J. Scheirs and D. B. Priddy, Eds. John Wiley & Sons, Ltd, 2003, pp. 341–362.
[38] O. Iwan, "Process for manufacturing plastic compositions and products obtained thereby," US1613673 A, 11-Jan-1927.
[39] W. H. Jo, C. D. Park, and M. S. Lee, "Preparation of functionalized polystyrene by reactive extrusion and its blend with polyamide 6," *Polymer*, vol. 37, no. 9, pp. 1709–1714, Apr. 1996.
[40] Z. Xing, M. Wang, G. Du, T. Xiao, W. Liu, D. Qiang, and G. Wu, "Preparation of microcellular polystyrene/polyethylene alloy foams by supercritical CO2 foaming and analysis by X-ray microtomography," *J. Supercrit. Fluids*, vol. 82, pp. 50–55, Oct. 2013.
[41] A. Krishnan K, C. Jose, R. K. R, and K. E. George, "Sisal nanofibril reinforced polypropylene/polystyrene blends: Morphology, mechanical, dynamic mechanical and water transmission studies," *Ind. Crops Prod.*, vol. 71, pp. 173–184, Sep. 2015.
[42] D. I. Collias and D. G. Baird, "Impact behavior of microcellular foams of polystyrene and styrene-acrylonitrile copolymer, and single-edge-notched tensile toughness of microcellular foams of polystyrene, styrene-acrylonitrile copolymer, and palycarbonate," *Polym. Eng. Sci.*, vol. 35, no. 14, pp. 1178–1183, Jul. 1995.
[43] G. Gao, C. Zhou, H. Yang, and H. Zhang, "Influence of core–shell rubber particles synthesized with different initiation systems on the impact toughness of modified polystyrene," *J. Appl. Polym. Sci.*, vol. 103, no. 2, pp. 738–744, Jan. 2007.
[44] B. B. Johnsen, A. J. Kinloch, and A. C. Taylor, "Toughness of syndiotactic polystyrene/epoxy polymer blends: microstructure and toughening mechanisms," *Polymer*, vol. 46, no. 18, pp. 7352–7369, Aug. 2005.
[45] S. Socrate, M. C. Boyce, and A. Lazzeri, "A micromechanical model for multiple crazing in high impact polystyrene," *Mech. Mater.*, vol. 33, no. 3, pp. 155–175, Mar. 2001.
[46] J. Y. Kim, C. H. Cho, P. Palffy-Muhoray, and T. Kyu, "Polymerization-induced phase separation in a liquid-crystal-polymer mixture," *Phys. Rev. Lett.*, vol. 71, no. 14, pp. 2232–2235, Oct. 1993.
[47] T. Tanabe, H. Furukawa, and M. Okada, "Salami pattern formation during phase separation induced by polymerization of 2-chlorostyrene in the presence of polystyrene," *Polymer*, vol. 44, no. 17, pp. 4765–4768, Aug. 2003.
[48] C. B. Bucknall and V. L. P. Soares, "Cavitation of rubber particles in high-impact polystyrene: Effects of crosslinking by ?-irradiation," *J. Polym. Sci. Part B Polym. Phys.*, vol. 42, no. 11, pp. 2168–2180, Jun. 2004.

[49] R. Rogers and S. Pidgeon, “Polymer Data Handbook Oxford University Press,” 1999. .
[50] J. D. Moore, “An electron microscope study of the microstructure of some rubber-reinforced polystyrenes,” *Polymer*, vol. 12, no. 8, pp. 478–486, Aug. 1971.
[51] C. D. Han, C. Sandford, and H. J. Yoo, “Effects of titanate coupling agents on the rheological and mechanical properties of filled polyolefins,” *Polym. Eng. Sci.*, vol. 18, no. 11, pp. 849–854, Aug. 1978.
[52] E. Piorkowska, A. S. Argon, and R. E. Cohen, “Size effect of compliant rubbery particles on craze plasticity in polystyrene,” *Macromolecules*, vol. 23, no. 16, pp. 3838–3848, Aug. 1990.
[53] Y. Liu, S.-S. Wang, W. Liu, Q.-X. Wan, H.-H. Wu, and G.-H. Gao, “Transition-Metal Catalyzed Carbon-Carbon Couplings Mediated with Functionalized Ionic Liquids, Supported-Ionic Liquid Phase, or Ionic Liquid Media,” *Curr. Org. Chem.*, vol. 13, no. 13, pp. 1322–1346, Sep. 2009.
[54] G. H. Gao, G. H. Im, M. S. Kim, J. W. Lee, J. Yang, H. Jeon, J. H. Lee, and D. S. Lee, “Magnetite-Nanoparticle-Encapsulated pH-Responsive Polymeric Micelle as an MRI Probe for Detecting Acidic Pathologic Areas,” *Small*, vol. 6, no. 11, pp. 1201–1204, Jun. 2010.
[55] S. Coiai, E. Passaglia, F. Ciardelli, D. Tirelli, F. Peruzzotti, and E. Resmini, “Modification of Cross-Linked Rubber Particles by Free Radical Polymerization,” *Macromol. Symp.*, vol. 234, no. 1, pp. 193–202, Feb. 2006.
[56] S. Coiai, E. Passaglia, and F. Ciardelli, “Gradient Density Grafted Polymers on Ground Tire Rubber Particles by Atom Transfer Radical Polymerization,” *Macromol. Chem. Phys.*, vol. 207, no. 24, pp. 2289–2298, Dec. 2006.
[57] N. Tsubokawa, K. Fujiki, and Y. Sone, “Radical Grafting from Carbon Black. Graft Polymerization of Vinyl Monomers Initiated by Peroxyester Groups Introduced onto Carbon Black Surface,” *Polym. J.*, vol. 20, no. 3, pp. 213–220, Mar. 1988.
[58] X. Wang and X. Lu, “Study on Properties of Ground Tire Rubber/Polystyrene Blend,” *China Rubber Ind.*, vol. 2011, no. 09, pp. 128–134, 2011.
[59] M. Pittolo and R. P. Burford, “Rubber-crumb modified polystyrene,” *J. Mater. Sci.*, vol. 21, no. 5, pp. 1769–1774, 1986.
[60] K. Kohlgrüber, Ed., *Co-Rotating Twin-Screw Extruder: Fundamentals, Technology, and Applications*. München: Carl Hanser Verlag GmbH & Co. KG, 2007.
[61] T. Villmow, B. Kretzschmar, and P. Pötschke, “Influence of screw configuration, residence time, and specific mechanical energy in twin-screw extrusion of polycaprolactone/multi-walled carbon nanotube composites,” *Compos. Sci. Technol.*, vol. 70, no. 14, pp. 2045–2055, Nov. 2010.
[62] H. Yazdani, M. Karrabi, I. Ghasmi, H. Azizi, and G. R. Bakhshandeh, “Devulcanization of waste tires using a twin-screw extruder: The effects of processing conditions,” *J. Vinyl Addit. Technol.*, vol. 17, no. 1, pp. 64–69, Mar. 2011.
[63] G. Gao, J. Zhang, H. Yang, C. Zhou, and H. Zhang, “Deformation mechanism of polystyrene toughened with sub-micrometer monodisperse rubber particles,” *Polym. Int.*, vol. 55, no. 11, pp. 1215–1221, Nov. 2006.
[64] M. A. Villalobos, A. E. Hamielec, and P. E. Wood, “Bulk and suspension polymerization of styrene in the presence of n-pentane. An evaluation of monofunctional and bifunctional initiation,” *J. Appl. Polym. Sci.*, vol. 50, no. 2,

pp. 327–343, Oct. 1993.
[65] C. Kotoulas, A. Krallis, P. Pladis, and C. Kiparissides, “A comprehensive kinetic model for the combined chemical and thermal polymerization of styrene up to high conversions,” *Macromol. Chem. Phys.*, vol. 204, no. 10, pp. 1305–1314, 2003.
[66] H. Yamazoe, P. B. Zetterlund, B. Yamada, D. J. T. Hill, and P. J. Pomery, “Free-Radical Bulk Polymerization of Styrene: ESR and Near-Infrared Spectroscopic Study of the Entire Conversion Range,” *Macromol. Chem. Phys.*, vol. 202, no. 6, pp. 824–829, Mar. 2001.
[67] P. J. Flory, “The Mechanism of Vinyl Polymerizations1,” *J. Am. Chem. Soc.*, vol. 59, no. 2, pp. 241–253, Feb. 1937.
[68] F. R. Mayo, “Chain Transfer in the Polymerization of Styrene: The Reaction of Solvents with Free Radicals1,” *J. Am. Chem. Soc.*, vol. 65, no. 12, pp. 2324–2329, Dec. 1943.
[69] F. R. Mayo, “Chain Transfer in the Polymerization of Styrene. VIII. Chain Transfer with Bromobenzene and Mechanism of Thermal Initiation1,” *J. Am. Chem. Soc.*, vol. 75, no. 24, pp. 6133–6141, Dec. 1953.
[70] F. R. Mayo and F. M. Lewis, “Copolymerization. I. A Basis for Comparing the Behavior of Monomers in Copolymerization; The Copolymerization of Styrene and Methyl Methacrylate,” *J. Am. Chem. Soc.*, vol. 66, no. 9, pp. 1594–1601, Sep. 1944.
[71] K. E. Russell and A. V. Tobolsky, “Thermal Initiation of Styrene Polymerization,” *J. Am. Chem. Soc.*, vol. 75, no. 20, pp. 5052–5054, Oct. 1953.
[72] W. A. Pryor and J. H. Coco, “Computer Simulation of the Polymerization of Styrene. The Mechanism of Thermal Initiation and the Importance of Primary Radical Termination,” *Macromolecules*, vol. 3, no. 5, pp. 500–508, Sep. 1970.
[73] P. Manaresi, V. Passalacqua, and F. Pilati, “Kinetics of graft polymerization of styrene on cis-1,4-polybutadiene,” *Polymer*, vol. 16, no. 7, pp. 520–526, Jul. 1975.
[74] N.-J. Huang and D. C. Sundberg, “Fundamental studies of grafting reactions in free radical copolymerization. III. Grafting of styrene, acrylate, and methacrylate monomers onto cis-polybutadiene using benzoyl peroxide initiator in solution polymerization,” *J. Polym. Sci. Part Polym. Chem.*, vol. 33, no. 15, pp. 2571–2586, 1995.
[75] G. Odian, *Principles of Polymerization*. John Wiley & Sons, 2004.
[76] A. E. Hamielec, J. W. Hodgins, and K. Tebbens, “Polymer reactors and molecular weight distribution: Part II. Free radical polymerization in a batch reactor,” *AIChE J.*, vol. 13, no. 6, pp. 1087–1091, Nov. 1967.
[77] A. W. Hui and A. E. Hamielec, “Thermal polymerization of styrene at high conversions and temperatures. An experimental study,” *J. Appl. Polym. Sci.*, vol. 16, no. 3, pp. 749–769, 1972.
[78] D. S. Achilias and C. Kiparissides, “Development of a general mathematical framework for modeling diffusion-controlled free-radical polymerization reactions,” *Macromolecules*, vol. 25, no. 14, pp. 3739–3750, 1992.
[79] G. A. O’neil, M. B. Wisnudel, and J. M. Torkelson, “Gel effect in free radical polymerization: model discrimination of its cause,” *AIChE J.*, vol. 44, no. 5, pp. 1226–1231, 1998.
[80] Y. J. Huang and L. J. Lee, “Optimization of diffusion-controlled free radical polymerizations in lumped-parameter systems,” *J. Appl. Polym. Sci.*, vol. 39, no. 11–12, pp. 2353–2375, 1990.

[81] L. Cavin, A. Rouge, T. Meyer, and A. Renken, “Kinetic modeling of free radical polymerization of styrene initiated by the bifunctional initiator 2, 5-dimethyl-2, 5-bis (2-ethyl hexanoyl peroxy) hexane,” *Polymer*, vol. 41, no. 11, pp. 3925–3935, 2000.
[82] J. D. Woloszyn, P. Hesse, K.-D. Hungenberg, and K. B. McAuley, “Parameter Selection and Estimation Techniques in a Styrene Polymerization Model,” *Macromol. React. Eng.*, vol. 7, no. 7, pp. 293–310, Jul. 2013.
[83] J. D. Woloszyn and K. B. McAuley, “Application of Parameter Selection and Estimation Techniques in a Thermal Styrene Polymerization Model,” *Macromol. React. Eng.*, vol. 5, no. 9–10, pp. 453–466, Oct. 2011.
[84] I. Capek, M. Riza, and M. Akashi, “On the kinetics of polymerization and copolymerization of poly(oxyethylene) macromonomers and styrene,” *Makromol. Chem.*, vol. 193, no. 11, pp. 2843–2860, Nov. 1992.
[85] V. D. Yenal’ev, N. A. Noskova, and I. S. Popov, “Study of the mechanism of styrene-rubber graft copolymerization,” *Polym. Sci. USSR*, vol. 16, no. 9, pp. 2332–2341, 1974.
[86] J. Qin, W. Guo, and Z. Zhang, “A kinetic study on bulk thermal polymerization of styrene,” *Polymer*, vol. 43, no. 26, pp. 7521–7527, Dec. 2002.
[87] J. Qin, H. Li, and Z. Zhang, “Modeling of high-conversion binary copolymerization,” *Polymer*, vol. 44, no. 8, pp. 2599–2604, Apr. 2003.
[88] J. Qin, W. Guo, and Z. Zhang, “Modeling of the bulk free radical polymerization up to high conversion—three stage polymerization model I. Model examination and apparent reaction rate constants,” *Polymer*, vol. 43, no. 4, pp. 1163–1170, 2002.
[89] T. H. Kim and N. Lee, “Melt-grafting of maleimides having hindered phenol group onto polypropylene,” *Bull.-KOREAN Chem. Soc.*, vol. 24, no. 12, pp. 1809–1813, 2003.
[90] M. Buback, R. G. Gilbert, R. A. Hutchinson, B. Klumperman, F.-D. Kuchta, B. G. Manders, K. F. O’Driscoll, G. T. Russell, and J. Schweer, “Critically evaluated rate coefficients for free-radical polymerization, 1. Propagation rate coefficient for styrene,” *Macromol. Chem. Phys.*, vol. 196, no. 10, pp. 3267–3280, 1995.
[91] S. Beuermann and M. Buback, “Rate coefficients of free-radical polymerization deduced from pulsed laser experiments,” *Prog. Polym. Sci.*, vol. 27, no. 2, pp. 191–254, 2002.
[92] H. Yamazoe and P. B. Zetterlund, “Free‐radical bulk polymerization of styrene: ESR and near‐infrared spectroscopic study of the entire conversion range,” *Macromol Chem Phys*, no. 202, pp. 824–829, 2001.
[93] P. B. Zetterlund, H. Yamazoe, B. Yamada, D. J. T. Hill, and P. J. Pomery, “High-Conversion Free-Radical Bulk Polymerization of Styrene: Termination Kinetics Studied by Electron Spin Resonance, Fourier Transform Near-Infrared Spectroscopy, and Gel Permeation Chromatography,” *Macromolecules*, vol. 34, no. 22, pp. 7686–7691, Oct. 2001.
[94] N. N. Tokareva and V. R. Duflyot, “Polymerization of vinyl monomers in three-dimensional networks,” *Polym. Sci. USSR*, vol. 32, no. 6, pp. 1181–1187, 1990.
[95] K. Novakovic, E. B. Martin, and A. J. Morris, “Modelling of the free radical polymerization of styrene with benzoyl peroxide as initiator,” in *Computer Aided Chemical Engineering*, vol. 14, A. K. and I. Turunen, Ed. Elsevier, 2003, pp. 815–820.
[96] M. Vicevic, K. Novakovic, K. V. K. Boodhoo, and A. J. Morris, “Kinetics of

styrene free radical polymerisation in the spinning disc reactor," *Chem. Eng. J.*, vol. 135, no. 1–2, pp. 78–82, Jan. 2008.

[97] J. P. Van Hook and A. V. Tobolsky, "The initiator efficiency of 2, 2′-azobisisobutyronitrile in the polymerization of styrene and methyl methacrylate, and dicumyl peroxide as a polymerization initiator," *J. Polym. Sci.*, vol. 33, no. 126, pp. 429–445, 1958.

[98] N. Tefera, G. Weickert, R. Bloodworth, and J. Schweer, "Free radical suspension polymerization kinetics of styrene up to high conversion," *Macromol. Chem. Phys.*, vol. 195, no. 9, pp. 3067–3085, 1994.

[99] W. J. Yoon and K. Y. Choi, "Kinetics of free radical styrene polymerization with the symmetrical bifunctional initiator 2,5-dimethyl-2,5-bis(2-ethyl hexanoyl peroxy) hexane," *Polymer*, vol. 33, no. 21, pp. 4582–4591, 1992.

[100] M. Kıranşan, A. Khataee, S. Karaca, and M. Sheydaei, "Artificial neural network modeling of photocatalytic removal of a disperse dye using synthesized of ZnO nanoparticles on montmorillonite," *Spectrochim. Acta. A. Mol. Biomol. Spectrosc.*, vol. 140, pp. 465–473, Apr. 2015.

[101] J. S. Torrecilla, M. L. Mena, P. Yáñez-Sedeño, and J. García, "Field determination of phenolic compounds in olive oil mill wastewater by artificial neural network," *Biochem. Eng. J.*, vol. 38, no. 2, pp. 171–179, Feb. 2008.

[102] M. Beale, M. T. Hagan, and H. B. Demuth, "Neural network toolbox," *Neural Netw. Toolbox Math Works*, vol. 5, p. 25, 1992.

[103] S. Karsoliya, "Approximating number of hidden layer neurons in multiple hidden layer BPNN architecture," *Int. J. Eng. Trends Technol.*, vol. 3, no. 6, pp. 713–717, 2012.

[104] M. Delnavaz, "Application of Artificial Neural Networks for Prediction of Photocatalytic Reactor," *Water Environ. Res.*, vol. 87, no. 2, pp. 113–122, Feb. 2015.

[105] A. R. Amani-Ghadim and M. S. S. Dorraji, "Modeling of photocatalyatic process on synthesized ZnO nanoparticles: Kinetic model development and artificial neural networks," *Appl. Catal. B Environ.*, vol. 163, pp. 539–546, Feb. 2015.

[106] F. L. Marten and A. E. Hamielec, "High-conversion diffusion-controlled polymerization of styrene. I," *J. Appl. Polym. Sci.*, vol. 27, no. 2, pp. 489–505, Feb. 1982.

[107] N. Tefera, G. Weickert, and K. R. Westerterp, "Modeling of free radical polymerization up to high conversion. I. A method for the selection of models by simultaneous parameter estimation," *J. Appl. Polym. Sci.*, vol. 63, no. 12, pp. 1649–1661, 1997.

[108] F. Triefenbach, "Design of experiments: The D-optimal approach and its implementation as a computer algorithm," *Bachelors Thesis Inf. Commun. Technol.*, 2008.

[109] A. I. Khuri and S. Mukhopadhyay, "Response surface methodology," *Wiley Interdiscip. Rev. Comput. Stat.*, vol. 2, no. 2, pp. 128–149, Mar. 2010.

[110] F. Avram, N. N. Leonenko, and N. Šuvak, "Parameter estimation for Fisher–Snedecor diffusion," *Statistics*, vol. 45, no. 1, pp. 27–42, Feb. 2011.

[111]P. F. de Aguiar, B. Bourguignon, M. S. Khots, D. L. Massart, and R. Phan-Than-Luu, "D-optimal designs," *Chemom. Intell. Lab. Syst.*, vol. 30, no. 2, pp. 199–210, Dec. 1995.

[112] L. I. Zheng-Hui, "Modélisation des Procédés de Polymérisation enEmulsion et d'Extrusion Réactive pour le Greffage sur Polypropylene," 2012.

[113] M. Nobelen, S. Hoppe, C. Fonteix, F. Pla, M. Dupire, and B. Jacques, “Modeling of the rheological behavior of polyethylene/supercriticalCO2 solutions,” *Chem. Eng. Sci.*, vol. 61, no. 16, pp. 5334–5345, Aug. 2006.
[114] F. James, *Statistical methods in experimental physics*. World Scientific, 2006.
[115] R. Kumar, S. C. Kaushik, R. Kumar, and R. Hans, “Multi-objective thermodynamic optimization of an irreversible regenerative Brayton cycle using evolutionary algorithm and decision making,” *Ain Shams Eng. J.*, Jul. 2015.
[116] J. Rached, S. Hoppe, D. Meimaroglou, C. Fonteix, and F. Pla, “Modeling and simulation of activated anionic polymerization of lauryllactam in the presence of a macroactivator,” *Chem. Eng. Sci.*, vol. 118, pp. 20–31, Oct. 2014.
[117] C. FONTEIX, F. BICKING, E. PERRIN, and I. MARC, “Haploid and diploid algorithms, a new approach for global optimization: compared performances,” *Int. J. Syst. Sci.*, vol. 26, no. 10, pp. 1919–1933, Oct. 1995.
[118] H. M. Hulburt and S. Katz, “Some problems in particle technology: A statistical mechanical formulation,” *Chem. Eng. Sci.*, vol. 19, no. 8, pp. 555–574, Aug. 1964.

Appendix I

Three stage polymerization model: [86]–[88]

$$R_p = -\frac{d[M]}{dt} = k_p[M^*][M] \tag{I.1}$$

$$R_i = 2fk_d[I] = R_t = 2k_t[M^*]^2 \tag{I.2}$$

Eliminating $[M^*]$ from Eqs (I.1) and (I.2):

$$R_p = -\frac{d[M]}{d\theta} = k_p\left(\frac{fk_d}{k_t}\right)^{1/2}[I]^{1/2}[M] \tag{I.3}$$

According to the classical kinetics of free radical polymerization, we have

$$[I] = [I]_0\exp(-k_d\theta) \tag{I.4}$$

Substituting Eq (I.4) into Eq (I.3), the following equation is obtained:

$$-\frac{d[M]}{[M]} = K_a[I]_0^{1/2}\exp(-k_d\theta/2)d\theta \tag{I.5}$$

Where

$$K_a = k_p(fk_d/k_t)^{1/2}$$

(a) Low conversion stage ($x \leqslant x_1$, $K_a = K_{1a}$)

Defining $$x = 1 - [M]/[M]_0$$

gives:

$$-\mathrm{In}(1-x) = K_1\left[\exp\left(-\frac{k_d\theta}{2}\right) - 1\right] \tag{I.6}$$

Where:

$$K_1 = (2/k_d)K_{1a}[I]_0^{1/2}$$

$$K_{1a} = k_{p1}(f_1k_d/k_{t1})^{1/2}$$

(b) Gel effect stage ($x_1 \leq x \leq x_2, K_a = K_{2a}$)

With the condition $[M]=[M]_1$ at $\theta=\theta 1$ and setting $[M]=[M]_0(1-x)$ and $[M]_1=[M]_0(1-x_1)$

$$-\mathrm{In}(1-x) = -\mathrm{In}(1-x_1) - K_2\left[\exp\left(-\frac{k_d\theta}{2}\right) - \exp\left(-\frac{k_d\theta 1}{2}\right)\right] \qquad \text{(I.7)}$$

Where

$$K_2 = (2/k_d)K_{2a}[I]_0^{1/2}$$

$$K_{2a} = k_{p2}(f_2 k_d/k_{t2})^{1/2}$$

(c) Glass effect stage ($x \geq x_2, K_a = K_{3a}$)

Similarly, we have:

$$-\mathrm{In}(1-x) = -\mathrm{In}(1-x_2) - K_3\left[\exp\left(-\frac{k_d\theta}{2}\right) - \exp\left(-\frac{k_d\theta 2}{2}\right)\right] \qquad \text{(I.8)}$$

Where:

$$K_3 = (2/k_d)K_{3a}[I]_0^{1/2}$$

$$K_{3a} = k_{p3}(f_3 k_d/k_{t3})^{1/2}$$

General polymerization rate functions:

Assuming that the quasi-steady-state approximation for radical concentration holds true and that the total polymerization rate is equal to the rate of monomer consumption, the reaction rate is written as:

$$R_{\mathrm{p}} = -\frac{dm}{dt} = k_p\left(\frac{k_d f \cdot I}{k_t}\right)^{1/2}[\mathrm{M}] \tag{I.9}$$

Substitute the Eq (I.2) to Eq (I.9), the following equation is obtained by:

$$-\frac{dm}{m} = k_p \cdot \left(\frac{fk_d I_0}{k_t}\right)^{1/2} \cdot \exp\left(-\frac{k_d \cdot t}{2}\right) \cdot dt \tag{I.10}$$

Integrating Eq. (I.10) and defining $x = \frac{m_0 - m}{m_0}$:

$$\ln(1-\mathrm{x}) = k_p\left(\frac{4f}{k_d k_t}\right)^{1/2} I_0^{1/2}\left[\exp\left(-\frac{k_d \cdot t}{2}\right) - 1\right] \tag{I.11}$$

Defining $\mathrm{A} = k_p\left(\frac{4f}{k_d k_t}\right)^{1/2} I_0^{1/2}$, the following equation is obtained:

$$\mathrm{x} = 1 - \exp\left[A \cdot \left(\exp\left(-\frac{kd \cdot t}{2}\right) - 1\right)\right] \tag{I.12}$$

$$\nu = \frac{k_p}{2(fk_d k_t)^{1/2}} \frac{[M]}{[I]^{1/2}} \tag{I.13}$$

$$\frac{1}{\overline{Xn}} = \frac{1}{\nu} + C_M + C_I \frac{[I]}{[M]} + Cs \frac{[S]}{[M]} \tag{I.14}$$

Appendix II

Rate functions of 'live' and 'dead' polymer / graft polymer:

'live' free polymer chains, R_n

$$\begin{aligned} rR_n = {} & [k_{i1}\cdot PR\cdot M + k_{fm}\cdot M\cdot(\textstyle\sum_{m=1}^{\infty} R_m + \sum_{m=1}^{\infty} GR_m)]\cdot\delta(n-1) \\ & + k_A\cdot AR\cdot M\cdot\delta(n-3) + k_B\cdot MR\cdot M\cdot\delta(n-2) + k_p(R_{n-1}-R_n)\cdot M \\ & - (k_{fm}\cdot M + k_{fg}\cdot G + k_{fa}\cdot AH)\cdot R_n \\ & + k_S\cdot PR\cdot\textstyle\sum_{m=n+1}^{\infty}(\frac{2}{m-1} D_m) - (k_{tc}+k_{td})\cdot R_n\cdot\sum_{m=1}^{\infty} R_m \\ & - (k_{tc}+k_{td})\cdot R_n\cdot\textstyle\sum_{m=1}^{\infty} GR_m - (k_{tpr}\cdot PR + k_{tprg}\cdot GPR)\cdot R_n \end{aligned} \qquad \text{(II.1)}$$

'dead' free polymer chains, D_n :

$$\begin{aligned} rD_n = {} & k_C\cdot AH\cdot M\cdot\delta(n-3) + (k_{fm}\cdot M + k_{fg}\cdot G + k_{fa}\cdot AH)\cdot R_n \\ & - k_S\cdot PR\cdot(n-1)\cdot D_n + k_S\cdot PR\cdot\textstyle\sum_{m=n+1}^{\infty}(\frac{2}{m-1} D_m) \\ & + 0.5\cdot k_{tc}\cdot\textstyle\sum_{m=1}^{n-1} R_m\cdot R_{n-m} + k_{td}\cdot R_n\cdot(\sum_{m=1}^{\infty} R_m + \sum_{m=1}^{\infty} GR_m) \\ & + k_{tpr}\cdot R_n\cdot PR \end{aligned} \qquad \text{(II.2)}$$

'live' graft polymer chains, GR_n:

$$\begin{aligned} rGR_n = {} & (k_{i2}\cdot GPR\cdot M)\,\delta(n-1) + k_{pG}\cdot(GR_{n-1} - GR_n)\cdot M \\ & - (k_{fm}\cdot M + k_{fg}\cdot G + k_{fa}\cdot AH)\cdot GR_n \\ & - (k_{tcG}+k_{tdG})\cdot GR_n\cdot\textstyle\sum_{m=1}^{\infty} GR_m \\ & - (k_{tc}+k_{td})\cdot GR_n\cdot\textstyle\sum_{m=1}^{\infty} R_m \\ & - (k_{tpr}\cdot PR + k_{tprg}\cdot GPR)\cdot GR_n \end{aligned} \qquad \text{(II.3)}$$

'dead' graft polymer chains, GD_n :

$$\begin{aligned} rGD_n = {} & (k_{fm}\cdot M + k_{fg}\cdot G + k_{fa}\cdot AH)\cdot GR_n \\ & + 0.5\cdot k_{tcG}\cdot\textstyle\sum_{m=1}^{n-1} GR_m\cdot GR_{n-m} + k_{tdG}\cdot GR_n\cdot\sum_{m=1}^{\infty} GR_m \end{aligned}$$

$$+ k_{td} \cdot GR_n \cdot \sum_{m=1}^{\infty} R_m$$

$$+ k_{tc} \cdot \sum_{m=1}^{n-1} GR_m \cdot R_{n-m}$$

$$+ k_{tpr} \cdot GRn \cdot PR + k_{tprg}(GR_n + R_n) \cdot GPR \qquad \text{(II.4)}$$

In the above expressions, δ(n) denotes the Kronecker's delta, defined by:

$$\delta(n-i) = \begin{cases} 1 \; for \; n = i \\ 0 \; for \; n \neq i \end{cases}$$

Moment rate functions:

Moment rate function for the 'live' polymer chains

$$r\lambda_k = k_{i1} \cdot PR \cdot M + k_{fm} \cdot M(\lambda_0 + v_0) + 3^k \cdot k_A \cdot AR \cdot M + 2^k \cdot k_B \cdot MR \cdot M$$

$$+ k_p \cdot M \cdot (\sum_{r=0}^{k} \binom{k}{r} \lambda_r \lambda_{k-r}) - (k_{fm} \cdot M + k_{fg} \cdot G + k_{fa} \cdot AH) \cdot \lambda_k$$

$$+ 2 \cdot k_S \cdot PR \cdot T_l - (k_{tc} + k_{td}) \cdot \lambda_k \cdot (\lambda_0 + v_0))$$

$$- (k_{tpr} \cdot PR + k_{tprg} \cdot GPR) \cdot \lambda_k \qquad \text{(II.5)}$$

Moment rate function for the 'dead' polymer chains:

$$r\mu_k = 3^k \cdot k_c \cdot AH \cdot M + (k_{fm} \cdot M + k_{fg} \cdot G + k_{fa} \cdot AH) \cdot \lambda_k$$

$$- k_s \cdot PR \cdot (\mu_{k+1} - \mu_k) + 2 \cdot k_s \cdot PR \cdot T_l$$

$$+ 0.5 \cdot k_{tc} \cdot \sum_{r=0}^{k} \binom{k}{r} \lambda_r \lambda_{k-r} + k_{td} \cdot (\lambda_0 + v_0) \cdot \lambda_k + k_{tpr} \cdot PR \cdot \lambda_k \qquad \text{(II.6)}$$

Moment rate function for the 'live' grafted polymer chains

$$rv_k = k_{i2} \cdot GPR \cdot M + k_{pG} \cdot M \cdot (\sum_{r=0}^{k} \binom{k}{r} v_r v_k)$$

$$- (k_{fm} \cdot M + k_{fg} \cdot G + k_{fa} \cdot AH) \cdot v_k$$

$$- (k_{tcG} + k_{tdG}) \cdot v_k \cdot v_0 - (k_{tc} + k_{td}) \cdot v_k \cdot \lambda_0$$

$$- (k_{tpr} \cdot PR + k_{tprg} \cdot GPR) \cdot v_k \qquad \text{(II.7)}$$

Moment rate function for the 'dead' grafted polymer chains:

$$r\xi_k = (k_{fm}\cdot M + k_{fg}\cdot G + k_{fa}\cdot AH)\cdot v_k + k_{tdG}\cdot v_k\cdot v_0 + k_{td}\cdot v_k\cdot \lambda_0$$
$$+ 0.5\cdot k_{tcG}\cdot \sum_{r=0}^{k}\binom{k}{r} v_r v_{k-r}$$
$$+ k_{tcG}\cdot \sum_{r=0}^{k}\binom{k}{r} v_r \lambda_{k-r}$$
$$+ k_{tpr}\cdot PR\cdot v_k + k_{tprg}\cdot GPR\cdot(v_k+\lambda_k) \quad \text{(II.8)}$$

The term T_1 corresponds to the following expression:

$$T_1 = \sum_{m=0}^{k}\binom{k}{m}\frac{B_m}{k-m+1}\mu_{k-m} \quad \text{(II.9)}$$

In the above, $\binom{n}{m}$ denotes the all the possible combinations of a set of n individuals into groups of m, defined as:

$$\binom{n}{m} = \frac{n!}{m!(n-m)!} \quad \text{(II.10)}$$

and B_m is the Bernoulli number series (i.e., B_0=1; B_1=-1/2; B_2=1/6, etc.). Finally, the closure technique of Hulburt and Katz (1964) has been applied in order to overcome the closure problem of the 'dead' polymer chain moments, deriving from the scission reaction[118]:

$$\mu_3 = \frac{\mu_2}{\mu_0\mu_1}(2\mu_0\mu_2 - {\mu_1}^2) \quad \text{(II.11)}$$

Appendix III

Diffusion-control model:

First stage of diffusion control:

$$k_{t,seg} = k_{to}\cdot(1+\delta_c C_p\, MW_m) \quad \text{(III.1)}$$

Second stage of diffusion control:

$$K = \overline{M_w}^{0.5} e^{(A/V_f)} \quad \text{(III.2)}$$

$$K_{cr} = A_{cr}\, e^{(Ecr/RT)} \quad \text{(III.3)}$$

$$V_f = [0.025+\alpha_P(T-T_{gp})]\frac{V_P}{V_t} + [0.025+\alpha_m\,(T-T_{gm})]\,\frac{V_m}{V_t} \quad \text{(III.4)}$$

$$k_T = k_{t0}\,(\frac{\overline{M_{wcr}}}{\overline{M_w}})^n\, e^{[-A(\frac{1}{V_f}-\frac{1}{V_{f,cr}})]} \quad \text{(III.5)}$$

$$k_{t,rd} = k_{t,rd,min}\, X + k_{t,rd,max}\,(1-X) \quad \text{(III.6)}$$

$$k_{t,rd,min} = 10^3 A_{min}\, k_{p,eff}\,[M]\, N_{av} \quad \text{(III.7)}$$

$$k_{t,rd,max} = 10\, A_{max}\, k_{p,eff}\,[M]\, N_{av} \quad \text{(III.8)}$$

$$A_{min} = \frac{4}{3}\pi\sigma\delta^2 \quad \text{(III.9)}$$

$$A_{max} = \frac{8}{3}\pi\delta^3 jc^{1/2} \quad \text{(III.10)}$$

$$k_{t,eff} = (\frac{1}{k_{t,seg}} + \frac{1}{k_T})^{-1} + k_{t,rd} \quad \text{(III.11)}$$

Where m and P denote monomer and polymer, respectively; T is polymerization temperature (K); V is volume; V_t is total volume of polymer and monomer, not including GTR;

Third stage of diffusion control:

$$V_{f,crm} = A_{crm}\, e^{(-\frac{E_{crm}}{RT})} \quad \text{(III.12)}$$

$$k_{p,eff}=k_{p0}\, e^{\left[-B\left(\frac{1}{V_f}-\frac{1}{V_{f,crm}}\right)\right]} \quad \text{(III.13)}$$

Fourth stage of diffusion control:

$$C_{rRatio}=\frac{V_{f,creff}}{V_{f,crm}} \quad \text{(III.14)}$$

$$f_{i,eff}=f_{i0}\, e^{\left[-C\left(\frac{1}{V_f}-\frac{1}{V_{f,creff}}\right)\right]} \quad \text{(III.15)}$$

Étude de la Cinétique de Polymérisation Radicalaire duStyrène dans un Réseau Tridimensionnel et Application à la Valorisation de Pneus Usagés

Cette thèse a pour objet de développer une nouvelle méthodologie pour valoriser les poudrettes de pneus usagés (PPU). Celles-ci résultent du broyage de la partie caoutchoutique des pneus usagés qui conserve l'excellente élasticité. L'idée est de profiter de leur élasticité pour renforcer la résistance au choc des polymères fragiles tels que le polystyrène (PS) en y incorporant les PPU. Cependant, la réalisation de cette idée a besoin de relever deux défis majeurs : (1) les PPU commerciales ont typiquement des diamètres de l'ordre de plusieurs centaines de micromètres. Or elles doivent être deux ordres de grandeur plus petits en taille pour pouvoir améliorer la résistance au choc des polymères fragiles. (2) L'adhésion interfaciale entre les polymères et les PPU est mauvaise et constitue donc des défauts mécaniques du matériau. Ces deux défis sont liés à la nature même des PPU qui sont intrinsèquement des réseaux réticulés chimiquement. Cette thèse choisit le PS pour représenter les polymères fragiles. La méthodologie visant à renforcer sa résistance au choc est de polymériser le styrène par voie radicalaire au sein des PPU. Cette polymérisation forme à la fois des chaines en PS libres et des greffons en PS liés chimiquement aux mailles du réseau des PPU. Les inclusions des chaines en PS libres facilitent la dispersion des PPU en taille plus petite lorsqu'une action mécanique leur est appliquée lors de l'extrusion par exemple. La formation des greffons en PS sur les mailles du réseau des PPU renforce l'adhésion interfaciale entre le PS et les PPU. Cette thèse a développé un modèle complet permettant de décrire la cinétique de polymérisation radicalaire du PS libre et celle des greffons en PS liés aux mailles du réseau des PPU. Elle l'a validé par un plan d'expériences judicieux.

Mots-clés: poudrettes de pneus usagés, polymérisation, polystyrène

Study of the Kinetics of Free Radical Polymerization of Styrene in a Three Dimensional Network and Applications for Used Tire Recycling

This thesis aims to develop a novel approach to value ground tire rubber (GTR). The latter results from grounding of the rubber part of used tires which retains excellent elasticity. The idea is to take the advantage of its elasticity to toughen brittle polymers such as polystyrene (PS) upon incorporating GTR into them. However, two challenges have to be overcome to realize this idea. (1) Commercial GTR is typically in the form of particles of a few hundreds of micrometers in diameter. However, it has to be at least one to two orders of magnitude smaller when incorporated in a brittle polymer so as to be able to improve its impact resistance. (2) The interfacial adhesion between the polymer and GTR is weak. These two challenges are related to the intrinsic nature of the GTR which is chemically cross-linked. This thesis chooses PS to represent brittle polymers. The approach aiming at toughening it is to polymerize styrene in a free radical manner inside cross-linked GTR particles. This leads to the formation of both free PS and PS that is grafted onto the GTR, denoted as grafted PS. The inclusions of the free PS inside the GTR particles help break them down by mechanical shear in a screw extruder for example and the formation of grafted PS improves the interfacial adhesion between the PS and the GTR. This thesis has developed a comprehensive kinetic model for the polymerization of free PS and that of grafted PS. This model is validated by experimental designs.

Keywords: ground tire rubber, polymerization, polystyrene